THE IMPACT OF DIETARY FAT AND EXERCISE ON INTESTINAL HOMEOSTASIS: A QUEST FOR ANTI-INFLAMMATORY MECHANISMS

By

PAUL J. WISNIEWSKI II

A dissertation submitted to the

School of Graduate Studies

Rutgers, The State University of New Jersey

In partial fulfillment of the requirements

For the degree of

Doctor of Philosophy

Graduate Program in Kinesiology & Applied Physiology

Written under the direction of

Sara C. Campbell

And approved by

_____

_____

_____

_____

_____

_____

New Brunswick, New Jersey

MAY 2020

ABSTRACT OF THE DISSERTATION

The impact of dietary fat and exercise on intestinal homeostasis: a quest for anti-inflammatory mechanisms

By PAUL J. WISNIEWSKI II

Dissertation Director:

Sara C. Campbell, PhD, FACSM

Excess consumption of saturated fat has shown to increase risk of colorectal cancer (CRC) development as well exacerbate inflammatory bowel disease (IBD) progression. In contrast, physical exercise has shown to significantly reduce the risk of CRC development and ameliorate symptoms of IBD. Although exercise has shown to exert profound anti-inflammatory effects in the colon, what is not well known are the exact mechanisms by which these health benefits are conferred. Of note are three primary processes that have been implicated in modulating intestinal inflammatory responses in the context of large bowel disorders. These include the production of intestinal mucus, the induction of the unfolded protein response (UPR) in the advent of endoplasmic reticulum (ER) stress, and the activation of inflammasomes which foster a microbe-host mutualism. The impact of dietary fat intake and physical activity on mucus thickness, the UPR and inflammasome activation where explored to elucidate putative mechanisms by which diet and exercise promote or disrupt intestinal homeostasis. In aim 1, we examined the extent to which 12 weeks of a 45% high-fat diet (HFD) contributes to colon inflammation and microbiota localization and whether voluntary wheel running could confer a therapeutic effect in 6-week-old male and female C57BL/6NTac mice. Voluntary wheel running attenuated HFD-induced colon

inflammation in female mice only while no differences in microbiota localization were observed between treatment groups. In addition, sedentary male mice consuming a control low 10% fat diet demonstrated a greater degree of inflammation compared to their female counterparts. These findings demonstrate that 12 weeks of a 45% HFD is not sufficient to induce any structural changes to intestinal mucus but have shown that regular physical activity can ameliorate colon inflammation. In aim 2, we replicated aim 1 in a second cohort of 6-week-old male and female C57BL/6NTac mice using a 60% HFD in order to accelerate the occurrence of overt colon pathologies and to compare our findings from aim 1. In addition, we explored the effects of dietary fat and voluntary wheel running on colonic epithelial ER stress and the UPR. In contrast to aim 1, voluntary wheel running attenuated HFD-induced colon inflammation in both male and female mice. In agreement with aim 1, a similar increase in inflammation in sedentary male mice fed a control 10% fat diet was observed. Female mice demonstrated an inherent increase in colon IL-10 concentrations, an improved proliferative phenotype and an increase in goblet cell density compared to males. Voluntary wheel running contributed to a significantly improved proliferative phenotype compared to exercised mice. Sedentary and exercised male mice consuming a 60% HFD exhibited a unique compensatory response characterized by an increase in inner mucus layer thickness and mucin 2 production. While a 60% HFD modulated the gene expression of ER stress sensors activating transcription factor 6 (Atf6) and inositol-requiring kinase 1β (IRE1β) in female mice, a 60% HFD increased the phosphorylation of eukaryotic initiating factor-2α (eIF2α) in male mice which was attenuated by a control 10% fat diet and voluntary wheel running. Findings from this aim further corroborate the efficacy of exercise in contributing to colon health and suggests that females may possess an inherent resistance against the development of colon pathologies. In addition, we are the first to demonstrate that voluntary wheel running attenuates HFD-induced colonic epithelial ER stress in male

mice. Utilizing the same cohort of animals from aim 2, aim 3 investigated the contribution of dietary fat and voluntary wheel running towards the transcription of inflammasome components and activation of caspase-1. Large increases in the gene expression of inflammasome components including the NOD-like receptor family pyrin domain containing (NLRP)3 and NLRP6 sensors, the adaptor PYD and CARD domain containing (Pycard), and caspase-1 where observed in sedentary female mice fed an HFD and in exercised female mice fed either diet relative to the sedentary control fed a 10% fat diet. This occurred in tandem with a non-significant increase in caspase-1 activation. In males, a non-significant and modest decrease in caspase-1 activation was observed, however. These findings illustrate putative sex differences in inflammasome activation in response to dietary fat and voluntary wheel running, but more rigorous analyses are required.

ACKNOWLEDGEMENTS

I would like to first thank my advisor, my mentor and dear friend, Dr. Sara C. Campbell. You saw something in me when I did not and gave me a chance at a better life. I am forever in your debt and thankful for all the wisdom you have imparted, both in academics and in life. There are no words to express the depth of my gratitude for all that you have done for me. I can only hope to uphold your respect as I begin the next chapter in my life.

Thank you, Dr. Laurie B. Joseph. You have become a dear mentor and an integral part of my success as a scientist and as a human being. You accepted me into your lab as if I were your own and demanded only excellence while asking nothing in return. You lead by example, have an immense heart and are fiercely loyal. I will forever endeavor to cultivate these qualities within myself and to make you both proud.

Thank you to Drs. Carol Gardner, Peihong Zhou, Tracy Anthony and Zoltan Szekely for all your wisdom and encouragement.

Thank you to my committee members Drs. Brandon Alderman, Lee Kerkhof, Shawn Arent and Dan Hoffman. Your input and support throughout this process has been invaluable.

Thank you to the Department of Kinesiology and Health, Department of Nutritional Sciences, Rutgers Center for Lipid Research and to the Institute for Food Nutrition and Health for the opportunities to present my research and financial assistance. I'd also like to give a special thanks to staff including Alejandro Diaz, Wendy Dobrynio, Janice Nappe and Amy Mathys for your support, belief and encouragement.

Finally, thank you to my fellow graduate students and lab mates including Robert Dowden, Candace Longoria, Lauren Hall, Tasleen Chawla, Dr. CJ Brush, Dr. Alan Walker, David Sanders, Katarina Smiljanec, Dr. Atreju Lackey, Gabriella Wahler, Rocio

Duran, Esther Mezhibovsky, Kevin Tveter, Ke Sui, Sai Santosh, Anastasia Diolintzi and Becca Melillo. For without you, graduate school would have been extremely difficult and life itself would be devoid of any authenticity and humanity. Thank you for your words of encouragement, for the time you took to listen, for your concerns and for your interest in my project. I am forever grateful to have been surrounded by such wonderful human beings.

DEDICATIONS

To my loving mother, Helina K. Wisniewski. You have been an inspiration since my earliest memories. From what you endured, what you suffered in life…the abuse, the poverty, the neglect, the violence…you managed to triumph over it all. You are a woman of fierce loyalty to family, who demonstrates a remarkable work ethic and who stands for truth above all else. I cannot tell you how fortunate I feel to have been raised by a woman of your strength and resilience. Thank you for always pushing me, for teaching me to be independent and for instilling the importance of education. You have given everything to ensure that Rob and I have a better life, now I will give everything to uphold that dream and to provide the same for my children. I love you mom.

To the memory of my father, Paul J. Wisniewski. Though you were with me only the first five years of my life, I am grateful to have spent every one of those days with you. I will never forget your story. That you had to give up your dream of becoming an Olympic swimmer after your father died to provide for your family. That you were a diesel mechanic, hands always calloused and stained with oil. That you never complained, worked hard and always had an unbreakable sense of humor. I will never forget our fishing trips after school. I will never forget the respect, love and affection you showed mom. I will never forget the kindness and love you showed me and Rob, even when you were at your sickest. But most importantly, I will never forget your smile. I will forever live to honor your kindness, humility and loving heart. I love you dad.

To my big bro, Robert E. Wisniewski. Your resilience, spirit and determination has always been an inspiration. You have helped me cultivate a sense of self and have encouraged me to not let doubt and fear get in the way of my own potential. I only hope that I can be an inspiration to you as much as you have been one for me. I love you bro.

To Rutgers University. I wasn't always the best student. I flunked out during my sophomore year and was forced to take year off. Having my eyes opened and a lesson learned, you allowed me to return and even provided me employment while continuing my education at night. I was a custodian, a grounds worker, a student worker, a writing tutor and a lab manager. Throughout this time, I learned the value of hard work, what it meant to earn a dollar, how to appreciate and connect with different cultures and most importantly, the value of education. For the past 15 years, you have allowed me to better myself. You have given me the opportunity to bet on my future and rise from failure. I am forever grateful.

To my Muay Thai coach, Chris Tran. I have never met a man who is as dedicated to their craft as they are to the betterment of their students. It has been 12 years and to this day, I feel I have so much more to learn from you. You have become a brother and a lifelong mentor. Through the art of Muay Thai, you have given me an immense appreciation for the gift of life itself and for the importance of challenging yourself. That through discipline as well as physical and mental hardship, I can grow deeper into the best man I can be. I owe you so much and am forever grateful. Thank you and I love you.

ACKNOWLEDGEMENT OF PREVIOUSLY PUBLISHED WORK

Chapter 2 of this dissertation, entitled “Voluntary Wheel Running Reduces Colon Inflammation in Female but not Male Mice Fed a High-fat Diet”, was originally published in *Comparative Exercise Physiology*. I was involved in the study design, data collection, statistical analyses, figure generation, original drafting of the manuscript, and final manuscript revisions.

The original article has been adapted with permission from:

Wisniewski PJ, Gardner C, Wahler G, Lightfoot SA, Joseph LB, Campbell SC (2019). Exercise reduces colon inflammation in female but not male mice fed a high-fat diet. *Comparative Exercise Physiology*, 15(1): 35-47.

TABLE OF CONTENTS

LIST OF TABLES

Chapter 2: Voluntary Wheel Running Reduces Colon Inflammation in Female but not Male Mice Fed a High-fat Diet

Chapter 3: High-fat diets and Voluntary Wheel Running Modulate Endoplasmic Reticulum Stress in Mouse Colon.

Chapter 4: The Effects of High-fat Diets & Exercise on Inflammasome Activity.

LIST OF FIGURES

Chapter 1: Introduction and Literature Review

Chapter 2: Voluntary Wheel Running Reduces Colon Inflammation in Female but not Male Mice Fed a High-fat Diet

Chapter 3: High-fat diets and Exercise Modulate Endoplasmic Reticulum Stress in Mouse Colon.

Chapter 4: The Effects of High-fat Diets & Exercise on Inflammasome Activity.

LIST OF ABBREVIATIONS

AB/PAS	Alcian blue-Periodic Acid Schiff
AMPs	Antimicrobial peptides
ATF6α	Activating transcription factor 6α
BiP	Immunoglobulin protein
BrdU	Bromodeoxyuridine
Card (ASC)	Apoptosis-associated speck-like protein containing a caspase activation and recruitment domain
CD	Crohn's disease
CHOP	CCAAT-enhance-binding protein homologous protein
COX-2	Cyclooxygenase-2
CRC	Colorectal cancer
DAMPs	Damage associated molecular patterns
DSS	Dextran sulfate sodium
eIF2α	Eukaryotic initiation factor-2α
ER	Endoplasmic reticulum
ERAD	ER associated protein degradation
F4/80	Marker for detection of murine macrophages
Fcgbp	IgGFc binding protein
Grp78	Glucose-regulated protein 78
HFD(s)	High-fat diet(s)
IBD	Inflammatory bowel disease
IgA	Immunoglobulin A
IL-10	Interleukin-10
IRE1β	Inositol-requiring kinase 1β
MIS	Mucosal immune system
Muc2	Mucin 2
NFκB	Nuclear factor kappa-light-chain-enhancer of activated B cells
NLRP3,6	NOD-like receptor family pyrin domain containing 3 or 6
NLRs	nucleotide-binding oligomerization domain (NOD)-like receptors
PAMPs	Pathogen associated molecular patterns
PCNA	Proliferating cell nuclear antigen
PERK	Pancreatic eIF2α kinase
PGC-1α	PPARγ coactivator 1 alpha
PPARγ	Peroxisome proliferator-activated receptor gamma
PRRs	Pattern recognition receptors
Pycard (ASC)	PYD and CARD domain containing
Relmβ	Resistin-like molecule beta
SFAs	Saturate fatty acids
TFF3	Trefoil factor 3
TLRs	Toll-like receptors
TNFα	Tumor necrosis factor alpha
UC	Ulcerative colitis
UPR	Uκolded protein response
XBP1	Transcription factor X box-binding protein 1

Chapter 1: Introduction & Literature Review

Introduction

The human intestine contains an immense and dynamic community of trillions of microorganisms. In exchange for protection and an ecological niche rich in both host and dietary derived nutrients, these microorganisms establish a symbiotic relationship with their host by making essential contributions to metabolic processes. The majority of these microorganisms are bacteria and predominately reside in the large intestine whose metabolites play a pivotal role in host energy production, immunity, lipid metabolism, glucose homeostasis and intestinal permeability (1); these microorganisms that inhabit the gut are commonly referred to as the 'gut microbiota' or microbial taxa. Though this relationship is primarily mutualistic in nature, the close association of a dense bacterial community with intestinal tissue poses serious health challenges. The sheer number of gut bacteria presents a persistent threat of microbial breach into systemic circulation which is compounded by a single-cell layer of epithelium and a large intestinal surface area (~32 m^2 in humans) (2). This opportunistic invasion by resident bacteria can degrade epithelial barrier integrity and contribute to pathologies such as chronic low-grade inflammation. The intestinal immune system therefore has an essential role in limiting tissue invasion by resident bacteria and is vital for preserving a symbiosis between the host and its gut microbiota.

2. Overview of Mucosal Homeostasis

The majority of immunological processes take place in the mucosa which is comprised of the epithelium, the underlying lamina propria and the muscularis mucosae, which is a thin muscle layer below the lamina propria (3) (Figure 1.1). The lamina propria consists of loosely packed connective tissue that forms the scaffolding for small intestinal villi and contains blood and nervous supply, and lymphatic drainage for the mucosa (3). Importantly, it is in the mucosa where cells of both the innate and adaptive

arms of the mucosal immune system (MIS) reside to maintain mucosal homeostasis. The MIS faces challenges unlike those faced by any other organ system as it must continuously cope with an enormous bacterial load distributed across a vast surface area and frequent pathogenic challenge from contaminated food and water (4). At the same time, the MIS must also avoid harmful overreactions that could damage intestinal tissue or alter crucial metabolic functions of the gut microbiota (5). Despite these challenges, the MIS is remarkably adept at minimizing the adverse health effects of the gut microbiota. Maintenance of mucosal homeostasis is thus achieved by three primary immunological barriers as previously suggested (5): *1)* limiting contact between bacteria and the epithelial cell surface, *2)* immune responses to penetrant bacteria and *3)* mucosal immune firewalls.

2.1. Segregation of the Epithelium and Gut Microbiota

Intestinal epithelial cells generate both physical and chemical barriers to minimize contact between the epithelial cell surface and the gut microbiota. The formation of a physical barrier is accomplished by the production of intestinal mucus from goblet cells which are specialized epithelial cells that secrete large glycoprotein polymers of mucins into the gut lumen forming a viscous gel-like substance. Mucus secretion from goblet cells is under direct regulation by the MIS through cytokines from T-helper type 2 (Th2) cells (6-8) including Interleukin (IL)-13, a major effector cytokine (9). Moreover, a recent study has shown that activation of the NOD-like receptor family pyrin domain-containing 6 (NLRP6) inflammasome drives mucus granule exocytosis from goblet cells (10), identifying the first innate immune regulatory pathway governing mucus secretion. In addition to the mucus layer covering the surface of the epithelium, of special importance is the enterocyte apical glycocalyx that is built by transmembrane mucins that projects into the intestinal lumen, and the tight junctions that firmly anchor

the cells to each other (11, 12). Together, these systems encompass the primary physical defense for limiting epithelial cell-microbe contact.

2.1.1. Mucin 2

The major component of intestinal mucus is the mucin 2 (muc2) mucin, the function of which has been determined only in recent years. Its structure is comprised of a protein core of approximately 5,179 amino acids, with a typical mucin PTS domain (13, 14) which has a high frequency of the amino acids proline, threonine, and serine (15). These domains become densely O-glycosylated in the golgi apparatus of a goblet cell, forming mucin domains whose appearance resemble a bottle brush with O-glycans extending in all directions like brush bristles; this extended conformation and high capacity of mucin glycans to bind water facilitate the gel-forming properties of the mucin domains (16). The Muc2 monomeric building block when fully glycosylated has a large mass of approximately 2.5 MDa and is polymerized in the endoplasmic reticulum (ER)-golgi secretory pathway of goblet cells, resulting in the formation of enormous net-like polymers (17). In addition, Muc2 also constrains the immunogenicity of gut antigens by delivering tolerogenic signals to dendritic cells (DCs) (18). Thus, its inherent complexity and contribution to host-microbe crosstalk corroborates the ecological importance of Muc2 in the gut.

2.1.2. Intestinal Mucus & Host Defense

The physicochemical properties of secreted mucus differ significantly in the small and large intestine, but the immune defenses employed by the host traverse the entire gut epithelium. In the small intestine the pore sizes in mucus are large, allowing bacteria and bacteria-sized particles to penetrate the secreted mucus (19). To prevent infection, antimicrobial proteins (AMPs) are secreted from crypt paneth cells and enterocytes into intestinal mucus which are of major importance in keeping bacteria at bay (20). Without

intestinal mucus, AMPs would quickly be diluted in the gut lumen. Intestinal mucus thus forms a diffusion barrier that concentrates AMPs near the epithelial cell surface and slows down bacterial penetration in the small intestine. In addition to the production of AMPs, another mechanism for sequestering resident bacteria involves the production of immunoglobulin A (IgA) from IgA^+ plasma cells. Production of IgA is facilitated by DCs that sample bacteria by phagocytosis at various mucosal sites (5). DCs located beneath the epithelial dome of Peyer's patches (lymphoid nodules primarily found in the ileum) sample penetrant bacteria (21) and DCs located in the lamina propria also sample small numbers of bacteria that are present at the apical surface of epithelial cells (22, 23). The bacteria-laden DCs then induce B cells to differentiate into plasma cells that produce IgA specific for intestinal bacteria (5). Secreted IgA then limits bacterial association with the intestinal epithelial surface (24) and restricts the penetration of bacteria across the gut epithelium (25). These defense mechanisms in the small intestine that limit microbe-epithelial cell contact are present in the colon apart from paneth cells and Peyer's patches, as these are exclusive to the small intestine. Consequently, the expression of AMPs are lower in the large intestine (26).

In the large intestine, goblet cells increase caudally from the duodenum to distal colon, paralleling an increase in bacterial load (27). The mucus layer is very thick (~ 50 μm in mice or 200 μm in humans) in the large intestine and is comprised of a two-layered design. The dense inner mucus layer is firmly anchored to intestinal goblet cells and is normally devoid of bacteria, while the loosely attached outer layer is laden with commensal bacteria (16, 28, 29). Conversion of the inner layer to the expanded outer layer is governed by endogenous proteases, such as the recently described calcium-activated chloride channel regulator 1 (CLCA1) which governs mucus growth as a metalloprotease (30). The expansion of the outer mucus layer increases pore size and penetrability to bacteria, providing a rich ecological niche for enteric microorganisms. In

contrast, pore size of the inner mucus layer is sufficiently smaller to hinder penetration of bacteria down to a 0.5 μm diameter (31). Together, the colon mucus barrier sequesters the gut microbiota and mediates the crosstalk between microbes and the host immune system.

2.2. Immune Responses to Penetrating Bacteria

The defenses employed to segregate the epithelium from the gut microbiota are not perfect, and some bacteria not only encounter the epithelial cell surface but may breach the epithelium. Penetrant bacteria typically succumb to rapid phagocytosis and elimination by resident macrophages in the lamina propria, however. Macrophages are present in high numbers in the mammalian gastrointestinal (GI) tract and are frequently in close contact with the epithelium (32). These innate immune cells rapidly phagocytize bacteria and kill the ingested organisms through mechanisms that include AMPs and reactive oxygen species (33). In addition to their phagocytic capacity, macrophages help to restore the physical integrity of the epithelium following injury by migrating to damaged areas and producing growth factors that enhance enterocyte proliferation (34).

In addition to innate immune responses, the adaptive immune system plays a large role in maintaining intestinal homeostasis. Specifically, $CD4^+$ T cells are an essential component of host-microbe mutualism. These cells differentiate into subset cell types, such as CD4+ T regulatory (T_{Reg}) and T helper (T_H) cells, in response to cytokine-induced signals via transcription factors originating from activated macrophages or DCs as well as epithelial cells. Each subset, as previously reviewed (5), produces their own characteristic cytokine profile which modulates inflammatory responses following mucosal injury or invasion as well as the activity of subset populations (35). This intrinsic regulation of CD4+ T cell differentiation and activity of subset cell populations is equally crucial for maintaining mucosal homeostasis as it promotes a tolerogenic response to penetrant bacteria without exacerbating epithelial tissue damage.

2.3. Mucosal Immune Firewalls

The MIS has the difficult task of confining the gut microbiota while maintaining an appropriate degree of inflammation to clear intestinal infections. The induction of both innate and adaptive immune responses is indeed tightly regulated and both arms of the MIS work in tandem to maintain mucosal homeostasis. Nevertheless, a ‘last resort’ or system of containment beneath the epithelial cell layer is still needed to prevent systemic infection.

Bacteria that enter the blood are mainly cleared by heterogeneous splenic macrophages populations (36) and those that enter the mesenteric (abdominal) vascular system are delivered through the portal vein to the liver to be cleared by hepatocytes, namely Kupffer cells (5). To reiterate and by contrast, penetrant bacteria in the mucosa are taken up by DCs which stimulate IgA secretion or are phagocytized by macrophages. As well, both B and T cells can be activated by low numbers of penetrant bacteria (21) and induce subsequent inflammatory responses (35). The inflammatory milieu generated by the MIS does not normally empty into systemic circulation but instead, drains into mesenteric lymph nodes preventing infiltration into systemic lymphoid structures (21). Not only does this ensure that the induction of mucosal immunity remains confined to the mucosa but that the effects of this induction can be distributed throughout the intestinal mucosa through recirculation of activated B and T cells via the mucosal lymphatics and vasculature (37-39). The mesenteric lymph node thus can be described as a mucosal immune “firewall” in that it provides a way for luminal microbial contents to be sampled and for adaptive immune responses to be induced but remain confined to the MIS, all while disseminating the local inflammatory responses across the entire mucosal surface.

3. Mechanisms of Inflammatory Bowel Disease

Inflammatory bowel disease (IBD) comprises a broad group of disorders that are characterized by chronic and sever inflammation of the gastrointestinal (GI) tract. IBD includes both ulcerative colitis (UC) and Crohn's disease (CD) which are distinct from one another based on clinical criteria; UC is a chronic inflammatory condition limited to the colon while CD can affect any part of the GI tract (40). Moreover, IBD is widely accepted as one of the most potent risk factors for colorectal cancer (CRC) development. Although the exact causes remain unclear, increasing evidence suggests that IBD arises from dysregulation of the MIS.

3.1. Muc2 Deficiency

Providing Muc2 is the primary component of intestinal mucus, Muc2 deficiency results in aberrant mucus properties and is linked to the onset of IBD where a strong correlation between mucosal inflammation and the suppression of Muc2 synthesis and secretion is found (41, 42). Of primary interest are seminal findings using Muc2 knockout ($Muc2^{-/-}$) mouse models that first established a causal relationship between Muc2 suppression and IBD and CRC development (43, 44), which have been confirmed by more recent studies (45, 46), as well as the function of Muc2 in protecting the host against pathogenic challenge (47).

3.1.1. CRC and IBD Onset

Most notably are the early findings of Velcich and colleagues who assessed the effects of Muc2 deficiency in the development of intestinal carcinogenesis (43). Muc2 knockout (KO) and wild type (WT) mice were maintained and sacrificed at 6 months and 1 year of age. It was found that tumors had spontaneously developed in the duodenum, colon and rectum within six months. At the age of 1 year, 65% of Muc2 KO mice had tumors. Interestingly, tumor formation was restricted to the small intestine in younger

mice, whereas tumors subsequently appeared in the large intestine and rectum in older mice. Likewise, histological analysis of duodenal, proximal and distal colon sections by Alcian blue staining showed a complete ablation of goblet cells as well as the elongation of colonic crypts. However, the absence of goblet cells was not due to a complete ablation of the differentiation pathway of this cell lineage because expression of intestinal trefoil factor 3 (TFF3), another product of fully differentiated goblet cells (48), remained detectable. Muc2 KO mice concomitantly demonstrated an enhanced epithelial cell proliferation in both the duodenum and colon relative to control mice as determined by immunohistochemical detection of incorporated bromodeoxyuridine (BrdU). Together, these findings indicate that Muc2 suppression induces intestinal carcinogenesis in a progressive manner, caudally down the GI tract, and that this induction is manifested as increased proliferation, decreased apoptosis and increased migration of intestinal epithelial cells. Further, some aspects of the differentiation program of the goblet cell lineage persist in Muc2 KO mice.

Following the work of Velcich et al. (43), Van der Sluis and colleagues later demonstrated that $Muc2^{-/-}$ mice elicit an even greater inflammatory response after 12 weeks of dextran sulfate sodium (DSS) treatment (44), a known agent that induces ulcerative colitis in mice. These mice showed evidence of colitis in as early as 5 weeks of age following treatment, which worsened as the mice aged, and demonstrated distinct changes in colonic morphology characterized by a progressive increase in mucosal thickness, in the flattening and ulceration of epithelial cells, and in crypt length as well as a severe loss of the architecture of the lamina propria which was more pronounced in older mice. Like the findings of Velcich et al. (43), colonic goblet cells in Muc2 KO mice were negative for Muc2 upon immunohistochemical analysis but TFF3 expression remained unchanged. Further, colonic goblet cells of Muc2 KO mice appeared smaller

and more condensed whereas the goblet cells of WT mice were round and bell shaped. In addition, Muc2 KO mice showed enhanced epithelial cell proliferation in the distal colon as evidenced by immunohistochemical detection of incorporated BrdU and increased infiltration of proinflammatory cytokines such as tumor necrosis factor α (TNF-α) and IL-1β but not of IL-6. In sum, these results further indicate that loss of Muc2 in the intestine degrades the epithelial barrier which leads to an abnormal mucosal and goblet cell morphology, contributing to colon inflammation and exacerbating chemically induced colitis.

3.1.2. Colonization Dynamics and Mucosal Inflammation

Providing the MIS maintains mucosal homeostasis by limiting microbe-epithelial cell contact, secretion of intestinal mucus is paramount in preventing breach of the epithelium by both pathogenic and commensal microbes and of subsequent inflammatory responses (28). Of note is an early study who sought to advance the understanding of mechanisms by which the host defends itself upon introduction of attaching and effacing (A/E) bacteria (e.g., *E. coli.*) (47). The goal of the study was to elucidate the role of Muc2 in host protection against such pathogens. To do so, $Muc2^{-/-}$ and WT mice were inoculated with *Citrobacter rodentium* via oral gavage, a murine A/E pathogen related to the common diarrheagenic *E. coli*. (47). To summarize the authors, Muc2 deficiency did not significantly impact the total number of bacteria that ultimately infected the mucosal surface but rather that it predisposed the large bowel to greater numbers of loosely adherent bacteria, increasing the overall burden of microbes and ulcer development; second, the host enhanced mucin synthesis and secretion to expunge pathogens and regulate total microbe density at the mucosal surface while Muc2 deficiency increased overall luminal burdens of microbes; and third, that this increased microbial burden induced by Muc2 deficiency exacerbated gut barrier

dysfunction by permitting translocation of both pathogenic and commensal microbes into systemic circulation (47).

3.2. Endoplasmic Reticulum Stress

The endoplasmic reticulum (ER) is a membrane-bound organelle crucial for the synthesis of polypeptides and posttranslational modification and folding of secretory or membrane proteins in eukaryotic cells. ER protein folding and modification are highly sensitive to disturbances in ER homeostasis including inflammatory stimuli (49). The accumulation of unfolded and misfolded proteins in the ER lumen is defined as ER stress and has been linked to high-fat diet (HFD)-induced inflammatory based diseases (50). ER stress activates the unfolded protein response (UPR) to rectify protein folding defects by three primary outcomes: decreased translation, restoration of protein folding and degradation of misfolded proteins through ER-associated protein degradation (ERAD), a process in which proteins in the ER are retro-translocated to the cytosol for proteasomal degradation (51). In addition, the UPR also orchestrates the induction of autophagy to degrade misfolded protein aggregates that cannot be removed by ERAD (52) whereas prolonged UPR activation induces ER stress-associated apoptosis to protect the organism all together (53).

Three protein sensors on the ER membrane initiate the UPR: (1) pancreatic ER eIF2α kinase (PERK), (2) inositol-requiring kinase 1 (IRE1) and (3) activating transcription factor 6 (ATF6) (49). Each of these stress sensors have an ER luminal domain that can sense the presence of unfolded and misfolded proteins. Under resting conditions, the ER chaperone binding immunoglobulin protein (BiP), also known as glucose-regulated protein 78 (Grp78), binds to the luminal domains of each stress sensor maintaining their inactive states (49). During ER stress, BiP dissociates from the luminal domains of the three stress sensors, activating them and initiating the UPR (54). BiP production is also upregulated in response to increased protein misfolding (55).

3.2.1. The Unfolded Protein Response

The most immediate response to ER stress is the activation of PERK. Activated PERK phosphorylates the alpha subunit of eukaryotic translation initiation factor 2 (eIF2α) and suppresses protein translation (53). Prolonged induction of PERK and subsequent phosphorylation of eIF2α activates the transcription factor ATF4 which upregulates the transcription factor CCAAT-enhance-binding protein homologous protein (CHOP) (56). The overexpression of CHOP promotes apoptosis, whereas CHOP-deficient cells are resistant to ER stress-induced apoptosis (57, 58). CHOP therefore plays an important role in the induction of apoptosis.

IRE1 is the most conserved ER stress transducer among the three and has two isoforms, IRE1α and IRE1β; IRE1α expression is ubiquitous (49) while IRE1β is found only in intestinal epithelial cells (59, 60). It is a ribonuclease that is activated by autophosphorylation following dissociation of BiP during ER stress (51). The major substrate for IRE1 is the mRNA encoding X box-binding protein 1 (XBP1) transcription factor. IRE1 splices XBP1 mRNA, converting it into a spliced and functionally active isoform (XBP1s) that induces UPR target gene expression such as those involved in ERAD signaling (61). These include members of the EDEM (ER degradation-enhancing α-mannosidase-like protein) family, which degrade misfolded glycoproteins (62).

ATF6 is a type II transmembrane protein, a basic leucine zipper (bZIP) transcription factor of the CREB/ATF family. In response to ER stress, ATF6 dissociates from BiP and travels to the golgi apparatus where it is then cleaved by site-1 protease (S1P) and S2P (51). The active transcription factor ATF6 is released into the cytoplasm which migrates to the nucleus to modulate gene expression of chaperones, components of ERAD and to induce ER biogenesis (49, 63). ATF6 also promotes protein folding, maturation and secretion (49). There are two isoforms, ATF6α and ATF6β. Though both isoforms are cleaved in response to ER stress, ATF6α is a potent activator of ER stress-response

genes whereas ATF6β acts to suppress the activity of ATF6α, serving as repressor to modulate the strength and duration of AFTF6α-mediated transcription (64).

3.2.2. ER Stress in Intestinal Secretory Cells

Goblet cells are specialized epithelial cells for the synthesis and secretion of intestinal mucus. Their name is derived from their goblet, cup like, appearance formed by the mucin granulae that fill the cytoplasm. This collection of secretory granules forms the theca, which is the morphologically defining characteristic of goblet cells. The major secretory product of intestinal goblet cells is Muc2, which undergoes extensive post-translational modification via *N*-glycosylation in the ER and *O*-glycosylation in the golgi apparatus occurs prior to secretion (31). In addition, intestinal mucus has a fast turnover of approximately 1 hr in the distal colon (65). It should also be stressed that goblet cells produce a range of other secretory products that are important functional components of the mucus barrier including TFF3 which is key to epithelial restitution after damage and injury (66), resistin-like molecule beta (Relmβ) which is critical for regulation of innate colonic function (67), and IgGFc binding protein (Fcgbp) which is covalently attached to Muc2 and may act as a mucus cross-linker (68). The complexity of the Muc2 protein and high secretory output of goblet cells makes Muc2 prone to misfolding which can activate the UPR. As such, ER stress in secretory cells is likely to promote intestinal inflammation in two ways as previously suggested by McGuckin et al. (51) : *1)* by reducing the effectiveness of the mucosal barrier caused by a decreased secretion of AMPs and mucins, and premature apoptosis and *2)* by UPR-initiated inflammatory signals released by stressed secretory cells. The details of which have been extensively reviewed (49, 51, 53) and more recently by Ma et al. (69).

3.3. Inflammasomes

The intestinal microenvironment represents a potentially hostile milieu in which a multitude of microorganisms, food-, and microbial-derived antigens constantly challenge the integrity of the intestinal epithelium. Prevention of epithelial breach is achieved by the production of intestinal mucus which acts as a physical and chemical barrier, by subsequent immune responses to penetrant bacteria and by prevention of systemic infection through the mesenteric lymphatic system and vasculature. Though intestinal epithelial cells function to keep bacteria from invading the body, they in fact have a complex and mutually beneficial relationship with the gut microbiota. The distinction between “friend vs. foe” is achieved through an array of pattern recognition receptors (PRRs) that recognize conserved molecular patterns, of both microbe and host origin, to initiate tolerogenic or defense responses (70). The first discovered family of PRRs are Toll-like receptors (TLRs), which are transmembrane receptors that recognize commensal- and pathogen-associated molecular patterns (PAMPs) (71). Several other classes of PRRs include nucleotide-binding oligomerization domain (NOD)-like receptors (NLRs). The NLR family of innate immune receptors have a wide range of endogenous and exogenous triggers, and downstream functions. Further, NLRs are a key component of inflammasomes which form in response to diverse microbial and host-derived stimuli (70).

Inflammasomes are cytoplasmic multi-protein complexes assembled around a set of core components that include a sensor protein, an adaptor protein (apoptosis-associated speck-like protein containing a caspase activation and recruitment domain (CARD)(ASC)) and an inflammatory caspase (72) of which caspase-1 seems to have a dominant role in inflammatory responses (73). In this regard, inflammasomes act as a multi-protein platform from which the activation of inflammatory caspases ensues. Inflammatory responses trigger proteolytic cleavage and activation of caspase-1,

resulting in the processing and release of proinflammatory cytokines IL-1β and IL-18, and in some cases pyroptotic cell death (74), an inflammatory form of programmed cell death. Activation of caspase-1 via the above pathway is known as canonical inflammasome signaling whereas non-canonical inflammasome signaling entails caspase-11 activation in mice or caspase-4 in humans (70). The role of inflammasomes in intestinal inflammation and infection is diverse and evidence suggests that the NOD-like receptor family pyrin domain containing 3 (NLRP3) and, more recently, the NLRP6 canonical inflammasomes are key players (70).

3.3.1. NLRP3 Inflammasomes

The NLRP3 inflammasome is expressed in both mucosal immune cells and epithelial cells and promotes inflammation through a caspase-1 dependent activation by cleavage of proinflammatory cytokines IL-1β and IL-18. Activation of the NLRP3 inflammasome is a two-step process, initiated by a priming signal that results in the nuclear factor kappa-light-chain-enhancer of activated B cells (NFκB)-dependent transcription of NLRP3 and processed (pro)-IL-1β. The second signal, binding of ligands, promotes inflammasome oligomerization and activation that culminates in caspase-1 activation and resultant cleavage of pro-IL-1β and pro-IL-18 into their biologically active forms, IL-1β and IL-18 (75). Ligands sensed by the NLRP3 inflammasome are diverse and include pathogen-associated molecular patterns (PAMPs) such as lipopolysaccharide (LPS); damage-associated molecular patterns (DAMPs) such as high concentrations of ATP (76); and ER stress (77). Given the diverse repertoire of ligands that can activate the NLRP3 inflammasome and its contribution to innate immunity, the NLRP3 inflammasome has been implicated in intestinal inflammation as well as in intestinal tumorigenesis which has recently been reviewed in depth (70).

3.3.2. NLRP6 Inflammasomes

Aberrant intestinal microbiota composition and function, termed dysbiosis, has been linked to multiple health conditions including metabolic disorders as well as IBD (1). Dysbiosis can be established in many ways including altered host genetics (78) and dietary modulation (79). Consequently, the host MIS participates in the organization of a "healthy" host-microbial interface by via IgA and mucus secretion, as well as the production of AMPs. Of note is the NLRP6 inflammasome which facilitates this mutualistic crosstalk.

The NLRP6 inflammasome is abundantly expressed in the intestinal epithelium, particularly in enterocytes and in secretory goblet cells, and is a key regulator of epithelial self-renewal and of goblet cell mucus secretion (10, 80-82). In addition, it is a regulator of the microbial ecology in the distal gut as mice deficient in NLRP6, ASC, or caspase-1 demonstrate a distinct form of dysbiosis that drives intestinal auto-inflammation, inflammation-induced colorectal cancer and features of metabolic syndrome (83-86). Exactly how the indigenous microbiota contributes to a healthy microbe-host interface has largely remained elusive, however. Findings of Levy et al (87) shed insight on this phenomenon in an elegant study design employing a NLRP6 deficient mouse model. Findings from this work indicated that IL-18 is necessary for AMP production and that the induction of AMP production by IL-18 is dependent on NFκB signaling as administration of IL-18 to germ free colon explants increased AMP levels and inhibition of NFκB prevented AMP production in WT mice, establishing an "inflammasome-AMP axis" in which the microbiota activates the Nlrp6 inflammasome, thereby stimulating production of mature IL-18 and subsequent AMP expression (87).

4. High-fat Diets and Inflammatory Bowel Disease

The prevalence of overweight (body mass index (BMI) ≥ 25 kg/m^2) and obesity (BMI ≥ 30 kg/m^2) has reached epidemic proportions with an estimated 2.1 billion adults worldwide overweight, of which 600 million are obese (88). Interestingly, the incidence and prevalence of IBD has risen in parallel with the obesity epidemic. Obesity may play a role in the pathogenesis of IBD and recent evidence suggests that impaired adipocyte metabolism and increased visceral adiposity, as well as dysbiosis of the gut microbiota are contributory factors (89); increased visceral adiposity is a risk factor CRC development as well (90). The use of HFDs in animal models has been used extensively to induce obesity and has shown to accelerate disease onset of CD-like ileitis independent of obesity (91). Findings from our previous work has demonstrated that HFDs induce an aberrant intestinal morphology and intestinal inflammation, and modulate tight junction protein expression in the small intestine (79).

4.1. HFDs and Intestinal Mucus

Studies that have examined the influence of HFDs on the physicochemical properties of colonic mucus are few and far between. For instance, Everard et al. (92) observed a thinner inner mucus layer in mice fed a 60% HFD in an early study. However, emerging evidence has gained further insight into how diet-induced metabolic disorders may contribute to aberrant mucus properties and predispose an individual to IBD. Most notably are the recent findings of Schroeder et al. (93), who demonstrated that 8 weeks of Western style diet (rich in SFAs and simple carbohydrates but depleted in dietary fiber) enhances colonic mucus penetrability and impairs mucus growth in mice which is accompanied by distinct alterations in the gut microbiota composition. The diet itself was comprised of 40.6% fat and 40.7% carbohydrates, of which only 4.0% was cellulose; in contrast, the normal chow diet contained 15.2% of neutral detergent fiber

(NDF) which measures most of the structural components in plant cells (94). Though no differences in inner mucus layer thickness were observed, mice given a WSD did demonstrate a more penetrable inner mucus layer following *ex vivo* analyses of colonic explants. Further, the authors observed a significantly slower mucus growth rate relative to chow-fed controls.

Following histological analysis of Carnoy-fixed colonic tissue sections by Alcian blue/periodic acid-Schiff (AB/PAS) staining, WSD-fed mice demonstrated a less organized inner mucus layer, more filled goblet cells and a trend towards more goblet cells per crypt (93). Likewise, goblet cells were more intensely stained in WSD-fed mice as determined by immunohistochemical detection of Muc2. These findings perhaps represent a compensatory response by the host as increased penetrability of the mucus allows more bacteria to access the epithelium and thus induces faster turnover and production of Muc2 (82, 95). In confirmation of this notion, more intense staining of immature (non-*O*-glycosylated) Muc2 was observed at the base of the crypts in WSD-fed mice. Moreover, WSD-fed mice secretion of mature (*O*-glycosylated) Muc2 was observed along the entire length of the crypt where it is normally confined to the crypt openings and epithelial surface. Evaluation of the mass spectrometry-based analysis of the mucus proteome revealed that WSD feeding did not cause major global alterations of the mucus protein composition, however, deleted in malignant brain tumour 1 (DMBT1) was abundant in WSD-fed mice which can agglutinate bacteria and is thus involved in mucosal innate immunity (96). The authors suggested that this response is perhaps another compensatory host response to the diet-induced mucus defects. Lastly, these mucus aberrations were prevented by treatment of *Bifidobacterium longum* and the dietary fiber inulin. In sum, these results demonstrate that a WSD can induce defects

in the physicochemical properties of intestinal mucus but can be rescued with sufficient intake of dietary fiber or a probiotic.

4.2. HFDs and Epithelial ER Stress

The impact of HFDs on ER stress remains largely ill-defined as well. In a more recent study however (78), Gulhane and colleagues examined the effects of prolonged high-fat feeding on epithelial cell oxidative/ER stress and intestinal mucin production in 6 – 8 wk old male WT and *Winnie* mice. *Winnie* mice have a missense mutation in the gene encoding for Muc2 which results in aberrant mucin assembly, inducing ER stress and spontaneous intestinal inflammation as seen in UC (97). *Winnie* colitis therefore results from an epithelial defect with a normal MIS, rather than major disruptions to the MIS as seen in many mouse models of IBD. The authors also assessed the extent to which exogenous IL-22 remediates HFD induced epithelial stress and inflammation as their previous report identified IL-22 as a potent suppressor of both oxidative and ER stress in pancreatic β-cells (98). Animals were given a 46% HFD or a normal chow 11% fat diet (NCD) and maintained for 3, 9 or 22 weeks. Those animals in the 22-week group were given a high (100 ng/g) or low dose (20 ng/g) of recombinant IL-22 or PBS as a control twice weekly by intra-peritoneal injection beginning at 18 weeks. It was found that increased mRNA levels of some inflammatory markers such as TNFα and of markers of ER stress were only observed after 22 weeks of a HFD; these included XBP1s, BiP and the ERAD chaperone ER degradation enhancing alpha-mannosidase like protein 1 (EDEM1). Likewise, increased protein levels of BiP and IRE1β in the distal colon were observed after 22 weeks of a HFD as well.

To ascertain whether the above induction of intestinal inflammation and ER stress altered the mucosal barrier, histological, gene expression and *in vitro* analyses were then performed in WT mice fed a HFD (78). No major changes of intracellular

mucin glycoproteins in goblet cells were observed with AB/PAS staining or with immunohistochemical detection of Muc2, though there was a suppression of Muc2 and TFF3 gene expression. Likewise, a significant decrease in the mRNA of transcription factors kruppel like factor 4 (KLF4) and SAM pointed domain ETS factor (SPDEF) was observed as well; KLF4 is required for the terminal differentiation of colonic goblet cells (99) whereas SPDEF is important for full maturation of goblet and paneth cells (100). Further, 22 weeks of a HFD led to the accumulation of the non-*O*-glycosylated Muc2 precursor, consistent with the induction of the UPR, as well as the suppression of the integral tight junction protein claudin-1 particularly at the apical surface of the epithelium. Concomitantly, endotoxin levels in serum were elevated following 11 and 22 weeks of a HFD (78). In *Winnie* mice, the HFD exacerbated colitis made evident by more severe and widespread colonic damage with prominent mucosal erosions and crypt abscesses. A concurrent upregulation of BiP and XBP1s mRNA, and suppression of KLF4 mRNA and claudin-1 protein expression was observed to a greater degree in *Winnie* mice fed a HFD. Interestingly and in contrast to the above findings of Benoit et al. (101), *in vitro* studies in human colonic LS174 secretory cells showed that palmitic acid treatment upregulated epithelial stress and reduced production of mature fully glycosylated Muc2 accompanied by an increase in the non-glycosylated Muc2 precursor and a reduction in Muc2 secretion. Likewise, a reduction in transepithelial electrical resistance was observed after 24 h of palmitic acid exposure. However, epithelial proliferation and apoptosis remained unchanged in WT mice fed a HFD or with IL-22 treatment. Lastly, administration of recombinant IL-22 suppressed both the HFD and palmitic acid-induced epithelial stress and mucosal inflammation in a dose dependent manner. In addition, IL-22 increased claudin-1 expression and reduced endotoxin levels in serum.

In sum, these findings demonstrate that prolonged high-fat feeding can induce ER stress in epithelial cells and challenge mucosal barrier integrity in tandem with a rise in serum endotoxin levels. In addition, HFDs can exacerbate the severity of genetically induced colitis. Lastly, exogenous IL-22 may promote mucosal barrier integrity and attenuate epithelial ER stress and mucosal inflammation in diet-induced obese mice.

4.3. HFDs and Inflammasomes

Though the role of HFDs on inflammasome regulation remains ill-defined, the recent work of Robblee et al. (102) demonstrated that a dietary excess of SFAs can activate the NLRP3 inflammasome through the induction of the ER stress sensor IRE1α in both human and mouse macrophages. Interestingly, SFA treatment has previously shown to activate IRE1α by a mechanism independent of the UPR (103). Taken together, the authors concluded that IRE1α may sense an altered membrane phospholipid composition which then mediates proinflammatory responses via inflammasome activation. HFD-induced macrophage infiltration and proinflammatory responses are commonly observed in metabolic disorders at affected tissues including adipocytes (104), hepatocytes (105) and in small intestinal villi (79). Thus, HFDs may potentiate intestinal inflammation through the activation of the NLRP3 inflammasome in recruited macrophages.

5. Exercise and Inflammatory Bowel Disease

Regular exercise provides a host of benefits to human health and is a potent preventative measure against the development of numerous chronic diseases. Exercise has been proposed as a powerful pharmacological agent given the myriad of health benefits exercise can confer providing the proper dosage (106). While exercise has the remarkable ability to modulate numerous physiological systems simultaneously, this also proves it difficult to elucidate the mechanisms behind these favorable effects. In the

context of IBD, a risk factor for the development of CRC, long-term participation in aerobic exercise has shown to significantly reduce the risk of IBD development (107-109) and ameliorate symptoms associated with IBD (110).

5.1. Putative Mechanisms of Inflammatory Control by Exercise in IBD

Though intense bouts of exercise can trigger systemic inflammation and a subsequent suppression of immunity, regular exercise may have anti-inflammatory actions mediated by auto-, para- and endocrine mediators produced by active skeletal muscle termed “myokines” (111-113). As summarized in a recent review (110), these myokines include IL-6, IL-8, IL-15 and brain-derived neurotrophic factor (BDNF) among several others which may suppress malignant cellular transformation and cancer development. In addition, endurance exercise has shown to upregulate the expression of the peroxisome proliferator-activated receptor-gamma (PPARγ) coactivator-1α (PGC-1α), which orchestrates the regulation of numerous adaptions derived from endurance training including fiber type transformation, mitochondrial biogenesis and angiogenesis along with improved insulin sensitivity (114). In addition, PGC-1α suppresses the transcriptional activity of NFκB, the master regulator of proinflammatory gene expression (115). Similarly, two concurrent studies by Liu et al. have shown that voluntary exercise prevents HFD induced colon inflammation and protects against ulcerative colitis by up-regulating PPARγ activity (116, 117) implicating PPARγ as a novel therapeutic target.

Additional studies have also demonstrated that exercise exerts anti-inflammatory and anticarcinogenic effects in the murine colon by suppression of cyclooxygenase-2 (COX-2) and proliferating nuclear cell antigen (PCNA) expression (118), and by increasing IL-10 production (119) which can act directly on goblet cells in the colon to reduce ER stress and promote mucus barrier function (120). We have also shown that voluntary exercise attenuates HFD-induced COX-2 expression in the small intestine (79) and in the colon of female mice (121). In sum, the above mechanisms indicate that

exercise confers its anti-inflammatory properties through a myriad of mediators as well as through distinct biochemical pathways involved in the modulation of inflammatory responses.

6. Conclusions

The present review highlights the complexity of mucosal homeostasis regulation and emphasizes that such regulation via the coordinate actions of both the innate and adaptive arms of the MIS requires an extreme elegance. As such, perturbations in mucosal homeostasis have been implicated in the pathogenesis of IBD and putative contributory mechanisms may include Muc2 deficiency, aberrant mucus properties, ER stress and inflammasome dysregulation. Diets high in SFAs may exacerbate or result in mucosal immune deficiencies and thus predispose an individual to IBD development through the discussed mechanisms. In contrast, exercise confers potent anti-inflammatory properties on the colon but its effect on intestinal mucus, ER stress and inflammasome activation remains ill-defined. Additional studies that further examine the impact of exercise on mucosal barrier and epithelial cell function remain vital.

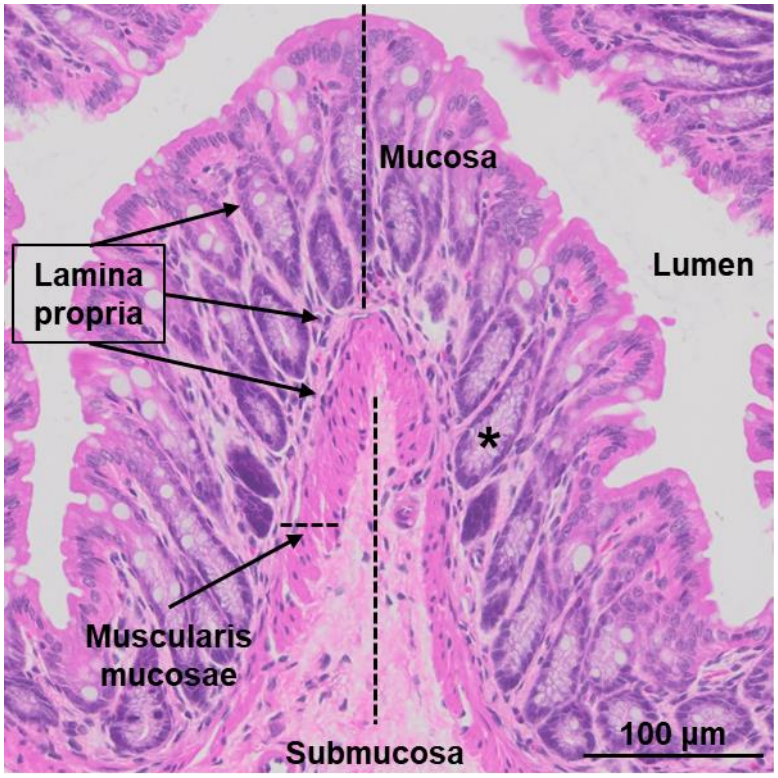

Figure 1.1. Gut mucosa overview. Histological section of mouse colon fixed in paraformaldehyde and sucrose was stained with H&E (original magnification x 400). Asterisk, crypt lumen.

Chapter 2: Voluntary Wheel Running Reduces Colon Inflammation in Female but not Male Mice Fed a High-fat Diet

Paul J. Wisniewski, Gabriella Wahler, Carol Gardner, Stanley A. Lightfoot, Laurie B. Joseph, Sara C. Campbell

Published in

Comparative Exercise Physiology, 15 (1), 35-47; 2019

Abstract

The influence of diet and exercise on intestinal mucus and the spatial organization of the microbiota is poorly understood. Though, it has been observed that the spatial organization of the microbiota can be altered extensively in Crohn's disease and ulcerative colitis. This study aims to investigate the pathophysiological events in mouse colon that are associated with a high fat diet and lack of exercise. Forty-eight, 6-week old C57BL/6NTac male and female mice were fed a normal or high-fat diet for 12 weeks and randomly assigned to free wheel running or sedentary groups. After 12 weeks, animals were sacrificed and distal colon tissue sections with and without fecal material were fixed for histomorphometric analysis, immunohistochemistry for cyclooxygenase-2 and mucin-2, or fluorescent *in situ* hybridization with the universal bacterial probe EUB338 (5'-GCTGCCTCCCGTAGGAGT-3'). Goblet cell counts and distance between the microbiota and epithelial surface were determined using ImageJ software. All mice had a normal colon morphology except for high-fat fed female mice who ran, which had less goblet cells compared to all male groups and a reduced mucin-2 expression. Voluntary wheel running attenuated high-fat diet induced COX-2 expression in female mice only. The distance between the microbiota and epithelial

surface remained the same. Taken together, these results show that voluntary wheel running protect against high-fat diet-induced inflammation in the distal colon of female mice and responses to changes in host behavior may differ between sex.

Key words: Colon; Inflammation; Gut microbiota; Intestinal mucin-2; Diet, high-fat

Introduction

Comorbidities associated with metabolic syndrome, particularly increased abdominal adiposity, are increased risk factors for colorectal cancer development (90). Further, aberrant colon mucus properties and chronic low-grade mucosal inflammation are closely involved in the pathophysiology of chronic gut inflammatory disease (122). Conversely, long-term participation in aerobic exercise has shown to significantly reduce the risk thereof (107-109) and ameliorate symptoms associated with inflammatory bowel disease (110). At present, there is a paucity of literature that has investigated the combined influence of high-fat diets (HFDs) and exercise on inflammation, the spatial organization of the microbiota and critical intestinal mucus proteins. In this paper, we examined the influence of host behavior on mucosal inflammation, *in situ* mucin protein expression and microbiota localization in male and female C57BL/6NTac mice.

Limiting contact between bacterial communities and colon epithelial tissue is important to ensure a balanced, tolerogenic mucosal inflammatory response (5). Among the immunological barriers in place, the first line of defense is a physical barrier which is employed through the production of a thick, highly glycosylated and hydrated mucus barrier comprised of two distinct parts: a dense, firmly attached inner layer that is normally devoid of bacteria and a loosely attached outer layer laden with commensal bacteria (16, 28, 29). The colon mucus barrier provides a rich ecological niche for enteric microbial life and mediates cross-talk between the host immune system and microbiota. These mucus layers are composed primarily of the MUC2 mucin, the most abundantly

secreted mucin in the gastrointestinal (GI) tract and primary component of intestinal mucus (16, 123). Studies have shown that MUC2 deficiency leads to the spontaneous development of ulcerative colitis and colorectal tumors in mice (43, 44, 46, 124). This is due to the aberrant mucus properties that allow resident bacteria to increase in proximity towards or make direct contact with the colon epithelial surface. Further, inflammatory bowel diseases such as ulcerative colitis and Crohn's disease induce changes in both the quality and quantity of intestinal mucus (41, 125-128). For this reason, it is becoming increasingly important to develop an understanding of the microbiota spatial organization as it relates to intestinal immunomodulation and colonization dynamics. However, the effect of HFDs on intestinal mucus and microbiota localization remains largely understudied and absent regarding the influence of exercise; only recently have studies began to examine the impact of HFDs on mucus thickness and MUC2 biosynthesis (78, 92, 101) in a rodent model.

The purpose of this study was to investigate the influence of voluntary wheel running on colon mucosal inflammation and microbiota localization in mice fed normal and HFDs. Our hypotheses were as follows: (1) voluntary wheel running attenuates high-fat diet induced colon inflammation; (2) high-fat diets result in the localization of the microbiota closer to the epithelial surface but is rescued by voluntary wheel running.

Methods

Animals, Diet & Activity Status

All animals received humane care in compliance with the institution's guidelines, as outlined in the Guide for the Care and Use of Laboratory Animals published by the National Institutes of Health. Experiments were completed at Rutgers University and approved by the Rutgers University Institutional Animal Care and Use Committee (IACUC). Forty-eight C57BL/6NTac male and female 6-week old mice (Taconic Farms,

Germantown, NY) were housed singly in an environmentally controlled room with a 12 hour light/dark cycle and maintained on the specified diet and water *ad libitum*. Animals were acclimated for two weeks before being randomly assigned to one of four groups: (1) control diet sedentary (CD-S); (2) high-fat sedentary (HF-S); (3) control diet running (CD-R); and (4) high-fat running (HF-R). Control diet groups consumed a control low-fat diet (D12450H, 10% kcal from fat, Research Diets, New Brunswick, NJ) and high-fat groups consumed a high-fat diet (D12451, 45% kcal from fat, Research Diets) which are matched for sucrose and protein content (Table 2.1). Food intake was monitored twice per week and animals were weighed once per week. Specifically, males and females were weighed in separate containers assigned to each sex on a scale designated for body weights only. For food intake, average daily consumption for each treatment group was calculated by dividing total group consumption in grams (g) by the number of animals per group and then by the number of days in between feeding days for each week; g/day were then converted into kcals/day. Animals in the running group had access to a free running wheel while sedentary groups could move freely within their cages, but had no running wheel (Coulbourn Instruments, Allentown, PA). At the end of 12 weeks, animals were sacrificed. Female mice were sacrificed in the metestrus stage of their estrous cycle to ensure low plasma estrogen (E2) as E2 has shown to be a potent modulator of metabolic inflammation (129) and of the inflammatory status in experimental colitis models (130). Estrous cycle was assessed using wet smears on the day of sacrifice as outlined by Caligioni (131). All animals in the study were healthy for the duration of the study. Tissue analysis was performed as described below.

Histochemistry

Distal colon sections without fecal material were fixed overnight at room temperature in 3% paraformaldehyde and 2% sucrose and then embedded in paraffin. Distal colon sections containing fecal material were carefully excised, fixed overnight at

room temperature in methanol-Carnoy fixative (60% dry methanol, 30% chloroform, 10% glacial acetic acid) and embedded in paraffin as previously described (132). For histological analysis, 5 μm tissue cross-sections were stained with hematoxylin and eosin (H&E) (Research Pathology Services and Office of Translational Science at Rutgers University, Piscataway, NJ) or Alcian blue-Periodic Acid Schiff (AB/PAS) (Thermo Fisher Scientific, Waltham, MA) which stains both acidic and neutral mucins. For histomorphometric analysis, all tissue sections were blindly scored by a board-certified pathologist (Dr. Stanley Lightfoot).

Immunohistochemistry

For immunohistochemical studies, 5 μm paraffin-embedded tissue sections fixed in paraformaldehyde and sucrose were deparaffinized, rehydrated, quenched of endogenous peroxidases with 3% H_2O_2 in CH_3OH and subsequently blocked with 10% or 100% normal goat serum at room temperature for 1 or 2 hr. Tissue sections were then incubated overnight at 4°C with primary rabbit affinity purified polyclonal antibodies against cyclooxygenase-2 (COX-2) (1:500, Abcam, Cambridge, MA), mucin-2 (H-300) (1:500, Santa Cruz, Dallas, TX) or rabbit IgG as a negative control (ProSci Inc., Poway, CA). The tissue sections were then incubated for 30 min with a biotinylated goat anti-rabbit secondary antibody (Vector Labs, Burlingame, CA). Each slide represented one sample and contained 1-3 cross-sections for both the primary antibody and IgG control. Antibody binding was visualized using a Vectastain Elite ABC Kit and DAB Peroxidase Substrate Kit (both from Vector Labs). Sections were photographed using the VS120-S5 system (Olympus, Center Valley, PA). For histomorphometric analysis, all tissue sections were blindly scored by a board-certified pathologist (Dr. Stanley Lightfoot). Slide staining was reported using a dual number system (#X#). The first number is the intensity of the stain and the second number is the amount of stain present in the specimen. The intensity was graded on a scale of 0–3: 0, no staining; 1, minimal; 2,

moderate; 3, high. The amount was indicated as follows: 1, 1-25%; 2, 26-50%; 3, 51-70%; 4, 71-100%. Total score is the product of both numbers.

Immunofluorescence

Following hybridization, 5 µm tissue sections fixed in methanol-Carnoy were blocked with 10% normal goat serum at 4℃ for 1 hr. Tissue sections were then incubated overnight at 4℃ with the primary rabbit affinity purified polyclonal antibody mucin-2 (H-300) (1:500). Tissue sections were then incubated for 2 hr at 4 ℃ with an Alexa Fluor 488-conjugated goat anti-rabbit IgG secondary antibody. Slides were mounted with Prolong Gold antifade with DAPI (Thermo Fisher Scientific). Sections were photographed using the Leica DMLB fluorescent microscope (Leica Microsystems Inc., Buffalo Grove, IL).

Fluorescent In Situ Hybridization (FISH)

As previously outlined (132), 5 µm paraffin-embedded tissue sections fixed in methanol-Carnoy were deparaffinized and washed in 99.5% ethanol. Tissue sections were then incubated overnight with the dissolved (1 µg/µL) Alexa Fluor 555-conjugated universal bacterial probe EUB338 (5'-GCTGCCTCCCGTAGGAGT-3') (133) or with a nonsense probe (5'-CGACGGAGGGCATCCTCA-3') as a negative control (both from Thermo Fisher Scientific) in hybridization solution (1:100, 20 mM Tris-HCl, pH 7.4, 0.9 M NaCl, 0.1% SDS, 35% formamide) at 50°C. Sections were then briefly rinsed in FISH washing buffer (20 mM Tris-HCl, pH 7.4, 0.9 M NaCl) at 50°C. Co-immunostaining was performed thereafter with the mucin 2 (H-300) antibody as described above.

Counting of Goblet Cells

Goblet cells along the crypts and surface of the epithelium were counted from images (5.5x) of H&E stained sections. Three areas per section were examined (n=6 animals/group) and averaged. Goblet cell parameters for each sex were determined using CD-S controls in an arbitrary (450x450 pixels) square region of interest (ROI) as

previously described (134). Specifically, binary color threshold and particle size range were determined and kept constant. Number of goblet cells within the ROI were recorded. Total length and average width of mucosa analyzed in each ROI was recorded. ImageJ software was used for data acquisition.

Measuring Distance Between Microbiota and Mucosa

Multiple measurements (13-34) were taken from images of methanol-Carnoy-fixed colon sections hybridized with EUB338 as previously described (135). Each measurement was taken perpendicular to the mucosa and border of the microbiota as indicated by FISH with co-immunostaining against mucin-2; sections with clearly defined and intact mucus layers were chosen for analysis. Two sections per animal were examined (n=4 animals/group) and averaged. ImageJ software was used for data acquisition.

Statistical Analysis

All analyses were performed using IBM SPSS version 25 (IBM Corp., Armonk, NY). Group means of anthropometrics, food intakes, goblet cell counts, and distances were analyzed using a one-way ANOVA for each sex as well as a three-way ANOVA for comparisons between factors sex, diet type and activity status with Fisher's Least Significance Difference (LSD) post hoc tests. Body weight change overtime was analyzed using a mixed model design with repeated measures. A difference of mean with a p value of ≤ 0.05 was considered statistically significant.

Results

Body weights and caloric intake

In females, no significant differences in body weight were found between CD-S, CD-R and HF-R groups (Table 2.2). In contrast, HF-S female mice had significantly greater body weights compared to all treatment groups. Both CD-R and HF-R groups

consumed significantly more kcals per day compared to their sedentary counterparts (CD-S and HF-S) and HF-R animals had the highest caloric intake compared to all treatment groups (Table 2.3). Despite this increased caloric intake, the HF-R group maintained a lower body weight compared to HF-S counterparts (24.7g vs. 30.3g). Further, a significant difference of mean body weights between CD-S and HF-S groups was first observed at week 6 (Figure 2.1).

In males, no significant difference in body weights were found between control groups (CD-S vs. CD-R) and HF groups (HF-S vs. HF-R). HF-S and HF-R animals had significantly greater body weights compared to their control-diet counterparts (CD-S and CD-R) (Table 2.2). Further, no significant differences were found between male HF-R and HF-S as well as CD-R and CD-S groups. Like the females, both male ran groups consumed significantly more kcals per day compared to their sedentary counterparts. HF-R animals had the highest caloric intake compared to all treatment groups (Table 3). In contrast to females, no significant differences in food intake were found between CD-S and HF-S groups (Table 2.3). A significant difference of mean body weights between CD-S and HF-S groups was first observed at week 5 (Figure 2.1).

Univariate analysis showed a significant main effect of sex for body weight (p = 0.000) and food intake (p = 0.004), as well as for diet (p = 0.000; p = 0.000) and activity status (p = 0.002; p = 0.000). Pairwise comparisons showed that females significantly weighed less with a mean difference of -9.4 g and consumed less kcals with a mean difference of -0.90 kcals compared to males. For diet, CD animals weighed significantly less than HF animals with a mean difference of -5.0 g. Likewise, CD animals consumed significantly less than HF animals with a mean difference of -1.760 kcals. For activity status, ran animals weighed significantly less but consumed more than sedentary animals with mean differences of -3.452 g for body weight and 3.780 kcals for food intake. A significant main effect of time (p = 0.000) and sex (p = 0.000) for body weight

change over study duration was found, as well as a significant time x activity status x diet interaction (p = 0.052) which was rendered non-significant when including sex (p = 0.078) (Figure 2.1). This suggests that the observed changes in body weight over time were due to activity status and diet, independent of sex.

Colon morphology and mucin distribution

Histomorphometric analysis of H&E stained colon sections showed that gross morphology was normal regardless of treatment in both females and males (Figure 2.2). Likewise, histomorphometric analysis of AB/PAS stained colon sections showed no significant differences in PAS staining and the distribution of neutral and acidic mucins along the crypts remained similar across all treatment groups (Figure 2.2).

Inflammatory status and MUC2 protein expression

In females, HF-S animals showed the greatest expression of COX-2 (Figure 2.3 and tables: total score). Expression was reduced in HF-R and, to a greater degree, in CD-R animals similar to their CD-S counterparts. In males, COX-2 expression was also reduced in CD-R mice. In contrast, CD-S male mice had an increased expression compared to CD-S female mice and remained the same compared to their HF-S male counterparts (Figure 2.3). Further, COX-2 expression did not change in male HF-R mice.

Expectedly, all MUC2 protein expression was centralized within goblet cells (GCs) with varying differences between the epithelium and crypts (Figure 2.4A). Expression of MUC2 was moderate (Figure 2.4A and tables: intensity of stain) and did not differ between treatment groups or sex except for HF-X female mice who had a weakened MUC2 expression (Figure 2.4A and tables: intensity of stain). In comparison to males, a significant main effect of sex was found (p = 0.018) for GC counts with a mean difference of -16.0; no difference in GC counts in comparison to all other female treatment groups were found though a reduction in HF-R GCs compared to female CD-S mice did approach significance (p = 0.064) (Figure 2.4B).

Microbiota localization

Bacteria were confined to the outer mucus layer and none were found in contact with the epithelial surface (Figure 2.5A). No significant differences in distance between the epithelial surface and border of the microbiota were found between treatment groups or sex (Fig. 2.5B) and an average distance of 15 μm was found for all mice.

Discussion

The present work examined the effects of high-fat diets and voluntary wheel running to explore and provide a basis for further studies on elucidating the mechanisms behind the inflammatory response in the colon and microbiota localization. To our knowledge, we are the first to show sex differences regarding the effect of voluntary wheel running on HFD-induced colon inflammation. Our results indicate that: (1) high-fat diets and voluntary wheel running do not affect colon tissue morphology apart from HF-R female mice who displayed a reduction of GCs; (2) high-fat diets increase colon inflammation in both males and females but is rescued by voluntary wheel running in female mice; (3) microbiota localization does not appear to be influenced by a 45% HFD or voluntary wheel running; and (4) significant body weight differences occur at 6 and 5 weeks of high-fat feeding in female and males compared to control low-fat fed counterparts.

We have previously shown that animals fed a high-fat diet exhibit distinct changes in small intestinal morphology including thickened and crowded villi which corresponded with enhanced COX-2 expression (79); these effects were rescued with voluntary wheel running and/or a control low-fat diet. In the present study, similar patterns in inflammatory status were observed in the distal colon. Sedentary animals fed a high-fat diet displayed the most significant inflammation which was attenuated with voluntary wheel running in female mice only. Although recent studies show that high-fat

diets induce colonic inflammation (78) and can be rescued with voluntary aerobic exercise (116), it is interesting that this protective effect was not seen in HF-R males. Further, no significant differences in body weight were found when compared to male high-fat sedentary counterparts, which contrasts our previous findings in which voluntary wheel running attenuated weight gain in the presence of a high-fat diet (79). Likewise, control-diet sedentary male mice showed an increased inflammatory tone compared to female counterparts. Given that running volume was not quantified, it is difficult to ascertain the cause of this discrepancy. These findings raise several questions regarding the influence of cohort and sex differences as well as control diets and voluntary wheel running. The observations in female mice still lend support to the importance of physical exercise in promoting colon health as early findings have demonstrated the potent anti-inflammatory effects of exercise training in the colon mucosa (118). Recent evidence further suggests that aerobic exercise exerts inflammatory control through activation of IL-10 (119) and by modulation of peroxisome proliferator-activated receptor gamma (PPARγ) (116). For subsequent studies, testing for a correlation between IL-10 and mucin gene/protein expression in tandem with PPARγ will be considered. Based on these data, physical exercise may promote intestinal homeostasis and prevent the development of chronic inflammation in the colon through mucosal immune modulation. In the present study, inflammation was assessed using only immunohistochemical detection of COX-2, a key enzyme involved in the production of prostanoids via the metabolism of free arachidonic acid and is induced by pro-inflammatory stimuli (136). Further, COX-2 plays an important role in both colonic inflammation and tumorigenesis through the COX-2/PGE_2 proinflammatory pathway (137). Therefore, more rigorous analyses will be necessary to fully examine the inflammatory mucosal milieu.

Intestinal goblet cells are a key epithelial cell type that are responsible for the synthesis and secretion of intestinal mucus. These cells are regulated directly by the immune system, primarily through characteristic cytokines produced by T helper type 2 cells (6-8). Consequently, goblet cell depletion may be indicative of impairments in mucosal immune function. If this is so, it is interesting that HF-R female mice demonstrated a reduction of goblet cells that approached significance and of MUC2 expression despite having an attenuated inflammatory response. As described in a recent review (138), this finding may be attributed to the process of compound exocytosis in which goblet cells respond to sufficient stimuli with a dramatic release of mucus granulae, emptying the whole cell interior and exposing the cytoplasm (139). As a result, these goblet cells are not readily detectable. The mechanisms involved and whether voluntary wheel running or diet contributes to this process remains unclear. Thus, comparing the cytokine profile of male and female mice, specifically IL-13 which is a major effector cytokine responsible for regulating goblet cell hyperplasia and increasing mucin protein expression (9), will prove to be more revealing in future studies.

The organizational principles that govern mucus attachment and localization of the microbiota remain poorly understood. The inflammatory status of the intestine appears to respond to and regulate the proximity and identity of gut microbes closest to the epithelium (95, 140-142). Although our FISH results did not show any significant differences in distance between the border of the microbiota and surface of the epithelium, a study that has reported a thinner intestinal mucus layer used a 60% HFD (92). In the present study, we used a 45% HFD to promote translatability and to limit potential confounding due to complications associated with diabetes. These findings suggest that the degree of change in microbiota localization may be dependent on the severity of intestinal inflammation. The extent of diet-induced inflammation observed using a 45% HFD may not be sufficient to alter the physicochemical properties of

intestinal mucus. Moreover, an average thickness of 15 μm was found in the present study while the thickness of the colonic inner mucus layer in mice is approximately 50 μm on live tissue (31). This large difference may be largely due to the effects of fixation which shrinks the luminal contents and intestinal mucus. In addition, the cleanliness of an animal facility can influence mucus development and thickness.

A limitation of the present study is the relatively short feeding duration of 12 weeks as indicated by a lack of observed pathologies in colon tissue. These findings suggest that prolonged high-fat feeding interventions may be needed to observe greater disturbances in metabolic and colon health; a longer feeding duration would also promote a greater likelihood of differences in body mass. Recent studies have utilized chronic high-fat feeding protocols of 20 – 24 weeks (78, 143, 144) and will be implemented in subsequent studies. Another limitation lies in the fact that voluntary wheel running is akin to physical activity as opposed to regimented exercise (145) and significant differences in derived exercise capacity exist between the former and forced treadmill running (146). Though as it stands in exercise studies using animal models, striking a fine balance between motivation and undue stress is paramount. For example, forced treadmill running exacerbates colon inflammation in colitic mice while voluntary wheel running remains protective (147). Lastly, running volume was not quantified and it is well established that female mice run farther, as well as faster, when given access to a running wheel relative to males (148). Thus, it is possible that the observed differences in both colon inflammatory status and goblet cell counts in females may be due to greater daily running volume and intensity. Yet, the extent of training effects in skeletal muscle, as commonly assessed by citrate synthase assays or succinate dehydrogenase (SDH) staining, was not determined. Still however, this notion of sex differences in wheel running activity corroborates our findings and supports the efficacy of enhanced physical activity in promoting colon health.

In summary, our results support the anti-inflammatory effects of voluntary wheel running against high-fat diet-induced colon inflammation. Microbiota localization does not appear to be affected by a high-fat diet or voluntary wheel running. Taken together, these data suggest that physical activity may contribute to intestinal homeostasis through inflammatory control in the presence of a high-fat diet. We have shown that responses to changes in host behavior may differ between sexes and subsequently affect goblet cell production. However, the mechanisms by which physical activity and/or exercise improve colon health are poorly understood given the complexity of intestinal host-microorganism interactions. In this regard, research that examines the influence of physical activity and/or exercise on colon mucosal homeostasis as it relates to immunomodulation and intestinal epithelial cell function will be vital.

Acknowledgements

The authors would like to thank Dr. Malin E.V. Johansson (University of Gothenburg, Department of Medical Biochemistry and Cell Biology) for kindly providing help with optimizing our FISH protocol. The authors would also like to thank Dr. David Feigley (Rutgers University, Department of Kinesiology and Health) for providing help with statistics.

Author Contributions

Conceived and designed the experiments: SCC PJW. Performed the experiments: PJW, LBJ,GC, SCC. Analyzed the data: SCC PJW SAL. Contributed reagents/materials/analysis tools: SCC CG LBJ. Wrote the paper: PJW. Provided editorial input on the manuscript: SCC LBJ.

This research did not receive any specific grant from funding agencies in the public, commercial, or not-for-profit sectors.

Table 2.1. Composition of experimental diets (Research Diets, Inc.).

	Control Diet	**High-fat Diet**
	kcal%	
Protein	20	20
Carbohydrate	70	35
Fat	10	45
Total	100	100
kcal/g	3.85	4.73
Ingredients	**g/kg total**	
Casein, 30 Mesh	200	200
L-Cystine	3	3
Corn Starch	452.2	72.8
Maltodextrin 10	75	100
Sucrose	172.8	172.8
Cellulose	50	50
Soybean Oil	25	25
Lard	20	177.5
Mineral Mix S10026	10	10
DiCalcium Phosphate	13	13
Calcium Carbonate	5.5	5.5
Potassium Citrate, $1H_2O$	16.5	16.5
Vitamin Mix V10001	10	10
Choline Bitartrate	2	2
FD&C Yellow Dye #5	0.04	/
FD&C Red Dye #40	0.01	0.05

Table 2.2. Final body weights and percent weight change.

	CD-S	HF-S	CD-R	HF-R
FEMALES				
Body Weight (g)	23.0±3.1	30.3±4.5*	22.3±2.4	24.7±1.4
% Weight Increase	48.39%	93.62%	47.48%	60.87%
MALES				
Body Weight (g)	33.8±3.4	39.0±4.6*	29.6±2.3	35.0±6.1*
% Weight Increase	75%	100%	55.64%	82.61%

Body weights and percent weight change after 12 weeks of treatment with control diet sedentary (CD-S), high-fat diet sedentary (HF-S), control diet running (CD-R) and high-fat diet running (HF-R) in female and male mice. Values are expressed as the mean ± SD, n = 6 for each treatment group. One-way ANOVA with LSD post-test for CD-S vs HF-S; CD-S vs CD-R; CD-S vs HF-R, HF-S vs CD-R, HF-S vs HF-R, CD-R vs HF-R in both females and males. * $p < 0.05$ from all other treatment groups in females; from CD groups having the same activity status (sedentary or running) in males.

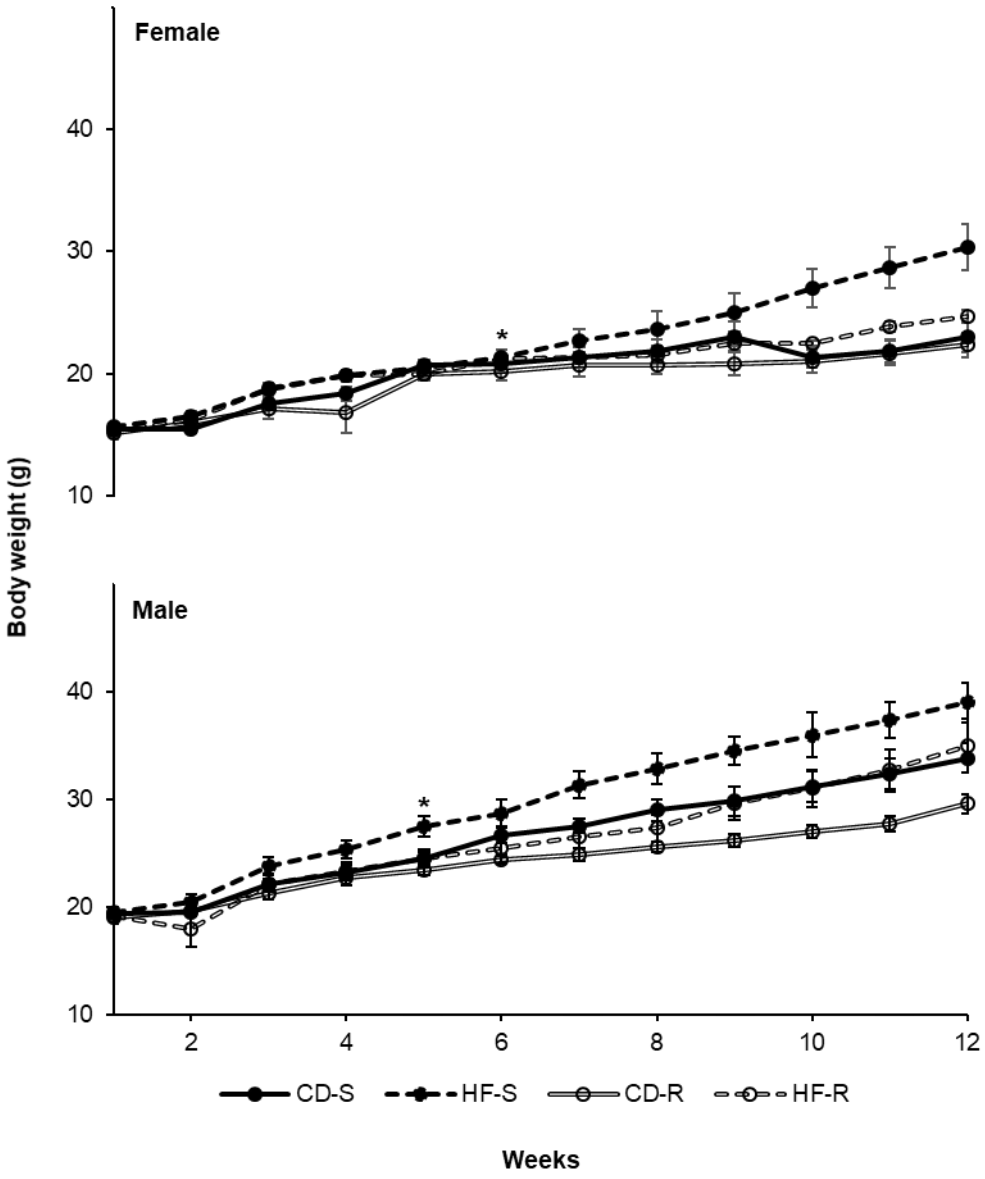

Figure 2.1. Body weight change over study duration. Body weights for each week during 12 weeks of treatment with control diet sedentary (CD-S), high-fat diet sedentary (HF-S), control diet running (CD-R) and high-fat diet running (HF-R) in female and male mice. Values are expressed as the mean ± SEM for each week, n = 6 for each treatment group. One-way ANOVA with LSD post-test for CD-S vs HF-S; CD-S vs CD-X; CD-S vs HF-X; HF-S vs CD-X; HF-S vs HF-X and CD-X vs HF-X for each sex at each week. * $p < 0.05$ for CD-S vs HF-S when first observed.

Table 2.3. Average kcals per day consumed over study duration.

	CD-S	HF-S	CD-R	HF-R
FEMALES				
Kcal/day	10.90±1.63*	12.68±1.95*	14.62±1.96*	16.50±2.34*
MALES				
Kcal/day	12.10±1.53+	13.22±1.87*	15.32±2.17*	17.58±2.10*

Average daily food intake over 12 weeks of treatment with control diet sedentary (CD-S), high-fat diet sedentary (HF-S), control diet running (CD-R) and high-fat diet running (HF-R) in female and male mice. Values are expressed as the mean ± SD, n = 6 for each treatment group. One-way ANOVA with LSD post-test for CD-S vs HF-S; CD-S vs CD-R; CD-S vs HF-R, HF-S vs CD-R, HF-S vs HF-R, CD-R vs HF-R in both females and males. * $p < 0.05$ from each other in females and males. + $p > 0.05$ from exercised groups in males.

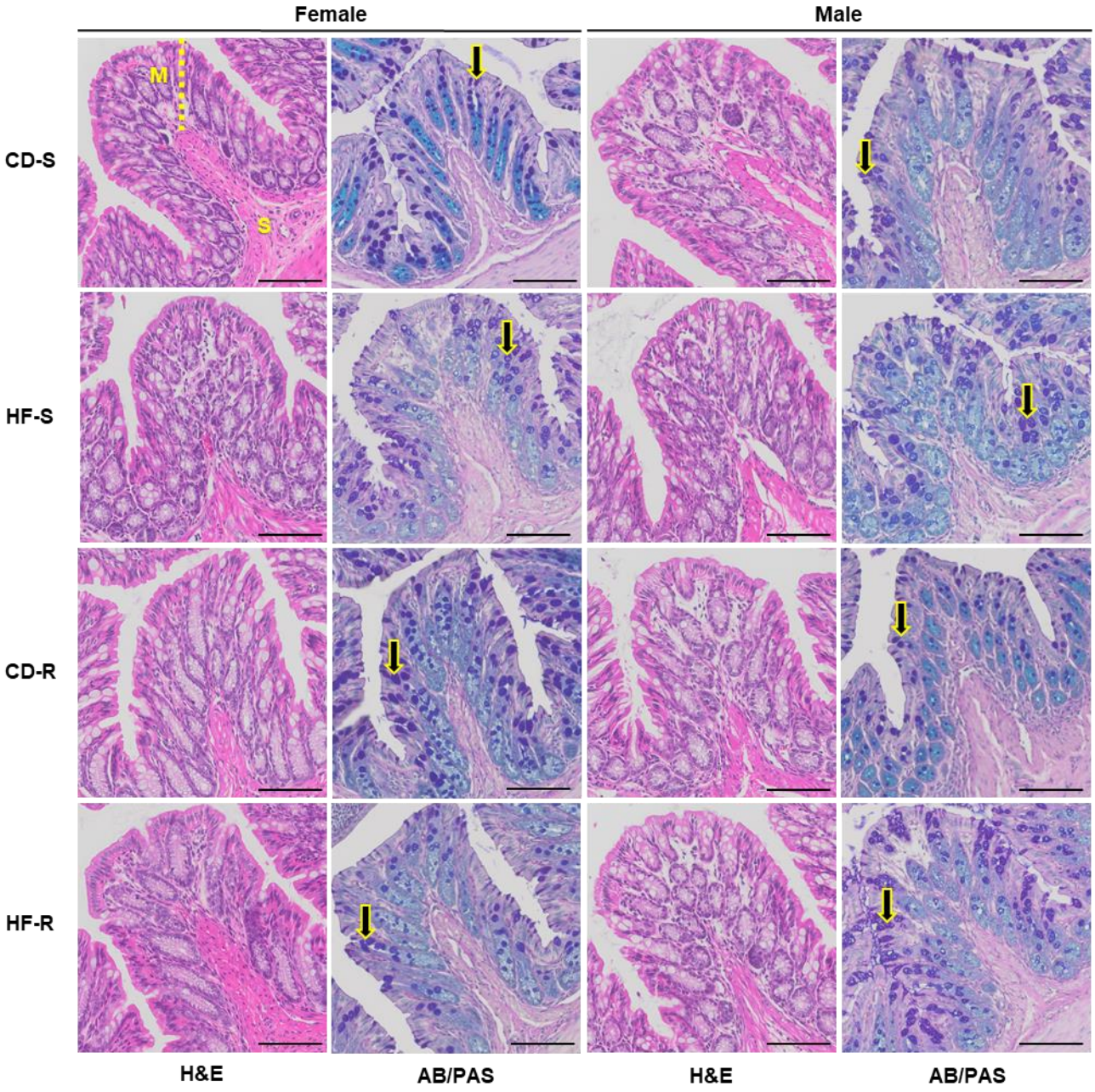

Figure 2.2. Effects of diet and voluntary wheel running on distal colon morphology and epithelial mucins. Histological sections fixed in paraformaldehyde and sucrose prepared after 12 weeks of treatment with control diet sedentary (CD-S), high-fat diet sedentary (HF-S), control diet running (CD-R) and high-fat diet running (HF-R) from female and male mice were stained with H&E or Alcian Blue/Periodic Acid-Schiff (AB/PAS). One representative section from 6 mice/treatment group for H&E and from 4 mice/treatment group for AB/PAS is shown (original magnification x 400; scale bars are 100 μm). Arrow, goblet cells; S, submucosa; M and dotted line, mucosa.

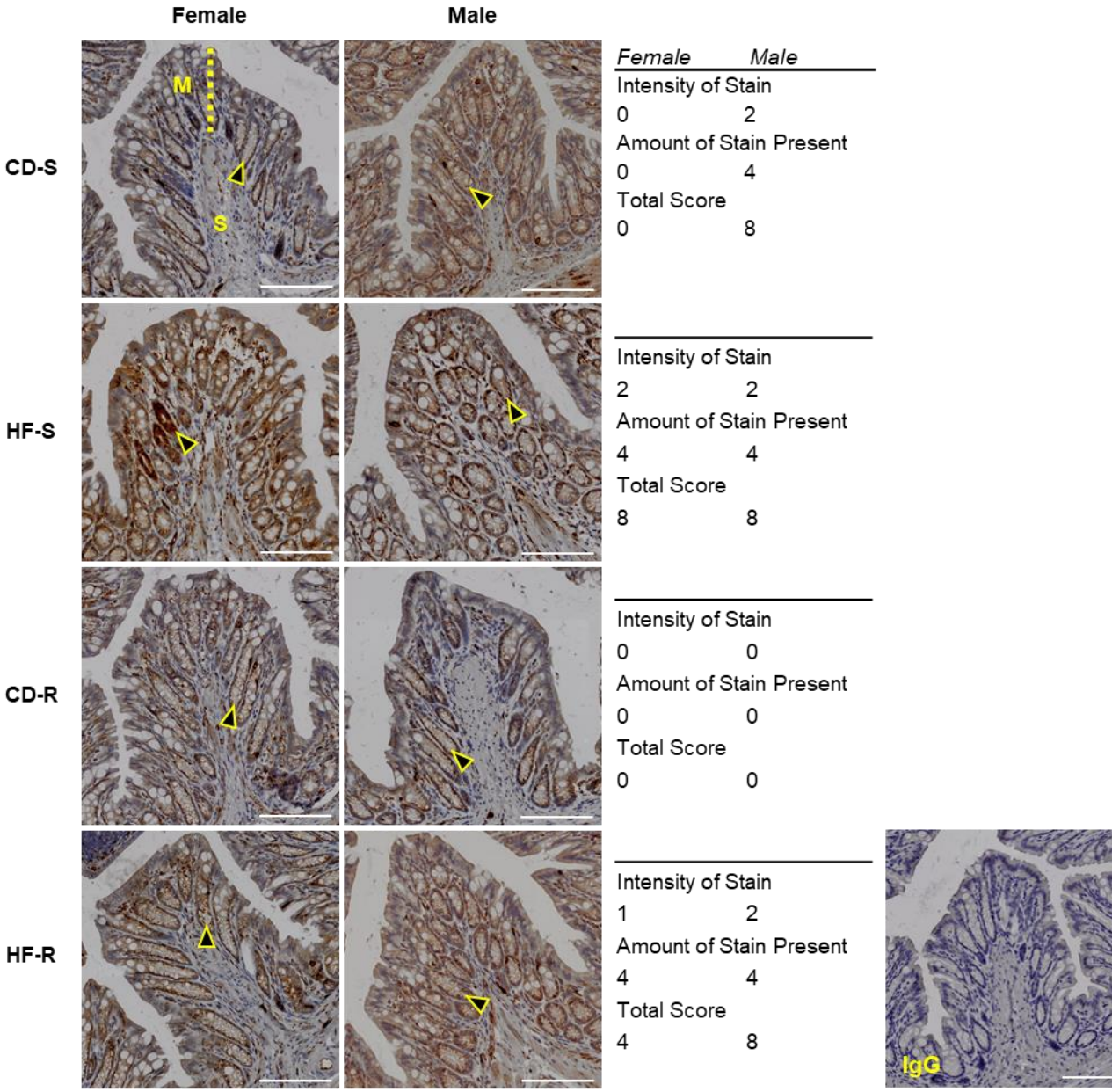

Figure 2.3. Effects of diet and voluntary wheel running on COX-2 expression in distal colon. Histological sections fixed in paraformaldehyde and sucrose prepared after 12 weeks of treatment with control diet sedentary (CD-S), high-fat diet sedentary (HF-S), control diet running (CD-R) and high-fat diet running (HF-R) from female and male mice were stained with an antibody for COX-2. One representative section from 4 mice/treatment group is shown (original magnification x 400; scale bars are 100 μm). An IgG negative control was used for immunohistochemical studies; one representative section is shown for all treatment groups and sexes. Table shows average scoring in both the epithelium and crypts combined for COX-2 expression. Slide staining is reported using a dual number system. The first number is the intensity of the stain and the second number is the amount of stain present in the specimen. The intensity is

graded on a scale of 0–3: 0, no staining; 1, minimal; 2, moderate; 3, high. The amount is indicated as follows: 1, 1-25%; 2, 26-50%; 3, 51-70%; 4, 71-100%. Total score is the product of both numbers. Arrowhead, base of colonic crypts; S, submucosa; M and dotted line, mucosa.

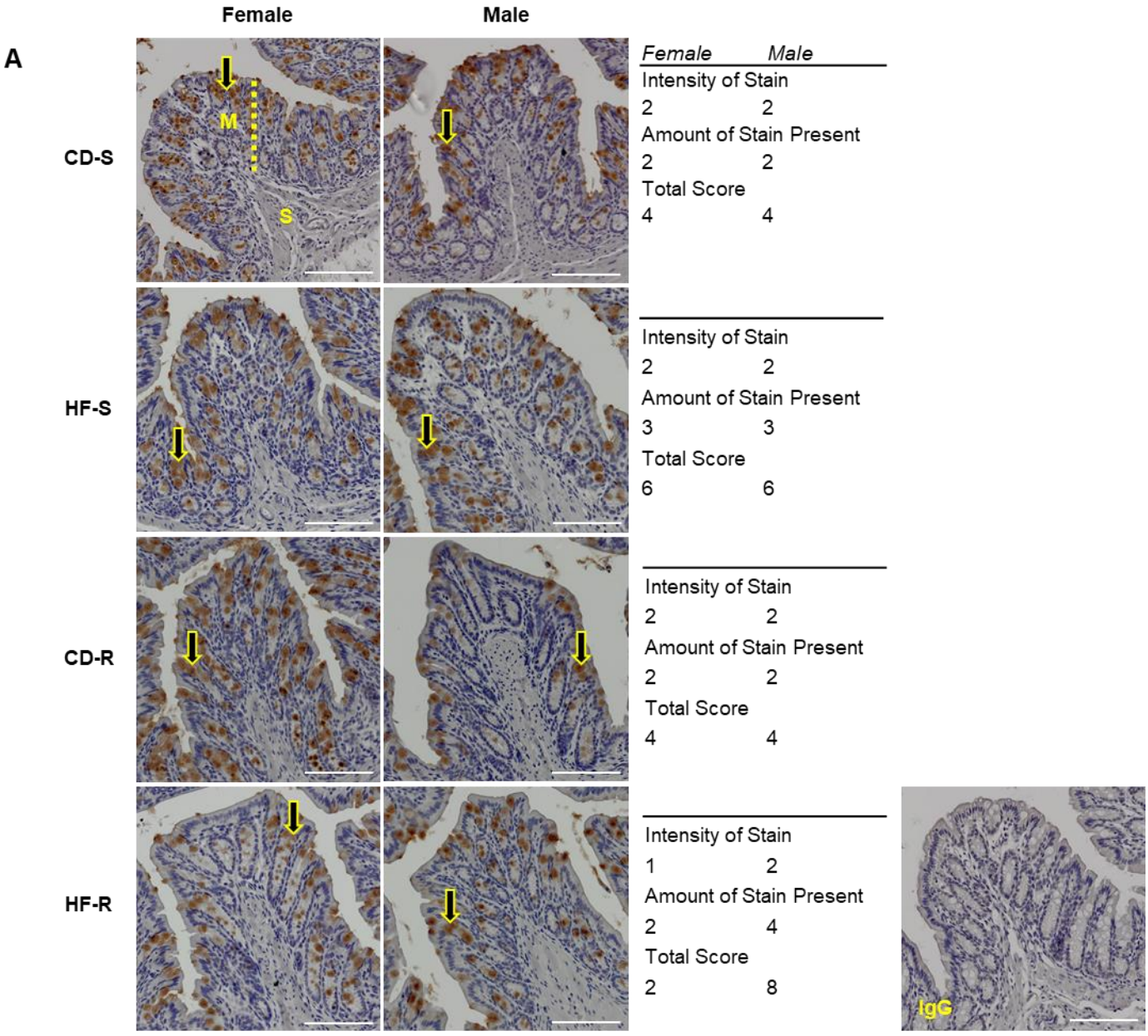
A
Female
Male
CD-S
HF-S
CD-R
HF-R
M
S
Female Male
Intensity of Stain
2 2
Amount of Stain Present
2 2
Total Score
4 4
Intensity of Stain
2 2
Amount of Stain Present
3 3
Total Score
6 6
Intensity of Stain
2 2
Amount of Stain Present
2 2
Total Score
4 4
Intensity of Stain
1 2
Amount of Stain Present
2 4
Total Score
2 8
IgG

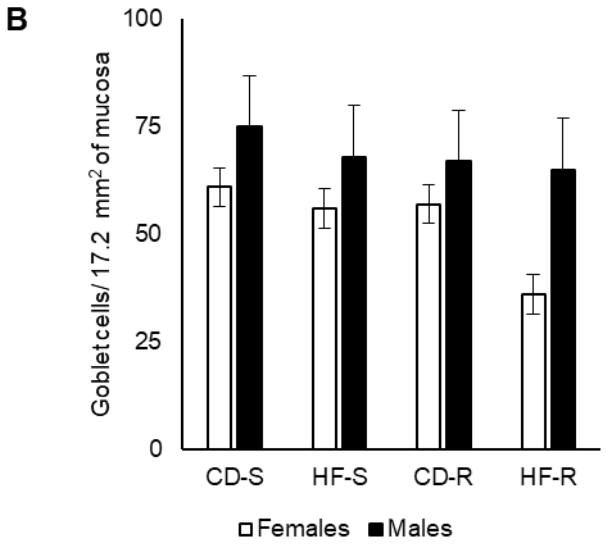

Figure 2.4. Effects of diet and voluntary wheel running on MUC2 expression in distal colon and goblet cell number. A. Histological sections fixed in paraformaldehyde and sucrose prepared after 12 weeks of treatment with control diet sedentary (CD-S), high-fat diet sedentary (HF-S), control diet running (CD-R) and high-fat diet running (HF-R) from female and male mice were stained with an antibody for MUC2. One representative section from 4 mice/treatment group is shown (original magnification x 400; scale bars are 100 μm). An IgG negative control was used for immunohistochemical studies; one representative section is shown for all treatment groups and sexes. **B.** Graph: goblet cell counts in each treatment group for each sex (means ± SEM, n = 6 mice/group). One-way ANOVA with LSD post-test for CD-S vs HF-S; CD-S vs CD-X; CD-S vs HF-X, HF-S vs CDX, HF-S vs HF-X, CD-X vs HF-X in both females and males. Table shows average scoring in both the epithelium and crypts combined for MUC2 expression. Slide staining is reported using a dual number system. The first number is the intensity of the stain and the second number is the amount of stain present in the specimen. The intensity is graded on a scale of 0–3: 0, no staining; 1, minimal; 2, moderate; 3, high. The amount is indicated as follows: 1, 1-25%; 2, 26-50%; 3, 51-70%; 4, 71-100%. Total score is the product of both numbers. Arrow, goblet cells; S, submucosa; M and dotted line, mucosa; asterisk, lumen.

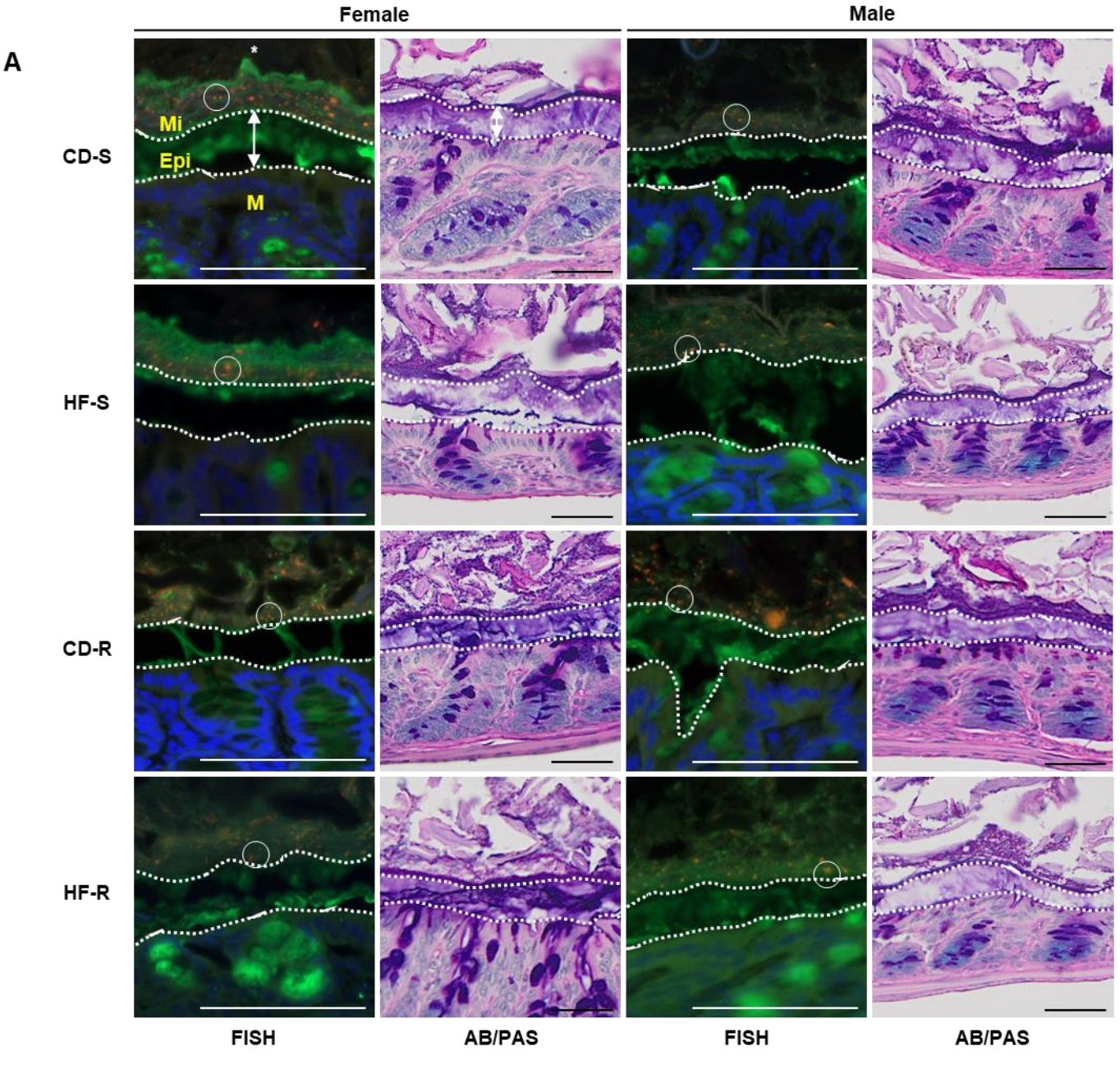
A
Female
Male
CD-S
HF-S
CD-R
HF-R
Mi
Epi
M
FISH
AB/PAS
FISH
AB/PAS

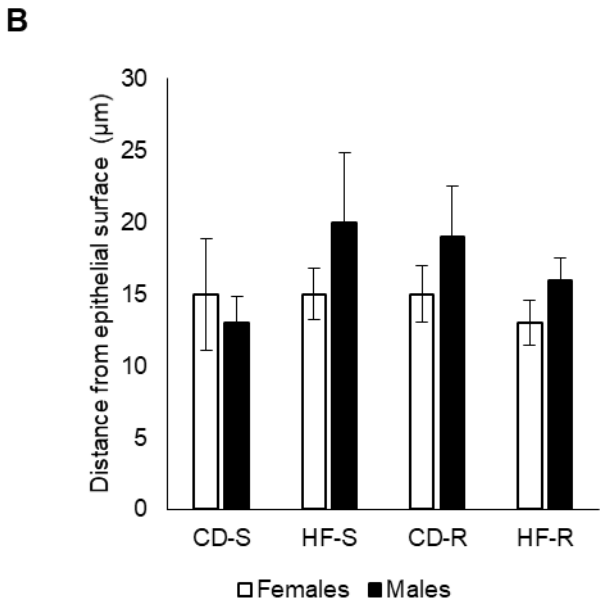

Figure 2.5. Effects of diet and voluntary wheel running on microbiota localization. **A.** Methanol-Carnoy fixed sections prepared after 12 weeks of treatment with control diet sedentary (CD-S), high-fat diet sedentary (HF-S), control diet running (CD-R) and high-fat diet running (HF-R) from female and male mice were hybridized with the Alexa Fluor 555-conjugated universal bacterial probe (EUB338) or with a nonsense (NS) probe or stained with AB/PAS. One representative section from 4 mice/treatment group is shown (original magnification x 400 for FISH and x 200 for AB/PAS; scale bars are 50 µm). White dotted lines; boundary of microbiota (Mi) and epithelial surface (Epi); double-sided arrow, distance measured; open circle, bacteria; M, mucosa; asterisk, lumen. **B.** Graph: distance between border of microbiota and epithelial surface (means ± SEM, n = 4 mice/group). One-way ANOVA with LSD post-test for CD-S vs HF-S; CD-S vs CD-X; CD-S vs HF-X, HF-S vs CDX, HF-S vs HF-X, CD-X vs HF-X in both females and males.

Chapter 3: High-fat diets and Voluntary Wheel Running Modulate Colon Inflammation and Endoplasmic Reticulum Stress

Introduction

Aberrant colon mucus properties and chronic low-grade mucosal inflammation are hallmark pathologies of chronic inflammatory bowel disease (IBD) (122). Evidence suggests that diets high in total fats are a risk factor for the development of IBD (149) , while long-term participation in aerobic exercise has shown to significantly reduce the risk thereof (107-109). There is growing evidence supporting the role of endoplasmic reticulum stress (ER) in disease and the failure to resolve this response as key components in the pathology of IBD. Given the potent anti-inflammatory effects of physical exercise, it is plausible that exercise may rescue HFD-induced ER stress. Thus, the present study examined the extent to which exercise and HFDs modulate the physical characteristics of intestinal mucus as well as colon inflammation and ER stress in male and female C57BL/6NTac mice.

Maintenance of intestinal homeostasis is essential for minimizing the adverse health effects of intestinal microorganisms, especially during environmental perturbations (5) such as changes in host behavior (i.e., diet and exercise). This is achieved through specialized immune adaptations that contribute to microbe-host mutualism by limiting bacterial invasion and mucosal inflammation (5). In the colon where the bacterial load is greatest, the primary physical defense limiting microbe-epithelial cell contact is a dual-layered mucus barrier; the primary component of this mucus barrier is the muc2 mucin, an *O*-linked glycoprotein produced by intestinal goblet cells (31). Folding and extensive post-translational modification of the muc2 protein occurs in the ER-golgi secretory pathway (31) and are critical for enabling the functional properties of mucins. The inherent complexity of mucin synthesis and high secretory output makes muc2 particularly prone to misfolding which activates the unfolded protein response (UPR) to resolve the protein folding defect and restore ER homeostasis (49).

Failure to resolve these defects results in the accumulation of unfolded and misfolded proteins in the ER lumen, defined as ER stress. ER stress and aberrant mucus properties have been implicated in the pathogenesis of UC (95, 97) and CD (127, 150). HFDs have recently shown to not only increase colon inflammation and ER stress (78), but also deteriorate colonic mucus as well (93). In addition, the UPR has been investigated as potential therapeutic target for colon cancer treatment (151-153). In this context, HFD-induced colon inflammation may be a contributing factor towards intestinal immune irregularities akin to UC and CD, which may also result in colon cancer development.

In contrast to HFDs, physical exercise has shown to ameliorate symptoms associated with IBD and significantly reduce the risk of colorectal cancer (CRC) development (107-110). Although the mechanisms by which exercise improves colon health are poorly understood, recent evidence suggests that aerobic exercise exerts anti-inflammatory control through activation of interleukin (IL)-10 (119). Of note is the finding that IL-10 is critical for colonic protection as it can act directly on goblet cells to reduce protein misfolding and ER stress as well as promote mucus barrier function (120). The influence of physical exercise on intestinal ER stress responses and epithelial cell function remains well understudied.

In these studies, we sought to replicate aim 1 using a 60% HFD and examine the expression of molecular targets involved in ER stress responses. Our hypotheses are as follows: (1) a 60% HFD results in the gut microbiota localizing closer to epithelial surface due to a thinner inner mucus layer but is prevented with voluntary wheel running; (2) voluntary wheel running increases IL-10 production concomitantly with a reduction of mucosal inflammation; (3) voluntary wheel running attenuates HFD-induced upregulation of UPR gene expression.

Methods

Animals, Diets and Activity Status

All animals received humane care in compliance with the IACUC guidelines, as outlined in the Guide for the Care and Use of Laboratory Animals published by the National Institutes of Health. Experiments were completed at Rutgers University and approved by the Rutgers University Institutional Animal Care and Use Committee (IACUC). Forty-Eight C57BL/6NTac male and female 6-week old mice (Taconic Farms, Germantown, NY) were housed singly in an environmentally controlled room with a 12 hour light/dark cycle and maintained on the specified diet and water *ad libitum*. Animals were acclimated for two weeks before being randomly assigned to one of four groups: (1) control diet sedentary (CDS); (2) very high-fat sedentary (VHFS); (3) control diet exercise (CDX); and (4) very high-fat exercise (VHFX). Control diet groups consumed a control low-fat diet (D12450J, 10% kcal from fat, Research Diets, New Brunswick, NJ) and very high-fat groups consumed a high-fat diet (D12492, 60% kcal from fat, Research Diets) which are matched for sucrose, dietary fiber and protein content (Table 3.1). Food intake was monitored twice per week and animals were weighed once per week. Specifically, males and females were weighed in separate containers assigned to each sex on a scale designated for body weights only. For food intake, average daily consumption for each treatment group was calculated by dividing total group consumption in grams (g) by the number of animals per group and then by the number of days in between feeding days for each week; g/day were then converted into kcals/day. Animals in the exercise groups had access to a free running wheel while sedentary groups could move freely within their cages, with no running wheel (Coulbourn Instruments, Allentown, PA). Physical activity was quantified daily using ClockLab (Actimetrics, Wilmette, IL). Rotations per day were converted into distance ran in meters per day by multiplying by running wheel circumference. At the end of 12

weeks, animals were sacrificed. Female mice were sacrificed in the metestrus stage of their estrous cycle to ensure low plasma estrogen (E2) as E2 has shown to be a potent modulator of metabolic inflammation (129) and of the inflammatory status in experimental colitis models (130). Estrous cycle was assessed using wet smears on the day of sacrifice as outlined by Caligioni (131). All animals in the study were healthy for the duration of the study. Just prior to sacrifice however, 8 females and 4 males died due to a malfunctioning metabolic chamber and 2 additional females died from an oral glucose tolerance test resulting in an n of 1 for CDS females, an n of 2 for VHFS females and an n of 3 for CDS males.

Histochemistry

Distal colon sections without fecal material were fixed overnight at room temperature in 3% paraformaldehyde and 2% sucrose and then embedded in paraffin. Distal colon sections containing fecal material were carefully excised, fixed overnight at room temperature in methanol-Carnoy fixative (60% dry methanol, 30% chloroform, 10% glacial acetic acid) and embedded in paraffin as previously described (132) for mucus thickness measurements. Remaining colon tissue was washed of fecal contents with cold 1x PBS and then snap frozen in liquid nitrogen or fixed in RNAlater at 4°C for 24 hrs and then stored in -80°C (Thermo Fisher Scientific, Waltham, MA). For histological analysis, 5 µm tissue cross-sections were stained with hematoxylin and eosin (H&E) (Research Pathology Services and Office of Translational Science at Rutgers University, Piscataway, NJ) or Alcian blue-Periodic Acid Schiff (AB/PAS) (Thermo Fisher Scientific) which stains both acidic and neutral mucins.

Immunohistochemistry

For immunohistochemical studies, 5 µm paraffin-embedded tissue sections were deparaffinized, rehydrated, quenched of endogenous peroxidases with 3% H_2O_2 in CH_3OH and subsequently blocked with 10% - 100% normal goat serum at room

temperature for 1 – 2 hr. Tissue sections were then be incubated overnight at 4°C with primary rabbit affinity purified polyclonal antibodies against cyclooxygenase-2 (COX-2) (1:500, Abcam, Cambridge, MA), mucin-2 (H-300) (1:500, Santa Cruz, Dallas, TX), F4/80, proliferating cell nuclear antigen (PCNA) or rabbit IgG as a negative control (ProSci Inc., Poway, CA). The tissue sections were then incubated for 30 min with a biotinylated goat anti-rabbit secondary antibody (Vector Labs, Burlingame, CA). Antibody binding was visualized using a Vectastain Elite ABC Kit and DAB Peroxidase Substrate Kit (both from Vector Labs). Sections were photographed using the VS120-S5 system (Olympus, Center Valley, PA).

Immunofluorescence

Following hybridization, 5 µm tissue sections fixed in methanol-Carnoy were blocked with 10% normal goat serum at 4℃ for 1 hr. Tissue sections were then incubated overnight at 4℃ with the primary rabbit affinity purified polyclonal antibody mucin-2 (H-300) (1:500). Tissue sections were then be incubated for 2 hr at 4 ℃ with an Alexa Fluor 488-conjugated goat anti-rabbit IgG secondary antibody. Slides were mounted with Prolong Gold antifade with DAPI (Thermo Fisher Scientific). Sections were photographed using the Leica DMLB fluorescent microscope (Leica Microsystems Inc., Buffalo Grove, IL).

Fluorescent In Situ Hybridization (FISH)

As previously outlined (132), 5 µm paraffin-embedded tissue sections fixed in methanol-Carnoy were deparaffinized and washed in 99.5% ethanol. Tissue sections were then incubated overnight with the dissolved (1 µg/µL) Alexa Fluor 555-conjugated universal bacterial probe EUB338 (5’-GCTGCCTCCCGTAGGAGT-3’) (133) or with a nonsense probe (5’-CGACGGAGGGCATCCTCA-3’) as a negative control (both from Thermo Fisher Scientific) in hybridization solution (1:100, 20 mM Tris-HCl, pH 7.4, 0.9 M NaCl, 0.1% SDS, 25% formamide) at 50°C. Sections were then briefly rinsed in FISH

washing buffer (20 mM Tris-HCl, pH 7.4, 0.9 M NaCl) at 50°C. Co-immunostaining was performed thereafter with the mucin 2 (H-300) antibody as described above.

Methods of Counting of Stained Sections and Scoring

Only U shaped crypts, with the base of the crypt touching the muscularis mucosae and its axis extending to the apical surface, were evaluated for proliferation index and goblet cell density. Proliferation index was defined as the ratio of PCNA stained nuclei to total nuclei measured for each crypt, a proxy for crypt height, as previously described (154). Likewise, goblet cell density was expressed as the ratio of muc2 stained goblet cells to total nuclei. Based on the 'running average' (155) data from two animal subjects pulled at random, we could show that 15 crypts were sufficient to determine a reliable proliferation index, total nuclei count and muc2 positive stained cell count (Figure 3.1). F4/80 positive cell counts were assessed across three sections per animal and were expressed relative to total area of mucosa measured using an arbitrary square region of interest (ROI) which was kept constant; ImageJ software was used for area measurements. PCNA positive nuclei, total nuclei, muc2 positive goblet cells and F4/80 positive cells were counted manually using a cell counter (Fisher Scientific, Waltham, Massachusetts) from images of stained sections (400x).

Measuring Inner Mucus Layer Thickness

Multiple measurements (27-80) were manually taken from images of methanol-Carnoy-fixed colon sections hybridized with EUB338 as previously described (135). Each measurement was taken perpendicular to the mucosa and border of the microbiota as indicated by FISH with co-immunostaining with muc2; sections with clearly defined and intact mucus layers were chosen for analysis. Two to three sections per animal were examined and averaged. ImageJ software was used for data acquisition.

Western Blot Analysis

Frozen colon samples (20 – 80 mg) were grinded by mortar and pestle in liquid nitrogen and homogenized mechanically in RIPA lysis buffer supplemented with protease and phosphatase inhibitor cocktails (Thermo Fisher Scientific). Samples were then centrifuged at 15,000 x g for 15 min at 4°C. Supernatants were aliquoted and frozen at -80°C until assay. Initial protein quantification of colon lysates was performed using a bicinchoninic acid (BCA) assay (Thermo Fisher Scientific). Equal amounts of protein (25 µg per lane) were loaded and separated by SDS-PAGE. Gels were then transferred to a nitrocellulose membrane using the Mini Gel Tank and Blot Module system (Thermo Fisher Scientific). Membranes were stained for total protein by Ponceau S staining solution (0.5% Ponceau S (w/v), 1% glacial acetic acid (v/v)), rinsed with deionized H_2O and then blocked with 5% (w/v) nonfat dried milk or bovine serum albumin (BSA) in 0.1% (v/v) Tween 20 Tris-buffered saline (TTBS) for 1hr at room temperature. Membranes were then incubated overnight at 4°C with primary rabbit affinity purified monoclonal antibodies (Cell Signaling, Danvers, MA) against phosphorylated eukaryotic initiation factor-2 (p-eIF2α) (1:500), eIF2α (1:1000), NFκB (1:1000), β-actin (1:1000) or muc2 (Thermo Fisher Scientific, 1:1000) in 5% BSA in 0.1% TTBS. Membranes were then incubated for 1 hr at room temperature with a horseradish peroxidase goat anti-rabbit secondary antibody (1:5,000 – 1:10,000, Cell Signaling). Membranes were developed using an enhanced chemiluminescence (ECL) detection kit (Thermo Fisher Scientific) and images were taken thereafter. Densitometric analysis of protein bands was performed using Image Studio Lite 5.2 (LI-COR Biosciences, Lincoln, NE) and normalized to β-actin or total protein. The results are expressed as arbitrary units. Precision Plus Protein™ Kaleidoscope™ Prestained Protein Standard (Bio-Rad, Hercules, CA) was used as a molecular weight standard.

Gene Expression Analysis

RNA was isolated from frozen colon tissue fixed in RNA*later* (Thermo Fisher Scientific) and purified using a RNeasy RNA purification kit (Qiagen, Venlo, Netherlands). RNA concentration and purity were determined by use of the Nanodrop 1000 Spectrophotometer (Thermo Fisher Scientific), followed by cDNA synthesis using 0.5 µg of RNA and the First Strand Kit (Qiagen) according to manufacturer's instructions. The expression of genes of interest were analyzed using quantitative real time-PCR (qRT-PCR) for a custom RT^2 PCR array (Qiagen) using the QuantStudio 3 PCR System (Applied Biosystems) and RT^2 SYBR Green ROX qPCR Mastermix (Qiagen). Ct values were generated and normalized to GAPDH and expressed relative to CDS groups using the $\Delta\Delta$Ct method.

Quantification of IL-10

Diluted colon lysates (1:10) were assessed for IL-10 concentration using an enzyme-linked immunosorbent assay (ELISA) (Thermo Fisher Scientific). All biological replicates were ran in duplicate.

Statistical Analysis

All analyses were performed using IBM SPSS version 25 (IBM Corp., Armonk, NY). Group means of experimental outcomes were analyzed using a one-way ANOVA for each sex with Tukey's post hoc tests as well as a three-way ANOVA for comparisons between factors sex, diet and activity status. Pre and post lean and fat mass were assessed using paired sample t tests for each treatment group. Body weight change overtime was analyzed using a mixed model design with repeated measures. A difference of mean with a p value of ≤ 0.05 was considered statistically significant.

Results

Body composition and caloric Intake

High-fat fed groups in both males and females had significantly greater bodyweights relative to their control diet counterparts (Table 3.2). In addition, VHFX mice had significantly reduced body weights compared to their VHFS counterparts. Surprisingly, while males exhibited a 111.5% weight increase over the study duration, females demonstrated a marked 154.8% increase in body weight (Table 3.2).

Univariate analysis showed a significant main effect of activity status, diet and sex for body weight (Table 3.4) as well as a significant activity status x diet interaction. Pairwise comparisons indicated that sedentary mice weighed more than exercised groups with a mean difference of 5.9 g; mice fed the control diet weighed less than high-fat fed groups with a mean difference of -12.6 g; and that female mice weighed less than males with a mean difference of -4.9 g. A significant main effect of time and sex for body weight change over study duration was found, as well as a significant time x activity status x diet interaction which was rendered non-significant when including sex (p = 0.245) (Figure 3.2). Further, the most marked differences in body weight change over time were observed in sedentary male and female mice fed a high-fat diet and this trend was significantly attenuated with exercise.

In agreement with the above findings, both males and female VHFX mice had significantly less fat mass compared to VHFS mice (Table 3.2) whereas VHFS groups displayed the greatest fat mass compared to all other treatment groups. In contrast to females, male CDS mice had significantly greater fat mass relative to their CDX counterparts. In females, a significant difference in fat mass between CDX and VHFX mice was not observed. A significant difference between CDX and VHFX in fat mass was observed in males, however. In females, both high-fat fed groups showed a significant increase in fat mass in comparison to their corresponding pre-study values

(Figure 3.3). The same observation was seen males with the additional finding that post-study fat mass was elevated in CDS animals compared to their pre-study values. Univariate analysis showed a significant main effect of sex for pre-study fat mass values as well as a significant main effect of activity status, of diet and a significant activity status x diet interaction for post-study fat mass values (Table 3.4). Pairwise comparisons concluded that female mice had a greater but modest amount of fat mass prior to the beginning of the study compared to males with a mean difference of 0.383 g. At the end of the study, pairwise comparisons indicated that sedentary mice had significantly greater fat mass compared to exercised counterparts with a mean difference of 5.3 g whereas mice fed a control diet had significantly less fat mass compared to high-fat fed mice with a mean difference of -10.1g (Table 3.4).

In both females and males, CDS mice consumed significantly less kcals/day compared to all other treatment groups (Table 3.3). VHFX mice consumed more kcals per day compared to their CDX counterparts. No significant differences between VHFS and exercised groups were observed, however. Univariate analysis showed a significant main effect of activity status and diet for average caloric intake over study duration (Table 3.4). Pairwise comparisons showed that sedentary mice and mice fed the control diet consume significantly less kcals per day compared to exercised and high-fat fed counterparts with mean differences of -2.7 kcal/d and -3.5 kcal/d. No significant differences in kcals per day were observed between male and female mice ($p = 0.898$). Lastly, significant activity status x diet and diet x sex interactions were found.

Morphological characteristics of colon and intestinal mucus

In males, a non-significant increase in inner mucus layer thickness was observed in VHFS mice compared to CDS ($p = 0.071$) (Figure 3.4, A). A significant increase was observed in VHFS mice compared to CDX mice (Figure 3.4, A). Interestingly, a modest but non-significant increase was also observed in VHFX mice compared to CDS and

CDX mice (p = 0.534, p = 0.347). Although no significant differences in inner mucus layer thickness were observed in female mice between treatment groups, significant diet x sex and activity status x diet x sex interactions were found (Table 3.5). For goblet cell density (Figure 3.4, B), both male CDX and VHFX mice showed a significant reduction compared to VHFS counterparts while no significant differences were observed in female mice. Further, a significant main effect of activity status and sex was found for goblet cell density as well a significant activity status x diet x sex interaction and a diet x sex interaction that approached significance (p = 0.066) (Table 3.5). No significant differences were found in male or female mice for total nuclei per crypt between treatment groups (Figure. 3.4, C); however, a significant main effect of sex and a modest decrease in total nuclei per crypt (-2.9 nuclei) was observed in female mice compared to males (Table 3.5).

In parallel to the above findings of inner mucus layer thickness, non-significant but modest increases in muc2 protein expression were observed in VHFS and VHFX male mice compared to CDS and CDX counterparts (p = 0.369, p = 0.805) (Figure 3.5). No significant differences in mu2 protein expression were observed in female mice. In contrast, non-significant increases in muc2 relative gene expression were observed in CDX and VHFX female mice (p = 0.069, p = 0.111) compared to VHFS counterparts demonstrating a 2.3 and 2.2 mRNA fold change (Figure 3.5); no significant differences in the relative gene expression of muc2 were found in male mice.

Colon inflammation and proliferation status

COX-2 expression was reduced in both male and female CDX and VHFX mice compared to VHFS counterparts (Figure 3.6). In contrast to females, in which a reduction of COX-2 expression was observed in CDS mice, male CDS mice demonstrated an increased COX-2 expression like that of VHFS counterparts. Further,

male VHFS and VHFX mice demonstrated a non-significant increase in the protein expression of NFκB compared to CDS (p = 0.369) and CDX (p = 0.805) counterparts (Figure 3.7, A); no significant differences were observed in the relative gene expression of NFκB, however (Figure 3.7, B). In contrast, female CDX and VHFX mice demonstrated a stark and significant increase in the relative gene expression of NFκB compared to VHFS counterparts demonstrating a 13.6 and 17.6 mRNA fold change; no significant differences were observed in total protein of NFκB.

Assessment of F4/80+ macrophages demonstrated a significant reduction in immunoreactive cells in female VHFX mice as well as in VHFS mice which approached significance (p = 0.057) compared to CDX counterparts (Figure 3.8). In contrast, no significant differences were found between any male treatment groups. Moreover, a significant main effect of diet for F4/80+ macrophages was found (Table 3.6). Overall expression of F4/80 appeared to predominately reside in the submucosa. In addition, no significant differences were found between any female treatment groups for IL-10 concentration (Figure 3.9) though a modest reduction was observed in VHFS and VHFX mice compared to CDS and CDX counterparts. In males, a difference between VHFX and CDS mice did approach significance (p = 0.078) in which VHFX mice demonstrated a modest increase in IL-10 concentration comparatively (Figure 3.9). Following univariate analyses, a main effect of sex approached significance (p = 0.055) in which females demonstrated an increase in colon IL-10 concentrations (+86.1 pg/mL) compared to males. A significant diet x sex interaction was found as well for IL-10 (Table 3.6).

For proliferation index, analyses confirmed that female CDX and VHFX mice demonstrated a reduced but non-significant index compared to VHFS counterparts (VHFS vs CDX, p = 0.071; VHFS vs VHFX, p = 0.098) (Figure 3.10). Likewise, male VHFX mice demonstrated a reduced index compared to VHFS, which approached

significance (p = 0.074), and CDS (p = 0.033) counterparts. Univariate analysis further confirmed a significant main effect of activity status as well as a main effect of sex that approached significance (p = 0.067) (Table 3.6). Pairwise comparisons indicated that sedentary mice had an increased proliferation index compared to exercised mice (+0.15, 30.4% difference); mice fed a 10% fat diet had a slightly lower proliferation index compared to mice fed a 60% fat diet (-0.02, -4.3% difference); and that female mice had a lower proliferation index compared to males (-0.07, -14.7% difference) (Table 3.6).

Gene expression of the unfolded protein response and phosphorylation of eIF2α

In females, significant differences were observed in the relative gene expression of ATF6 and IRE1β between VHFS and VHFX mice in which voluntary wheel running prevented an HFD-induced decrease in gene expression (0.6 vs 0.9 mRNA fold change for ATF6, 0.6 vs 1.1 mRNA fold change for IRE1β) (Figure 3.11). In males, no significant differences in the expression of any assessed gene was observed (Figure 3.11).

In females, a non-significant increase in the protein expression of phosphorylated (p-) eIF2α was observed in CDX mice compared to all other treatment groups (p = 0.216 vs VHFS; p = 0.074 vs VHFX) (Figure 3.12). In males, expression was significantly reduced in CDX and VHFX mice compared to VHFS animals. In addition, a non-significant (p = 0.093) increased expression was observed in male VHFS mice compared to CDS counterparts (Figure 3.12). No significant differences were observed in the protein expression of eIF2α between any treatment group in both male and female mice (Figure 3.12). When expressed as the ratio of p-eIF2α to eIF2α, CDS, CDX and VHFX male mice demonstrated a significantly reduced ratio compared to VHFS counterparts (Figure 3.12). In females, a non-significant increase in CDX mice was observed compared to all other treatment groups (p = 0.224 vs VHFS; p = 0.897 vs VHFX).

Discussion

The present study sought to examine the impact of excess dietary fat consumption and voluntary wheel running on the physical characteristics of colonic mucus, colon inflammation and ER stress responses. In contrast to our first hypothesis, we observed a thickening of the inner mucus layer in sedentary male mice consuming an HFD while no changes were observed in females. In partial fulfillment of our second, voluntary wheel running did reduce HFD-induced colon inflammation independent of diet type though no robust changes in IL-10 were observed in exercised mice. Interestingly however, female mice had greater IL-10 concentrations overall compared to males. Lastly, only slight changes in the gene expression of the UPR in females were observed with males showing no distinct changes in any assessed target. In contrast, sedentary males consuming an HFD demonstrated a significant increase in the phosphorylation of eIF2α which was prevented with voluntary wheeling running and a reduced fat control diet.

Growing evidence supports the role of diet in contributing to both the destabilization of the gut microbiota and the colonic mucus barrier (156). Specifically, consumption of a western style diet (WSD), characterized by an excess of saturated fat and simple carbohydrates but depleted in dietary fiber, has shown to deteriorate colonic mucus and augment microbial community structure in the distal gut (93, 157). Although our experimental diets were not fiber-deficient, we observed an increase in inner mucus layer thickness in sedentary male mice consuming an HFD with a concomitant increase in goblet cell density. We also observed a non-significant increase in total muc2 protein in sedentary and exercised male mice consuming an HFD. Together, these findings suggest that consumption of excess saturated fat stimulate an increase in mucus production independent of activity status in males. Recent findings by Schroeder et al. (93) have demonstrated similar increases in mucus production following an acute

exposure to a WSD though observed a decrease in mucus thickness which normalized after 28 days, as did mucus production, indicating that initial changes in mucus thickness and synthesis following consumption of a WSD are transient. In contrast, we observed a thickening of the inner mucus layer as well as an increase in mucus production following 12 weeks of an HFD suggesting that prolonged excess consumption of saturated fat with sufficient dietary fiber intake provoke a unique compensatory host response. Moreover, the lack of changes in mucus thickness and production observed in female mice suggest that females may be resistant to diet-induced disruptions of colonic mucus as estradiol has shown to demonstrate extensive protective effects in the gastrointestinal tract (158) and modulate the physicochemical properties of intestinal mucus (159). In agreement with this notion, females displayed an increase in goblet cell density compared to males corroborating an innate protective advantage. Changes in goblet cell density and their implications may be context dependent as exercised mice demonstrated an overall reduction in goblet cell density compared to sedentary mice, however. It is plausible that this response may be due to an improved gastrointestinal motility as aerobic exercise has shown to decrease colonic transit time (160). Enhanced gastric motility may therefore stimulate an increase in goblet cell secretion of intestinal mucus into the gut lumen thus making them readily undetectable in the mucosa by histological or immunohistochemical staining.

Previously in aim 1, we showed that intestinal COX-2 expression was attenuated by voluntary wheel running in female mice on either diet but only in male mice consuming a control diet. In contrast, the present study shows that voluntary wheel running attenuates HFD-induced colon inflammation in both exercised male and female mice consuming a high 60% fat diet. This discrepancy may be due to the difference in dietary sucrose content compared to aim 1 using 45% HFD, which had double the amount of sucrose content compared to the present 60% HFD used (172.8 g/kg vs. 68.8

g/kg). Excess sucrose intake is associated with an increased risk of IBD development (161) and has shown to enhance susceptibility to colitis as well as promote colon inflammation (162). In agreement with aim 1, however; a similar degree of inflammation was observed in sedentary male mice consuming a control diet further indicating that sedentary male mice may be more susceptible to intestinal inflammation compared to their female counterparts. Following the assessment of F4/80 expression, a cell-surface glycoprotein on murine tissue-resident macrophages, it was observed that F4/80+ macrophages were predominately confined to the submucosa. Macrophages found in this compartment of intestinal tissue are thought to be involved in maintaining the integrity of the submucosal vasculature (163). In activated macrophages, F4/80 expression is suppressed (164). Interestingly, we observed that in sedentary and exercised female mice consuming an HFD, F4/80+ expression was suppressed. Mice consuming a high 60% fat diet displayed an overall reduction in F4/80+ cells compared to mice on the control 10% fat diet. Together, these findings suggest that HFDs may augment the activity of submucosal macrophages and that females may be more susceptible to these dietary fat-induced effects despite demonstrating a reduced degree of mucosal inflammation.

In addition to COX-2 and F4/80 expression, NFκB expression was assessed as it serves as a pivotal mediator of inflammatory responses (165). NFκB is comprised of a family of five structurally related transcription factors, including RelA/p65, which plays a pivotal role in the induction of the canonical NFκB pathway (166). In male sedentary and exercised mice on an HFD, a non-significant increase in total protein for NFκB was observed. While no differences in total protein were observed in female mice, exercised female mice consuming either diet showed an increase in the gene expression of NFκB compared to sedentary counterparts consuming an HFD. Though the mechanisms behind this response in female mice remain unclear, these findings may indicate sex-

specific differences in the transcriptional and translational regulation of NFκB which may also be modulated by exercise in females. In the context of inflammatory status however, activation of NFκB is a better indicator of induced pro-inflammatory responses. What determines the activation of these subunits is the degree of phosphorylation, constituting the extensive regulation of NFκB activation in inflammatory responses (167). In the present study, only total protein and the gene expression of RelA/p65 was assessed. Examining the extent of phosphorylation of RelA/p65 would therefore provide additional insight when assessing colon inflammatory status.

Aerobic exercise has shown to promote colon health by attenuating inflammation (116, 118) and via the production of IL-10 (119), a potent anti-inflammatory cytokine. In the present study however, IL-10 production was not increased from voluntary wheel running. This may be due to the fact that voluntary wheel running is akin to physical activity in humans as opposed to regimented exercise (145) where significant differences in derived exercise capacity exist between the former and forced treadmill running in mice (146). Voluntary wheel running may therefore not be sufficient to induce such training adaptations that could elicit overt changes in IL-10 production. Nevertheless, female mice displayed an overall increase in IL-10 compared to males further illustrating that estradiol may confer additional anti-inflammatory benefits. Yet the significant interaction of diet x sex as well as the modest reduction in IL-10 in female mice consuming a HFD of either activity status suggests that female mice are more susceptible to changes in immune regulation by dietary fat; the mechanisms behind these interactions and their implications remain ill-defined, however.

In addition to its anti-inflammatory benefits, long-term participation in aerobic exercise has shown to significantly reduce the risk of CRC development (107-109). In humans, clinical measures are implemented to assess disease risk and can be utilized in animal studies to foster a translational approach. Of note is the assessment of PCNA

expression, a marker of cellular proliferation, which is known to be an effective predictor in colorectal cancer development in humans (168-170). As changes in the proliferative characteristics of the colonic mucosa precede the development of overt neoplasia in experimental carcinogenesis (171-173), proliferative phenotype in mice may constitute an important clinical marker to model disease risk in humans. To this end, evaluation of proliferative phenotype by proliferation index with PCNA has been established as a viable measure (154). In the present study, we observed a marked 30.4% increase in the proliferation index of sedentary mice compared to exercised counterparts suggesting that increasing physical activity still confers a significant degree of colonic protection compared to sedentary behavior. In addition, female mice demonstrated a 14.7% decrease in proliferation index indicating that females may be less at risk for the development of CRC. As dietary fat had no effect on proliferation index, these findings together suggests that activity status and sex are primary predictors of proliferative phenotype in colon tissue.

Recent evidence has shown that HFDs induce colonic ER stress (78). In sedentary female mice consuming an HFD, we observed a modest but unexpected suppression in the gene expression of ER stress sensors ATF6 and IRE1β, contrasting our initial hypothesis. In the advent of ER stress, ATF6 promotes protein folding, maturation and secretion (49) while IRE1 splices XBP1 mRNA, converting it into its functionally active isoform (XBP1s) that induces UPR target gene expression such as those involved in ERAD signaling (61). Although the effects of dietary fat on IRE1β regulation remain unclear, the ubiquitous isoform, IRE1α, potentiates obesity-associated inflammation (174). This was not assessed in the present study as the IRE1β isoform is predominately expressed in intestinal epithelial cells. In contrast, ATF6 has shown to possess a multitude of regulatory characteristics in embryonic development, as well as in the development of female reproductive structures and in adipogenesis and lipogenesis

(175). For instance, animal studies in female mammals have determined ATF6 to be a crucial regulator of follicular physiological processes (176, 177) and embryonic implantation (178). In addition, ATF6 has shown to suppress sterol regulatory element-binding protein (SREBP)-2-mediated lipogenesis (179) which controls cellular lipid metabolism and homeostasis. Although estrous cycle was not assessed over the duration of the present study nor was the expression of SREBP-2, it is reasonable to consider that the observed suppression of ATF6 in female mice might have occurred in tandem with HFD-induced changes to their estrous cycle as well as in the regulation of lipid metabolism. Recent findings by Chakraborty et al. illustrate that prolonged (25-27 weeks) consumption of a 60% fat diet markedly effects estrous cycle in mice, characterized by a complete acyclicity or rather the elongation or skipping of cycles (e.g., diestrus) or both, indicating a profound disruption in the reproductive cycle (180). In addition, excess storage of triglycerides in hypertrophic adipocytes activate SREBP-2 (181). In agreement with this notion, we observed a marked percent increase in body weight in sedentary female mice consuming an HFD compared to male counterparts (154.8% vs 111.5%). Taken together, the observed suppression of ATF6 in high-fat fed sedentary female mice may have occurred due to systemic changes in lipid metabolism, perhaps by an opposing upregulation of SREBP-2 in adipose tissue, and to a disrupted reproductive cycle. How this translates to alterations of colonic epithelial ER homeostasis remains ill-defined, however.

In contrast to the above findings in female mice, we observed no significant changes in the gene expression of any protein in male mice. Instead, exercised male mice consuming either diet or sedentary controls demonstrated a significant reduction in the phosphorylation of eIF2α compared to high-fat fed sedentary counterparts indicating that 12 weeks of a 60% HFD induces colonic epithelial ER stress in male mice. Further, we are the first to demonstrate that voluntary wheel running can attenuate this response. As

in many pathways, phosphorylation events are key to determining the activation or suppression of involved proteins. The lack of any overt changes in females suggests that 12 weeks of an HFD is not sufficient to induce any overt irregularities in colonic epithelial ER homeostasis. Moreover, the lack of changes in the gene expression of proteins involved in the UPR in male mice further indicate that changes in phosphorylation status may precede transcriptional activity as phosphorylation of eIF2α by PERK is the most immediate response to ER stress (53). Additional analyses examining the phosphorylation of PERK and IRE1 as well as the splicing of XBP1 would provide further insight as well.

Conclusions

In sum, these results illustrate a unique compensatory response in males consuming an HFD characterized by a thickening of the inner mucus layer and an increased production of muc2 independent of activity status. We have shown that voluntary wheel running attenuates HFD-induced colon inflammation, while HFDs may augment the activity of submucosal macrophages. Our findings also suggest that females have a decreased propensity for colon inflammation and a reduced CRC risk due to an inherent elevation of IL-10 and a decreased proliferation index. In contrast, being sedentary may dramatically increase risk of CRC development due to an aberrant proliferative phenotype while being more physically active can prevent this response. Lastly, we are the first to demonstrate that voluntary wheel running attenuates HFD-induced colonic epithelial ER stress in males. Taken together, these findings corroborate the efficacy of exercise in promoting colon health primarily by reduction of inflammation, improvements in proliferative status and restoration of ER homeostasis. We also highlight unique sex-specific differences that require further exploration.

Table 3.1. Composition of experimental diets (Research Diets, Inc.).

	Control Diet	High-fat Diet
		kcal%
Protein	20	20
Carbohydrate	70	20
Fat	10	60
Total	100	100
kcal/g	3.82	5.21
Ingredients		**g/kg total**
Casein, 30 Mesh	200	200
L-Cystine	3	3
Corn Starch	506.2	/
Lodex 10	125	125
Sucrose	72.8	72.8
Fiber (Solka Floc)	50	50
Soybean Oil	25	25
Lard	20	245
Mineral Mix S10026B	50	50
Choline Bitartrate	2	2
Vitamin Mix V10001C	1	1
FD&C Yellow Dye #5	0.04	/
FD&C Blue Dye #1	0.01	0.05

Table 3.2. Final body weights (g), fat mass (g) and percent weight change for each treatment group.

	CDS	VHFS	CDX	VHFX
females				
body weight (g)	23.0 ± 1.7	43.1 ± 7.8*	23.3 ± 0.8	30.3 ± 6.8*
fat mass (g)	2.0 ± 0.9	18.0 ± 6.7*	1.0 ± 0.3	7.2 ± 6.0
% weight increase	34.2%	154.8%	38.1%	81.2%
males				
body weight (g)	30.3 ± 3.4	44.7 ± 2.5*	27.7 ± 1.7	36.4 ± 3.8*
fat mass (g)	4.9 ± 1.8[a]	15.7 ± 2.6*	2.0 ± 1.6[b]	9.4 ± 3.7[a, b]
% weight increase	43.2%	111.5%	30.2%	74.7%

Body weights, fat mass and percent weight change after 12 weeks of treatment with control diet sedentary (CDS), very high-fat diet sedentary (VHFS), control diet exercise (CDX) and high-fat diet exercise (VHFX) in female and male mice. Values are expressed as the mean ± SD, n = 7 for each treatment group. One-way ANOVA with Tukey's post-test for CDS vs VHFS; CDS vs CDX; CDS vs VHFX, HFS vs CDX, HFS vs VHFX, CDX vs VHFX in both females and males. *$p < 0.05$ from CD groups undergoing the same intervention (sedentary or exercise) and each other in both males and females for body weight or from all other groups for fat mass. Values that share the same superscript are significantly ($p < 0.05$) different from each other.

Table 3.3. Average kcals per day consumed over study duration for each treatment group.

	CDS	VHFS	CDX	VHFX
females				
Kcals/day	11.1 ± 1.5§	16.9 ± 3.1	15.8 ± 1.6*	18.1 ± 2.0*
males				
Kcals/day	12.2 ± 1.7§	16.4 ± 2.3	15.9 ± 1.9*	17.5 ± 1.1*

Average daily food intake over 12 weeks of treatment with control diet sedentary (CDS), very high-fat diet sedentary (VHFS), control diet exercise (CDX) and very high-fat diet exercise (VHFX) in female and male mice. Values are expressed as the mean ± SD, n = 7 for each treatment group. One-way ANOVA with Tukey's post-test for CDS vs VHFS; CDS vs CDX; CDS vs VHFX, HFS vs CDX, HFS vs VHFX, CDX vs VHFX in both females and males. *$p < 0.05$ from each other in females and males; §$p < 0.05$ from all groups in males and females.

Table 3.4. Analysis of body weight, fat mass and average food intake over study duration by independent factors.

pairwise comparisons

	activity status (AS)			diet (D)			sex (S)		
parameter	*sedentary*	*exercise*	mean difference	*control 10% fat*	*very high 60% fat*	mean difference	*female*	*male*	mean difference
final body weight (g)	35.3 ± 0.8	29.4 ± 0.8	5.9 ± 1.1*	26.1 ± 0.8	38.6 ± 0.8	-12.6 ± 1.1*	29.9 ± 0.8	34.8 ± 0.8	-4.9 ± 1.1*
Pre-study[a] fat mass (g)	1.2 ± 0.1	1.3 ± 0.1	-0.1 ± 0.1	1.3 ± 0.1	1.3 ± 0.1	-0.04 ± 0.1	1.5 ± 0.1	1.1 ± 0.1	0.4 ± 0.1*
post-study fat mass (g)	10.1 ± 0.7	4.9 ± 0.7	5.3 ± 1.0*	2.5 ± 0.7	12.6 ± 0.7	-10.1 ± 0.1*	7.0 ± 0.7	8.0 ± 0.07	-1.0 ± 0.1
food intake (kcals)	14.1 ± 0.2	16.8 ± 0.2	-2.7 ± 0.3*	13.8 ± 0.2	17.2 ± 02	-3.5 ± 0.3*	15.5 ± 0.2	15.5 ± 0.2	-0.04 ± 0.3

3-way ANOVA *p*-values

parameter	AS	D	S	AS x D	AS x S	D x S	AS x D x S
final body weight (g)	0.000	0.000	0.000	0.000	0.710	0.386	0.111
pre-study[a] fat mass (g)	0.495	0.734	0.002	0.848	0.611	0.912	0.499
post-study fat mass (g)	0.000	0.000	0.343	0.001	0.513	0.324	0.101
food intake (kcals)	0.000	0.000	0.898	0.000	0.359	0.042	0.358

Values of each parameter are expressed as the mean ± SEM. Three-way ANOVA for comparisons between activity status, diet and sex. [a]Measurement of fat mass was taken at the end of the 2-week acclimation period at 6 weeks of age. *$p \leq 0.05$.

Table 3.5. Analysis of morphological characteristics by independent factors in mouse colon.

pairwise comparisons

	activity status (AS)			diet (D)			sex (S)		
parameter	*sedentary*	*exercise*	mean difference	*control 10% fat*	*very high 60% fat*	mean difference	*female*	*male*	mean difference
total nuclei per crypt	31.9 ± 1.0	33.2 ± 0.7	-1.2 ± 1.2	31.8 ± 0.9	33.3 ± 0.7	-1.6 ± 1.2	31.1 ± 0.9	34.0 ± 0.7	-2.9 ± 1.1*
goblet cell density[a]	0.34 ± .01	0.27 ± .01	-0.06 ± 0.02*	0.32 ± 0.01	0.30 ± .01	0.03 ± 0.015	0.32 ± 0.01	0.29 ± .01	0.04 ± 0.015*
thickness (μm) of IML	38.1 ± 1.7	34.9 ± 1.2	3.2 ± 2.1	35.1 ± 1.6	37.9 ± 1.3	-2.8 ± 2.1	36.1 ± 1.7	37.9 ± 1.2	-0.8 ± 2.1
muc2 protein[b]	4996.6 ± 1243.7	5179.9 ± 771.0	-183.2 ± 1463.3	4414.4 ± 1162.4	5762.1 ± 889.0	-1347.7 ± 1463.3	5073.6 ± 1190.1	5102.8 ± 851.5	-29.2 ± 1463.3

3-way ANOVA *p*-values

parameter	AS	D	S	AS x D	AS x S	D x S	AS x D x S
total nuclei per crypt	0.301	0.195	0.023	0.530	0.270	0.403	0.186
goblet cell density[a]	0.000	0.106	0.020	0.607	0.102	0.066	0.012
thickness (μm) of IML	0.140	0.198	0.701	0.173	0.953	0.008	0.020
muc2 protein[b]	0.901	0.365	0.984	0.449	0.335	0.165	0.483

Values of each parameter are expressed the mean ± SEM. Three-way ANOVA for comparisons between activity status, diet and sex. *$p \leq 0.05$. [a]Density refers to number of positively stained goblet cells for mucin 2 relative to total nuclei per crypt. [b]Expressed as density normalized to total protein. IML, inner mucus layer.

Table 3.6. Analysis of inflammation markers, proliferation index and phosphorylation of eIF2α by independent factors in mouse colon.

pairwise comparisons

	activity status (AS)			diet (D)			sex (S)		
parameter	*sedentary*	*exercise*	mean difference	*control 10% fat*	*very high 60% fat*	mean difference	*female*	*male*	mean difference
F4/80+ cells[a]/mm^2	1.0 ± 0.2	1.2 ± 0.1	-0.2 ± 0.4	1.4 ± 0.2	0.8 ± 0.1	0.6 ± 0.2*	1.3 ± 0.2	0.9 ± 0.1	0.4 ± 0.2
IL-10 (pg/mL)	376.4 ± 37.9	411.9 ± 20.8	-35.5 ± 43.2	408.3 ± 34.5	380.0 ± 26.0	28.3 ± 43.2	437.2 ± 36.0	351.1 ± 23.9	86.1 ± 43.2*
RelA/NFκB p65 protein[b]	2285.7 ± 901.1	2219.3 ± 558.6	66.4 ± 1060.2	1847.1 ± 842.2	2658.0 ± 644.1	-810.9 ± 1060.2	2142.2 ± 862.3	2362.9 ± 617.9	-220.7±1060.2
p-eIF2α/eIF2α[c]	0.80 ± 0.14	0.71 ± 0.08	0.08 ± 0.17	0.70 ± 0.13	0.79 ± 0.1	-0.09 ± 0.17	0.66 ± 0.14	0.84 ± 0.09	-0.19 ± 0.17
proliferation index	0.56 ± 0.03	0.41 ± .02	0.15 ± 0.04* (30.4 %)	0.47 ± 0.03	0.49 ± 0.02	-0.02 ± 0.04 (4.3 %)	0.45 ± 0.03	0.51 ± 0.02	-0.07 ± 0.04 (14.7 %)

3-way ANOVA *p*-values

parameter	AS	D	S	AS x D	AS x S	D x S	AS x D x S
F4/80+ cells[a]/mm^2	0.425	0.014	0.093	0.563	0.963	0.138	0.773
IL-10 (pg/mL)	0.417	0.516	0.055	0.733	0.531	0.013	0.757
RelA/NFκB p65 protein[b]	0.951	0.451	0.837	0.933	0.705	0.161	0.547
p-eIF2α/eIF2α[c]	0.613	0.587	0.270	0.006	0.000	0.180	0.568
proliferation index	0.001	0.562	0.067	0.422	0.664	0.131	0.443

Values of each parameter are expressed the mean ± SEM. Proliferation index is defined as the ratio of immunoreactive nuclei for PCNA to the total nuclei counted per crypt; percent difference is shown in parentheses. Three-way ANOVA for comparisons between activity status, diet and sex. *$p \leq 0.05$. [a]Counted F4/80+ cells normalized to total area of mucosa measured. [b]Expressed as density normalized to total protein. [c]Expressed as the ratio of normalized densities (to total protein) of p-eif2α to eif2α. PCNA, proliferating cell nuclear antigen.

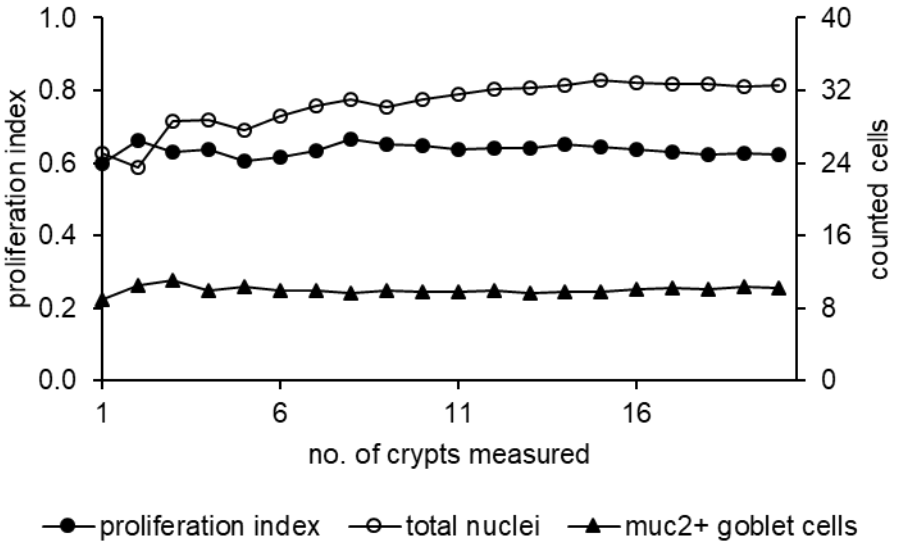

Figure 3.1. Determination of running averages for stained cell counting. The running average of proliferation index, total nuclei and immunoreactive goblet cells for muc2 in normal looking colonic mucosa from one representative animal. Muc2, mucin 2.

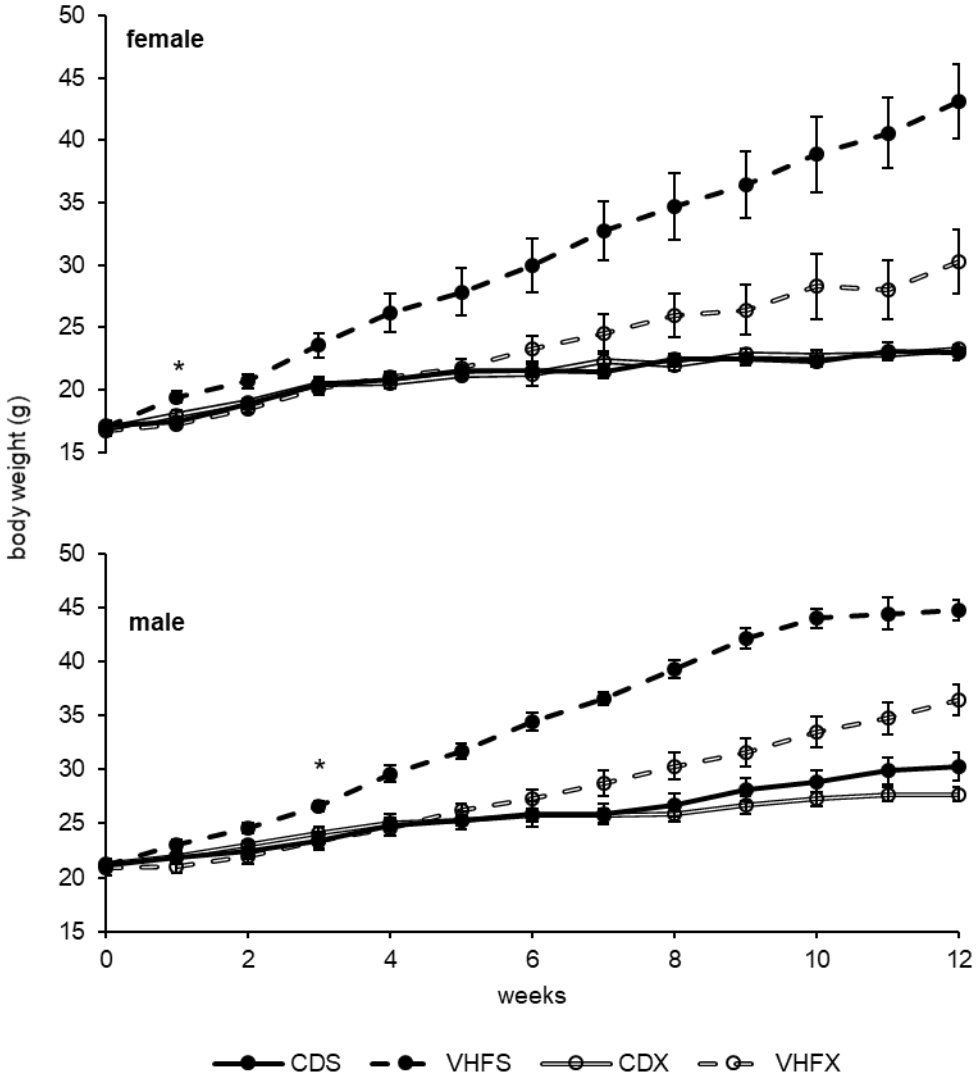

Figure 3.2. Body weight change over study duration. Body weights for each week during 12 weeks of treatment with control diet sedentary (CDS), very high-fat diet sedentary (VHFS), control diet exercise (CDX) and very high-fat diet running (VHFX) in female and male mice. Values are expressed as the mean ± SEM for each week, n = 7 mice/group. One-way ANOVA with Tukey's post-test for CDS vs VHFS; CDS vs CDX; CDS vs VHFX; HFS vs CDX; HFS vs VHFX and CDX vs VHFX for each week in both females and males. * $p < 0.05$ for CDS vs VHFS when first observed.

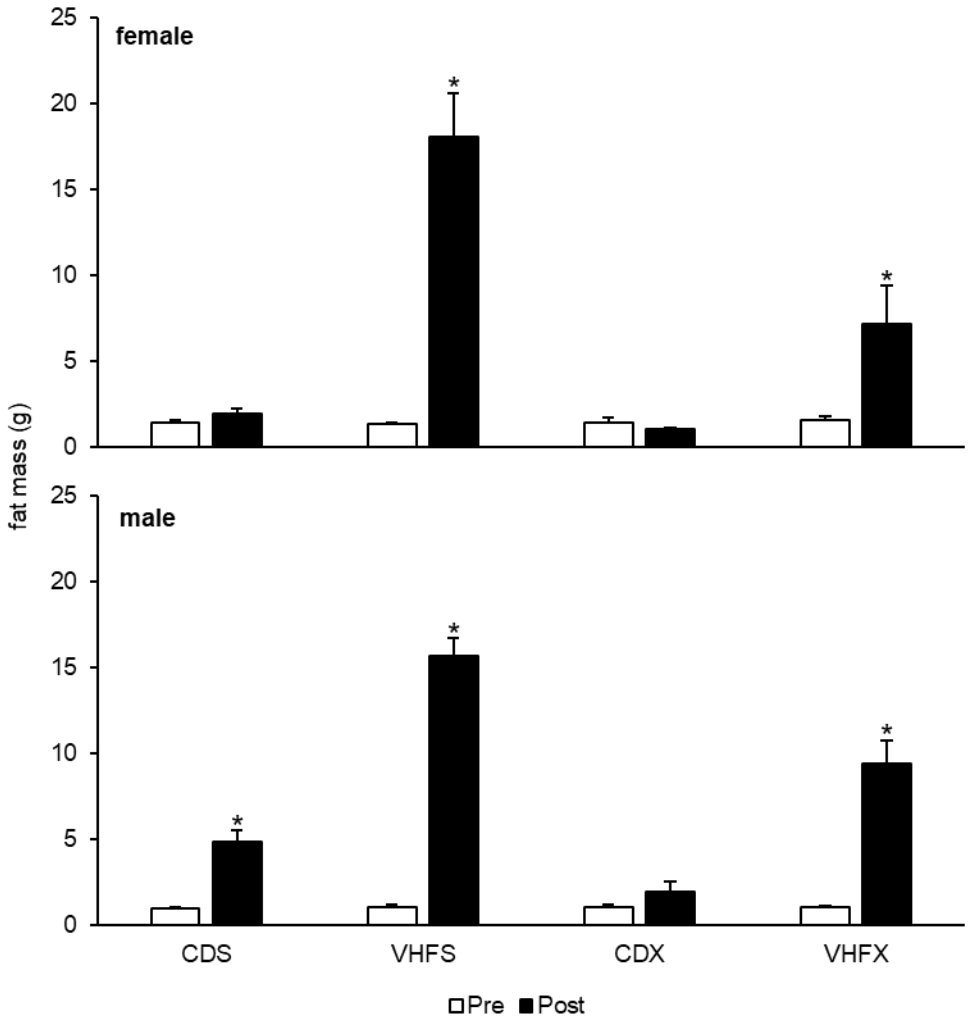

Figure 3.3. Comparisons of pre and post fat mass between treatment groups. Pre and post study fat mass following 12 weeks of treatment with control diet sedentary (CDS), very high-fat diet sedentary (VHFS), control diet exercise (CDX) and very high-fat diet running (VHFX) in female and male mice. Values are expressed as the mean ± SEM, n = 7 mice/group. Paired samples t-test between pre (open bars) and post (filled) fat mass for each treatment group. *$p < 0.05$ compared to pre fat mass.

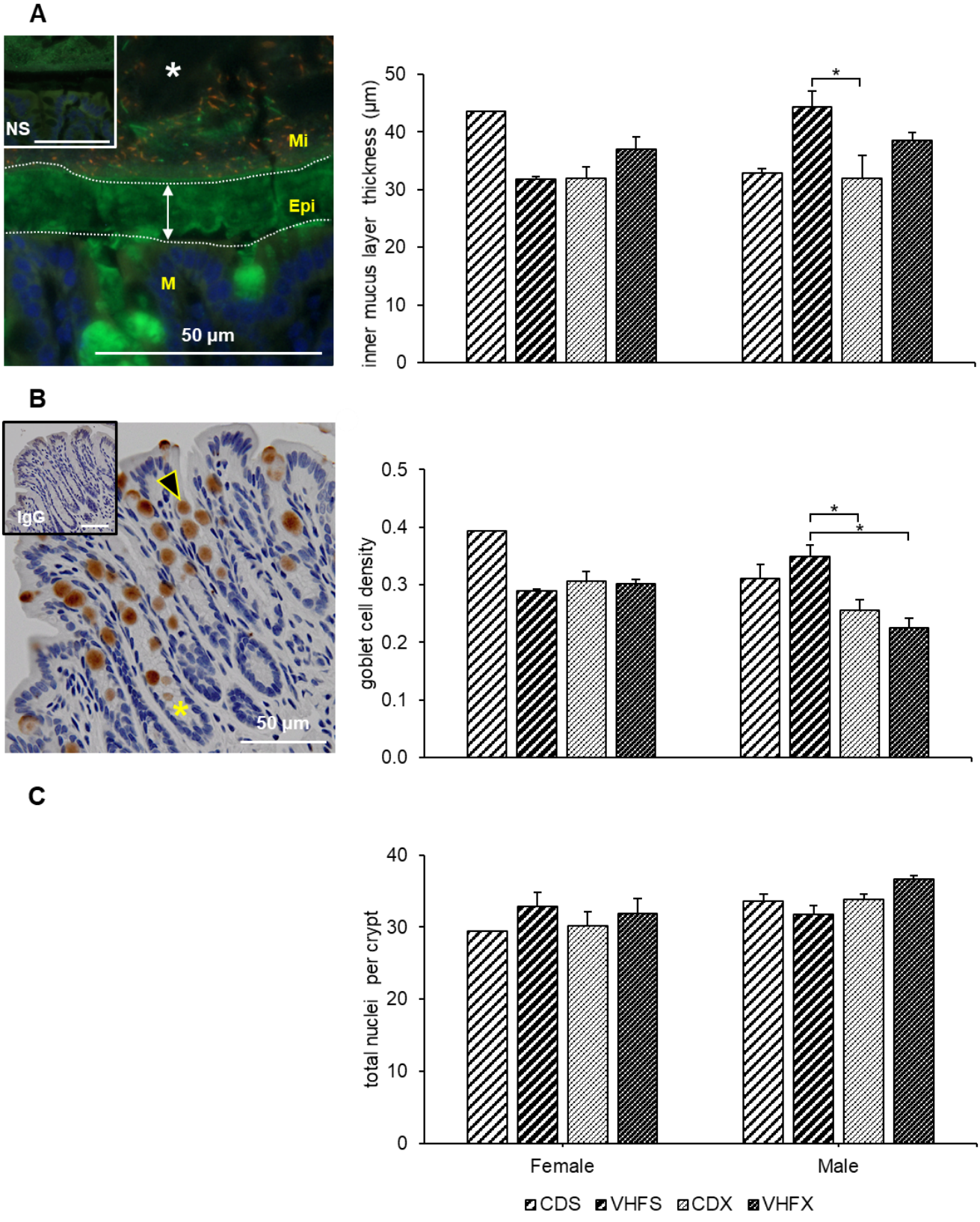
A
NS
*
Mi
Epi
M
50 µm
inner mucus layer thickness (µm)
0
10
20
30
40
50
*
B
IgC
*
50 µm
goblet cell density
0.0
0.1
0.2
0.3
0.4
0.5
*
*
C
total nuclei per crypt
0
10
20
30
40
Female
Male
CDS
VHFS
CDX
VHFX

Figure 3.4. Effects of diet and voluntary wheel running on inner mucus layer thickness and goblet cell density in colon. A. panel: methanol-Carnoy fixed sections prepared after 12 weeks of treatment with control diet sedentary (CDS), very high-fat diet sedentary (VHFS), control diet exercise (CDX) and very high-fat diet exercise (VHFX) from female and male mice were hybridized with the Alexa Fluor 555-conjugated universal bacterial probe (EUB338) or with a nonsense (NS) probe. Co-immunofluorescent staining was performed for muc2. One representative section is shown for each probe (original magnification x 400). Inset, NS control. Graph: inner mucus layer thickness. **B.** panel: immunohistochemical staining for muc2 in histological sections fixed in paraformaldehyde and sucrose. One representative section is shown (original magnification x 400). Inset, IgG control. Graph: goblet cell density, defined as the number of positively stained goblet cells for mucin 2 per crypt relative to total nuclei per crypt. **C.** graph: total nuclei per crypt. Values are expressed as the mean ± SEM, n = 1-4 mice/group. One-way ANOVA with Tukey's post-test for CDS vs VHFS; CDS vs CDX; CDS vs VHFX, VHFS vs CDX, VHFS vs VHFX, CDX vs VHFX in both females and males. *$p \leq 0.05$. White dotted lines; boundary of microbiota (Mi) and epithelial surface (Epi); double-sided arrow, distance measured; open circle, bacteria; M, mucosa; white asterisk, lumen; yellow asterisk, base of single crypt; black and yellow arrow, immunoreactive goblet cell for mucin 2.

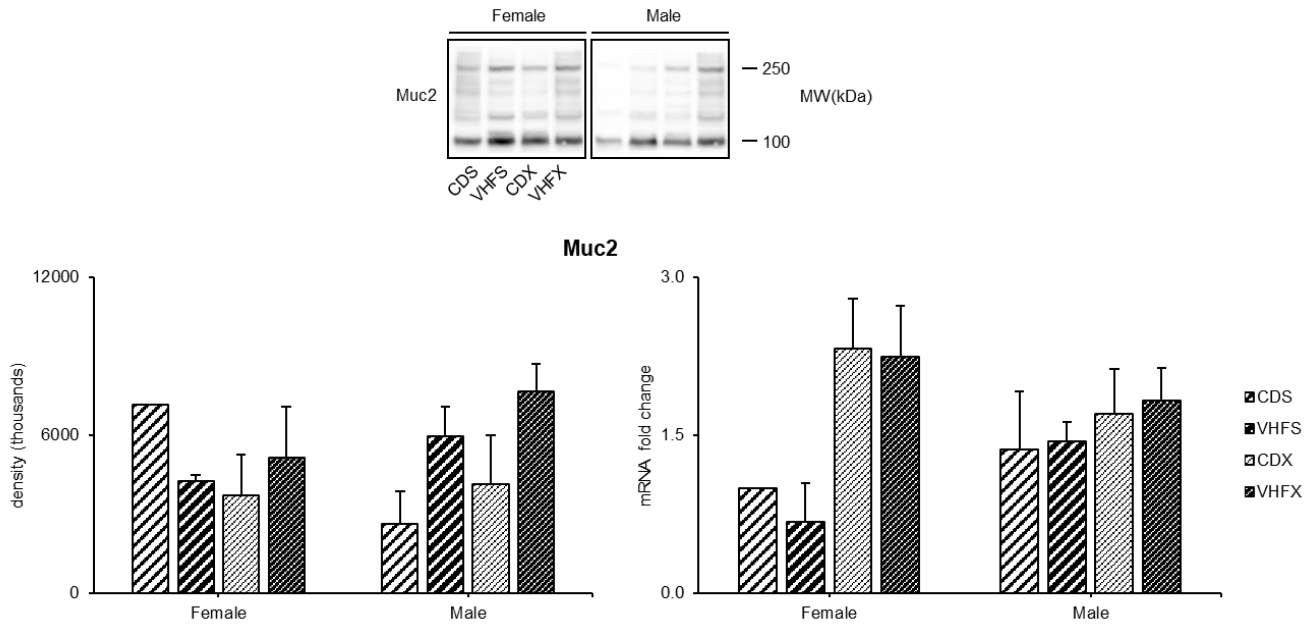

Figure 3.5. Effects of diet and voluntary wheel running on muc2 expression in colon. Immunoblotting (left graph) with an antibody for muc2 following SDS-PAGE of colon lysates after 12 weeks of treatment with control diet sedentary (CDS), very high-fat diet sedentary (VHFS), control diet exercise (CDX) and very high-fat diet exercise (VHFX). Densities are expressed as the mean ± SEM, normalized to total protein as determined by ponceau S staining, n = 1-7 mice/group. Quantitative real-time PCR of RNA extracts (right graph). Values are expressed as the fold change relative to CDS groups ± SEM, n = 1-7 mice/group. One-way ANOVA with Tukey's post-test for CDS vs HFS; CDS vs CDX; CDS vs VHFX; HFS vs CDX; VHFS vs VHFX and CDX vs VHFX for densities and ΔCt values. Muc2, mucin 2.

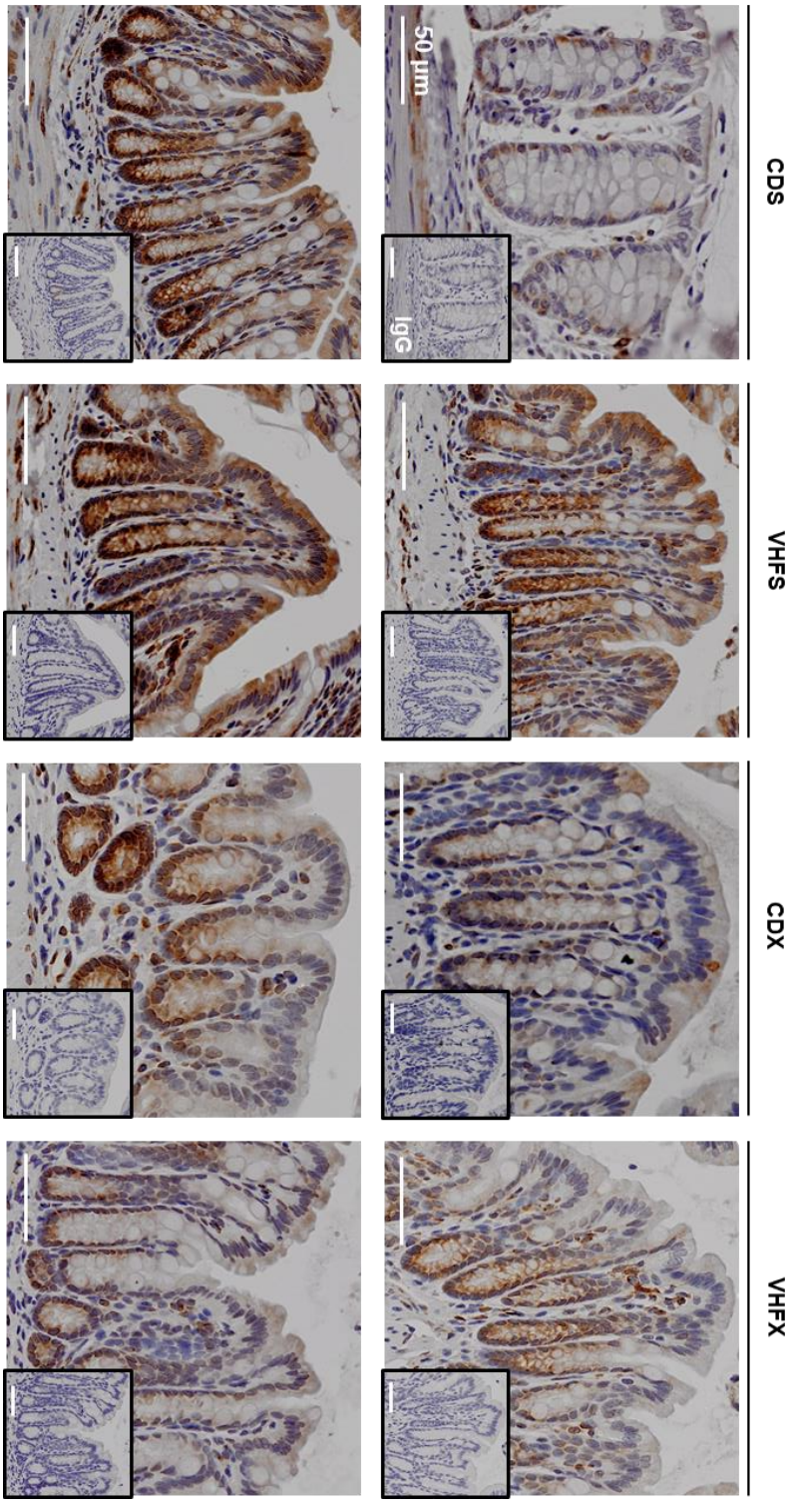
CDS
VHFS
CDX
VHFX
Female
Male
50 um
IgG

Figure 3.6. Effects of diet and voluntary wheel running on COX-2 expression in colon. Histological sections fixed in paraformaldehyde and sucrose prepared after 12 weeks of treatment with control diet sedentary (CDS), very high-fat diet sedentary (VHFS), control diet exercise (CDX) and very high-fat diet exercise (VHFX) in female and male mice were stained with an antibody for COX-2. One representative section from 1-4 mice/group is shown (original magnification x 400). Inset, IgG control.

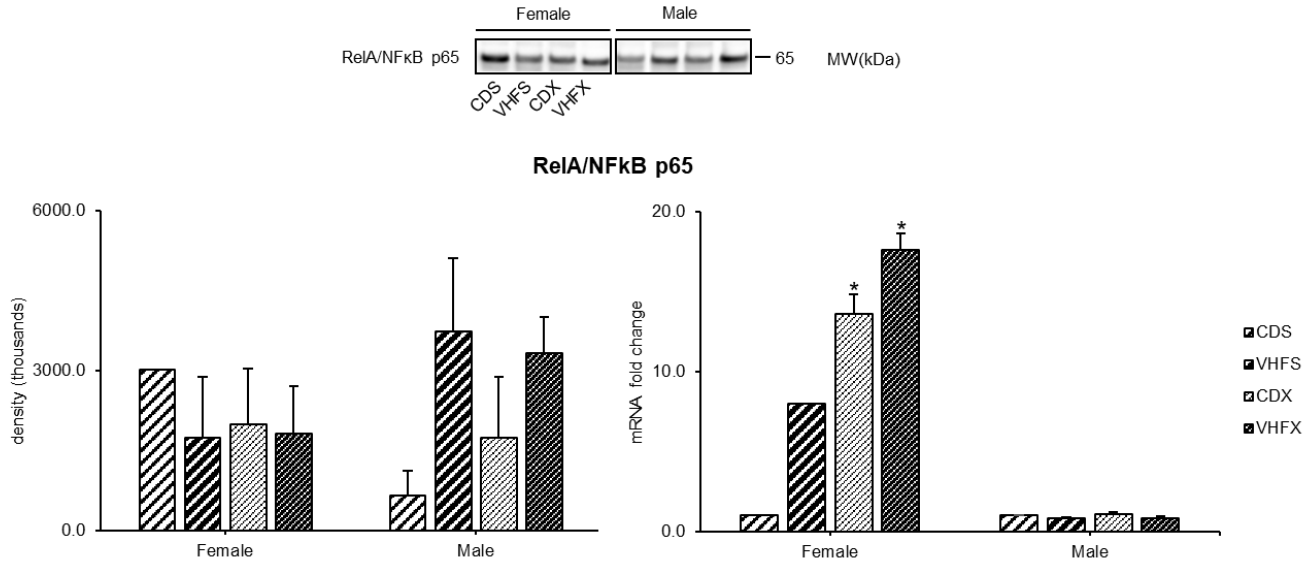

Figure 3.7. Effects of diet and voluntary wheel running on NF-κB expression in colon. A. Immunoblotting (left graph) with an antibody for RelA/NFκB p65 following SDS-PAGE of colon lysates after 12 weeks of treatment with control diet sedentary (CDS), very high-fat diet sedentary (VHFS), control diet exercise (CDX) and very high-fat diet exercise (VHFX). Densities are expressed as the mean ± SEM, normalized to total protein as determined by ponceau S staining, n = 1-7 mice/group. Quantitative real-time PCR of RNA extracts (right graph). Values are expressed as the fold change relative to CDS groups ± SEM, n = 1-7 mice/group. One-way ANOVA with Tukey's post-test for CDS vs HFS; CDS vs CDX; CDS vs VHFX; HFS vs CDX; VHFS vs VHFX and CDX vs VHFX for relative density and ΔCt values. *p ≤ 0.05 compared to VHFS. RelA/NFκB, p65/nuclear factor kappa-light-chain-enhancer of activated B cells.

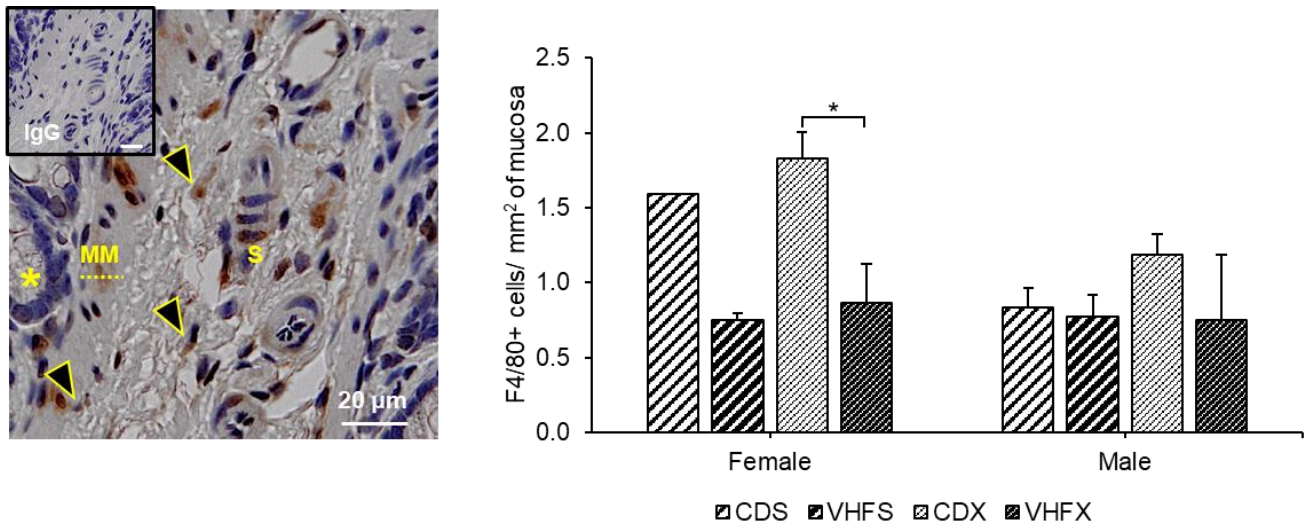

Figure 3.8. Effects of diet and voluntary wheel running on F4/80+ macrophages in colon. Panel: histological sections fixed in paraformaldehyde and sucrose prepared after 12 weeks of treatment with control diet sedentary (CDS), very high-fat diet sedentary (VHFS), control diet exercise (CDX) and very high-fat diet exercise (VHFX) in female and male mice were stained with an antibody for F4/80. One representative section is shown (original magnification x 400). Inset, IgG control. Graph: analysis of total F4/80+ stained cells counted relative to total area of mucosa measured. Values are expressed as the mean, n = 1-4 mice/group. One-way ANOVA with Tukey's post-test for CDS vs VHFS; CDS vs CDX; CDS vs VHFX, HFS vs CDX, HFS vs VHFX, CDX vs VHFX in both females and males. *$p \leq 0.05$. Asterisk, base of single crypt; MM, muscularis mucosae; S, submucosa; black and yellow arrow, immunoreactive cells.

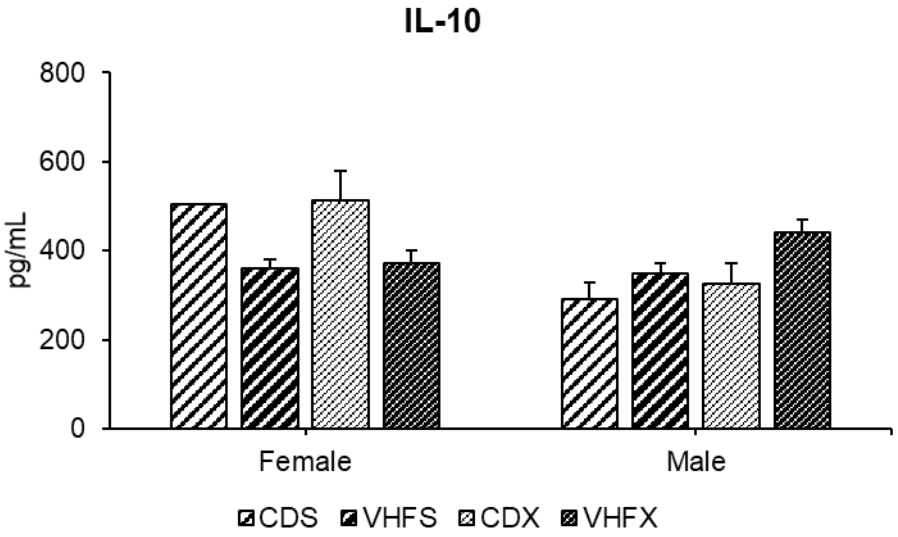

Figure 3.9. Effects of diet and voluntary wheel running on IL-10 in colon. Quantification of IL-10 concentration by ELISA from colon lysates following 12 weeks of treatments with control diet sedentary (CDS), very high-fat diet sedentary (VHFS), control diet exercise (CDX) and very high-fat diet exercise (VHFX) in female and male mice. Values are expressed as the mean ± SEM, n = 1-7 mice/group. One-way ANOVA with Tukey's post-test for CDS vs VHFS; CDS vs CDX; CDS vs VHFX, HFS vs CDX, HFS vs VHFX, CDX vs VHFX in both females and males.

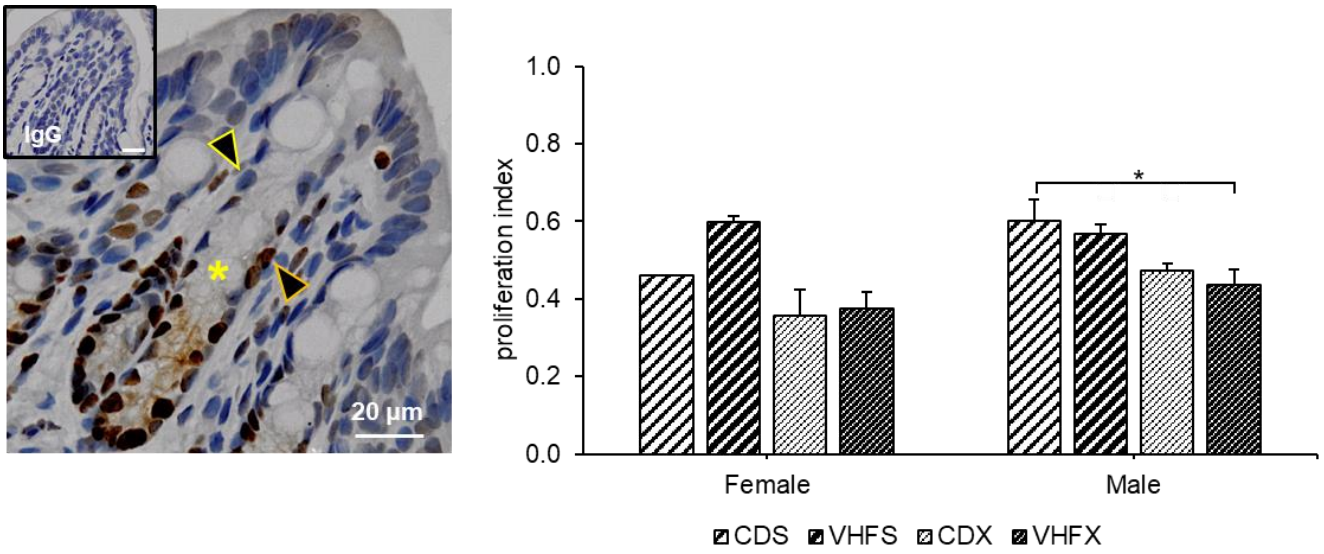

Figure 3.10. Effects of diet and voluntary wheel running on proliferation index in colon. Panel: histological sections fixed in paraformaldehyde and sucrose prepared after 12 weeks of treatment with control diet sedentary (CDS), very high-fat diet sedentary (VHFS), control diet exercise (CDX) and very high-fat diet exercise (VHFX) in female and male mice were stained with an antibody for PCNA. One representative section is shown (original magnification x 400). Inset, IgG control. Graph: analysis of proliferation index. Proliferation index is defined as the ratio of immunoreactive nuclei for PCNA to the total nuclei counted for a crypt. Values are expressed as the mean ± SEM, n = 1-4 mice/group. One-way ANOVA with Tukey's post-test for CDS vs VHFS; CDS vs CDX; CDS vs VHFX, HFS vs CDX, HFS vs VHFX, CDX vs VHFX in both females and males. *$p \leq 0.05$. Asterisk, single crypt; black and yellow arrow, nuclei; black and orange arrow, immunoreactive nuclei; PCNA, proliferating cell nuclear antigen.

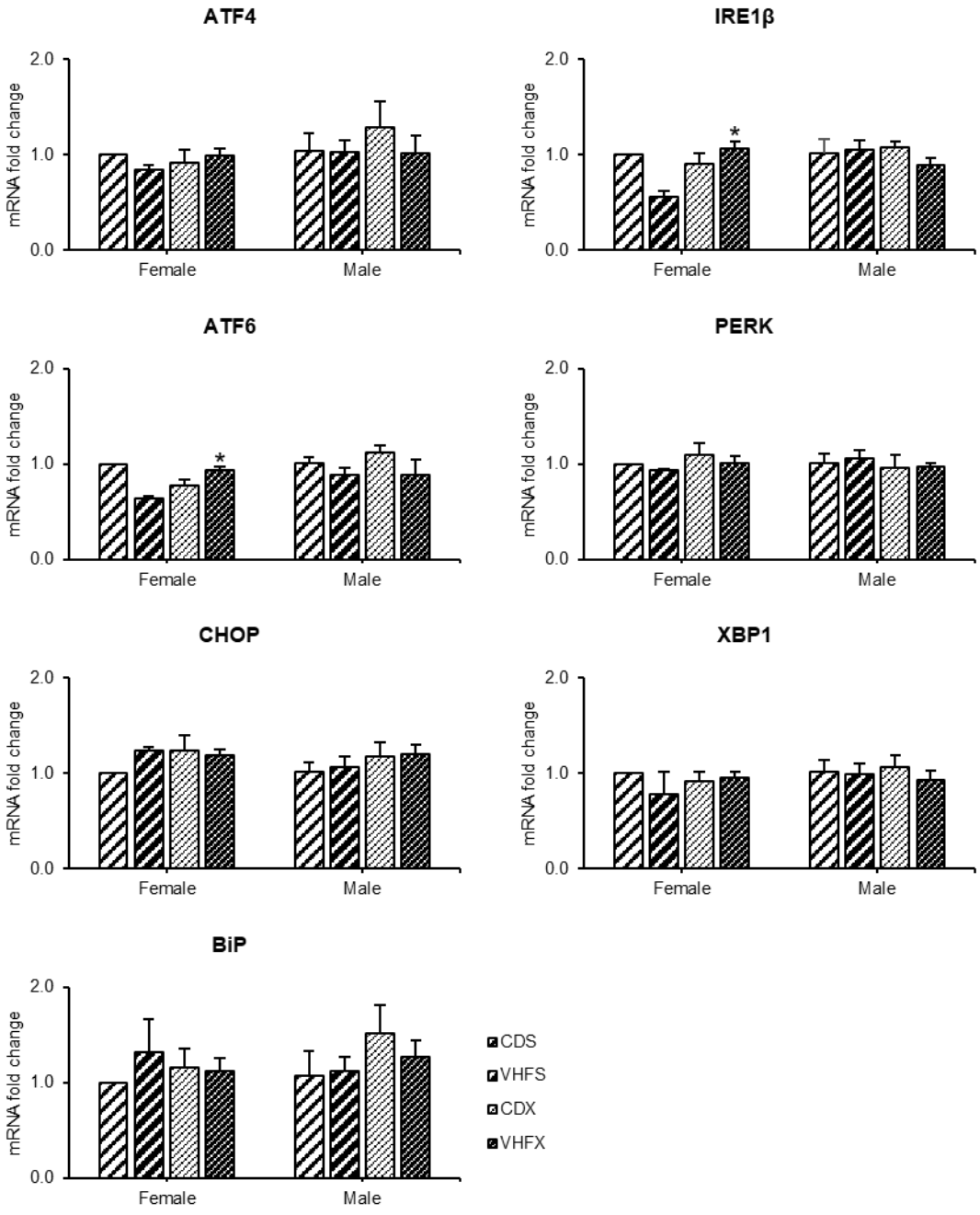
ATF4
IRE1β
ATF6
PERK
CHOP
XBP1
BiP
mRNA fold change
2.0
1.0
0.0
Female
Male
*
CDS
VHFS
CDX
VHFX

Figure 3.11. Effects of diet and voluntary wheel running on relative gene expression of the unfolded protein response in colon. Relative gene expression of the unfolded protein response following 12 weeks of treatment with control diet sedentary (CDS), very high-fat diet sedentary (VHFS), control diet exercise (CDX) and very high-fat diet running (VHFX) in female and male mice colon. Values are expressed as the fold change relative to CDS groups ± SEM, n = 1-7 mice/group. One-way ANOVA with Tukey's post-test for CDS vs VHFS; CDS vs CDX; CDS vs VHFX; VHFS vs CDX; VHFS vs VHFX and CDX vs VHFX for ΔCt values. ∆Ct was calculated as $Ct_{target} - Ct_{reference}$. * $p < 0.05$ compared to VHFS. ATF4 & 6, activating transcription factor; CHOP, CCAAT-enhance-binding protein homologous protein; Grp78, glucose-regulated protein 78/ binding immunoglobulin protein (BiP); IRE1β, inositol-requiring kinase 1 beta; PERK, pancreatic endoplasmic reticulum eukaryotic initiating factor-2 alpha kinase; XBP1, transcription factor X box-binding protein 1.

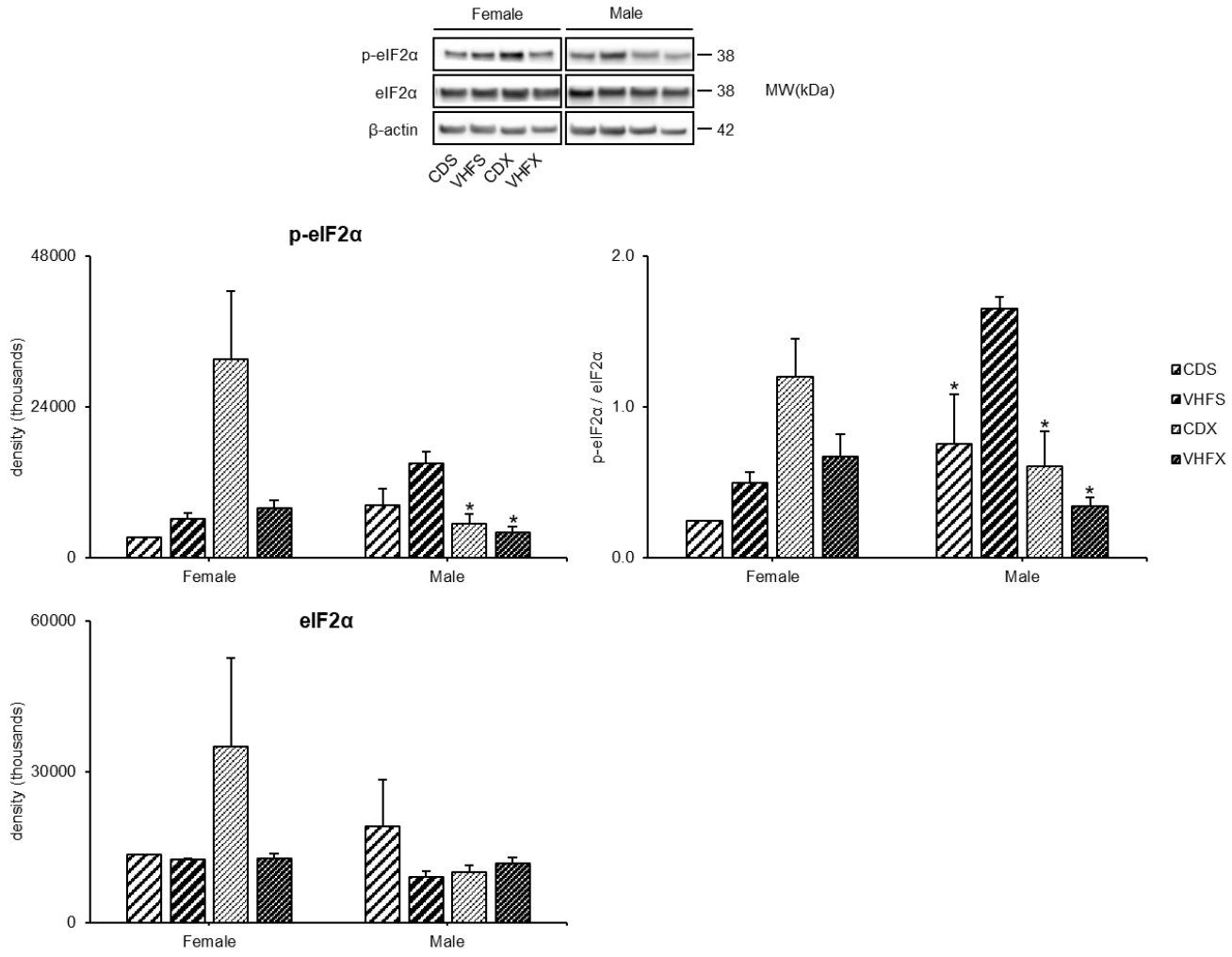

Figure 3.12. Effects of diet and voluntary wheel running on phosphorylation of eIF2α in colon. Immunoblotting with cellular stress marker antibodies for p-eIF2α and eIF2α following SDS-PAGE of colon lysates after 12 weeks of treatment with control diet sedentary (CDS), very high-fat diet sedentary (VHFS), control diet exercise (CDX) and very high-fat diet exercise (VHFX). Densities are expressed normalized to β-actin ± SEM, n = 1-7 mice/group. Ratio of normalized densities between p-eIF2α and eIF2α ± SEM. One-way ANOVA with Tukey's post-test for CDS vs HFS; CDS vs CDX; CDS vs VHFX; HFS vs CDX; VHFS vs VHFX and CDX vs VHFX for densities and ratios. *p ≤ 0.05 compared to VHFS. p-eIF2α, phosphorylated eukaryotic initiation factor-2 alpha; eIF2α, eukaryotic initiation factor-2 alpha.

Chapter 4: High-fat Diets & Voluntary Wheel Running Alter the Gene Expression of Inflammasomes

Introduction

Determination of a healthy host-microbe interface is achieved by a myriad of pattern recognition receptors (PRRs) along the gut epithelium that recognize conserved molecular patterns of both microbe and host origin to initiate tolerogenic or defense responses (70). Of note are nucleotide-binding oligomerization domain (NOD)-like receptors (NLRs) which are a key component of inflammasomes that form in response to diverse microbial and host-derived stimuli. Of primary interest are the NOD-like receptor family pyrin domain containing 3 and 6 (NLRP3 and 6) inflammasomes which have been implicated in intestinal inflammation and tumorigenesis (70) as well as in the governance of intestinal mucus secretion (10) and microbial composition (87). At present, there is a paucity of literature that has examined the combined influence of high-fat diets (HFDs) and exercise on inflammasome activity. Thus, the present study examined the extent to which voluntary wheel running and HFDs modulate inflammasome signaling in male and female C57BL/6NTac mice.

The intestinal microenvironment represents a potentially hostile milieu in which a multitude of microorganisms, food-, and microbial-derived antigens constantly challenge the integrity of the intestinal epithelium. Prevention of epithelial breach is achieved by a delicate balance between the actions of multiple immunological barriers (5). Though the cells lining the intestine function to keep bacteria from invading the body, intestinal epithelial cells in fact have a complex and mutually beneficial relationship with the gut microbiota. The distinction between “friend vs. foe” is thus achieved through an array of PRRs including NLRs which constitute the inflammasome. Inflammasomes are cytoplasmic multi-protein complexes assembled around a set of core components that include a sensor protein, an adaptor protein (apoptosis-associated speck-like protein containing a caspase activation and recruitment domain (CARD)(ASC)) and an

inflammatory caspase (72) of which caspase-1 has a dominant role in inflammatory responses (73). In this regard, inflammasomes act as a multi-protein platform from which the activation of inflammatory caspases ensues and converts the pro-inflammatory cytokines IL-18 and IL-1β into their biological active forms. Activation of caspase-1 via the above pathway is known as canonical inflammasome signaling whereas non-canonical inflammasome signaling entails caspase-11 activation in mice or caspase-4 in humans (70). The role of inflammasomes in intestinal inflammation, infection and carcinogenesis is diverse and evidence suggests that the NLRP3 and, more recently, the NLRP6 canonical inflammasomes are key players in both the perpetuation and attenuation thereof (70). However, the effect of HFDs on inflammasome activity remains largely understudied and absent regarding the influence of exercise. One study has shown that diets rich in saturated fatty acids (SFAs) activates the NLRP3 inflammasome and subsequent proinflammatory cytokine production in human and murine macrophages (102). The effects of HFDs on inflammasome regulation in intestinal epithelial cells remain ill-defined, however.

The purpose of this study was to investigate the influence of voluntary wheel running on the gene expression of inflammasome components, including the gene expression of the NLRP3 and NLRP6 sensors, and on the activation of caspase-1 in mice fed normal and HFDs. Our hypotheses were as follows: (1) voluntary wheel running attenuates HFD-induced transcription of the NLRP3 sensor but promotes the expression of the NLRP6 sensor; and (2) voluntary wheel running suppresses HFD-induced caspase-1 activation.

Methods

Animals, Diets and Activity Status

All animals received humane care in compliance with the institution's guidelines, as outlined in the Guide for the Care and Use of Laboratory Animals published by the National Institutes of Health. Experiments were completed at Rutgers University and approved by the Rutgers University Institutional Animal Care and Use Committee (IACUC). Forty-Eight C57BL/6NTac male and female 6-week old mice (Taconic Farms, Germantown, NY) were housed singly in an environmentally controlled room with a 12 hour light/dark cycle and maintained on the specified diet and water *ad libitum*. Animals were acclimated for two weeks before being randomly assigned to one of four groups: (1) control diet sedentary (CDS); (2) very high-fat sedentary (VHFS); (3) control diet running (CDR); and (4) very high-fat running (VHFR). Control diet groups consumed a control low-fat diet (D12450J, 10% kcal from fat, Research Diets, New Brunswick, NJ) and very high-fat groups consumed a high-fat diet (D12492, 60% kcal from fat, Research Diets) which are matched for sucrose and protein content (Table 3.1). Food intake was monitored twice per week and animals were weighed once per week. Specifically, males and females were weighed in separate containers assigned to each sex on a scale designated for body weights only. For food intake, average daily consumption for each treatment group was calculated by dividing total group consumption in grams (g) by the number of animals per group and then by the number of days in between feeding days for each week; g/day were then converted into kcals/day. Animals in the exercise groups had access to a free running wheel while sedentary groups could move freely within their cages, but had no running wheel (Coulbourn Instruments, Allentown, PA). Physical activity was quantified daily using ClockLab (Actimetrics, Wilmette, IL). Rotations per day will be converted into distance ran in meters per day by multiplying by running wheel circumference. At the end of 12 weeks, animals were sacrificed. Female mice were

sacrificed in the metestrus stage of their estrous cycle to ensure low plasma estrogen (E2) as E2 has shown to be a potent modulator of metabolic inflammation (129) and of the inflammatory status in experimental colitis models (130). Estrous cycle was assessed using wet smears on the day of sacrifice as outlined by Caligioni (131). All animals in the study were healthy for the duration of the study. Just prior to sacrifice however, 8 females and 4 males died due to a malfunctioning metabolic chamber and 2 additional females died from an oral glucose tolerance test resulting in an n of 1 for CDS females, an n of 2 for VHFS females and an n of 3 for CDS males.

Western Blot Analysis

Frozen colon samples (20 – 80 mg) were grinded by mortar and pestle in liquid nitrogen and homogenized mechanically in RIPA lysis buffer supplemented with protease and phosphatase inhibitor cocktails (Thermo Fisher Scientific). Samples were then centrifuged at 15,000 x g for 15 min at 4°C. Supernatants were aliquoted and frozen at -80°C until assay. Initial protein quantification of colon lysates was performed using a bicinchoninic acid (BCA) assay (Thermo Fisher Scientific). Equal amounts of protein (25 µg per lane) were loaded and separated by SDS-PAGE. Gels were then transferred to a nitrocellulose membrane using the Mini Gel Tank and Blot Module system (Thermo Fisher Scientific). Membranes were stained for total protein by Ponceau S staining solution (0.5% Ponceau S (w/v), 1% glacial acetic acid (v/v)), rinsed with DI H_2O and then blocked with 5% (w/v) nonfat dried milk or bovine serum albumin (BSA) in 0.1% (v/v) Tween 20 Tris-buffered saline (TTBS) for 1hr at room temperature. Membranes were then incubated overnight at 4°C with primary rabbit affinity purified monoclonal antibodies (Cell Signaling, Danvers, MA) against cleaved caspase-1 (1:500) and caspase-1 (1:1000) in 5% BSA in 0.1% TTBS. Membranes were then incubated for 1 hr at room temperature with a horseradish peroxidase goat anti-rabbit secondary antibody (1:10,000, Cell Signaling). Membranes were developed using an enhanced

chemiluminescence (ECL) detection kit (Thermo Fisher Scientific) and images were taken thereafter. Densitometric analysis of protein bands was performed using Image Studio Lite 5.2 (LI-COR Biosciences, Lincoln, NE) and normalized to total protein. The results are expressed as arbitrary units. Precision Plus Protein™ Kaleidoscope™ Prestained Protein Standard (Bio-Rad, Hercules, CA) was used as a molecular weight standard.

Gene Expression Analysis

RNA was isolated from frozen colon tissue fixed in RNA*later* (Thermo Fisher Scientific) and purified using a RNeasy RNA purification kit (Qiagen, Venlo, Netherlands). RNA concentration and purity were determined by use of the Nanodrop 1000 Spectrophotometer (Thermo Fisher Scientific), followed by cDNA synthesis using 0.5 µg of RNA and the First Strand Kit (Qiagen) according to manufacturer's instructions. The expression of genes of interest were analyzed using quantitative real time-PCR (qRT-PCR) with RT^2 PCR primer assays (Qiagen) using the QuantStudio 3 PCR System (Applied Biosystems) and RT^2 SYBR Green ROX qPCR Mastermix (Qiagen). Ct values were generated and normalized to GAPDH and expressed relative to CDS groups using the $\Delta\Delta$Ct method.

Statistical Analysis

All analyses were performed using IBM SPSS version 25 (IBM Corp., Armonk, NY). Group means of experimental outcomes were analyzed using a one-way ANOVA for each sex with Tukey's post hoc tests as well as a three-way ANOVA for comparisons between factors sex, diet and activity status. A difference of mean with a p value of $\leq$ 0.05 was considered statistically significant.

Results

Gene expression of inflammasome components

In females, increases in the gene expression of PYCARD, casp1, IL-18, NLRP3 and NLRP6 relative to the CDS control were observed in sedentary mice fed an HFD as well as in exercised mice fed either diet (Figure 4.1). For PYCARD, a 2.9 mRNA fold change was observed in VHFS mice; 2.9 in CDX mice; and 2.9 in VHFX mice. For casp1, a 2.6 mRNA fold change was observed in VHFS mice; 3.6 in CDX mice; and 2.9 in CDX mice. For IL-18, a 45.5 mRNA fold change was observed in VHFS mice; 41.2 in CDX mice; and 85.5 in VHFX mice. For NLRP3, a 2.4 mRNA fold change was observed in VHFS mice; 6.7 in CDX mice; and 20.3 in VHFX mice. For NLRP6, a 12.2 mRNA fold change was observed in VHFS mice; 18.6 in CDX mice; and 15.0 in VHFX mice. Between groups, consumption of an HFD suppressed the gene expression of IL-1β compared to sedentary and exercised counterparts (CDX vs VHFS, $p = 0.031$; CDX vs VHFX, $p = 0.072$). In contrast, a non-significant increase in the gene expression of IL-18 in VHFX mice was found compared to CDX mice ($p = 0.084$). Lastly, a gradual increase in the gene expression of NLRP3 was observed with VHFX mice demonstrating the highest mRNA fold change (VHFX vs VHFS, $p = 0.000$; VHFX vs CDX, $p = 0.002$).

In males, significant differences were observed in the gene expression of PYCARD and NLRP3 (Figure 4.1). For PYCARD, significant differences in the mRNA fold change between VHFS and VHFX mice were found (1.4 vs 0.8, $p = 0.023$). For NLRP3, both exercised groups demonstrated a significant increase in mRNA fold change compared to VHFS mice (3.4 in CDX mice and 3.0 in VHFX mice vs 1.3 in VHFS mice, $p = 0.021$ and 0.013).

Cleavage of caspase-1

In females, a non-significant increase in the ratio of cleaved casp1 to casp1 was observed in both exercised groups compared to sedentary mice on either diet (Figure

4.2). In contrast, a modest but non-significant decrease in the ratio was observed in both male exercised groups compare to sedentary mice on either diet. No significant effect of any independent factor was observed for the ratio of cleaved casp1 to casp1 (Table. 4.1).

Discussion

The present study sought to examine the impact of excess dietary fat consumption and voluntary wheel running on the gene expression of inflammasome components, including the NLRP3 and NLRP6 sensors, as well as on the activation of caspase-1. In contrast to our first hypothesis, we observed marked increases in all inflammasome components in sedentary high-fat fed female mice and in exercised female mice fed either diet. These mice demonstrated a concomitant, albeit non-significant, increase in caspase-1 activation. Moreover, HFDs suppressed the transcription of IL-1β but increased the transcription of IL-18 as did voluntary wheel running. In males, voluntary wheel running increased the gene expression of the NLRP3 sensor as opposed NLRP6 but modestly suppressed the activation of caspase-1 in mice fed either diet.

The NLRP3 inflammasome has been implicated in the pathogenesis of IBD (70) but recent findings indicate that it possess both pathogenic and anti-inflammatory properties as well. Specifically, studies have shown that mice with deficiencies in the sensor NLRP3, in the adaptor PYCARD or in caspase-1 present more sever experimental colitis (182, 183). In addition, findings by Yao et al. indicate that hyperactivation of the NLRP3 inflammasome may confer a protective advantage against experimentally induced colitis in mice (184). Alternatively, the NRLP6 inflammasome has shown to be critical for the maintenance of colonic homeostasis (10, 87). In the present study, we observed an increase the gene expression of the NLRP3 and NLRP6 sensors

in sedentary female mice fed an HFD and in exercised female mice consuming either diet. However, a non-significant increase in the activation of caspase-1 was observed only in exercised female mice suggesting that voluntary wheel running may potentiate an additional therapeutic effect in the colon by activating either the NLRP3 or NLRP6 inflammasome or both. Moreover, it is interesting that HFDs suppressed the gene expression of IL-1β but increased the expression of IL-18 as did voluntary wheel running. As protein concentrations of IL-18 and IL-1β were not assessed, it is difficult to ascertain the implications of these findings though IL-18 equilibrium has been implicated in the governance of mucosal barrier function in experimental colitis (185) and maturation of IL-18 is required for the NLRP6 inflammasome antimicrobial axis (87). In males, the opposite was observed in which voluntary wheel running increased the gene expression of the NLRP3 sensor but modestly reduced the activation of caspase-1. Together, these results suggest that voluntary wheel running may promote intestinal homeostasis in female mice by increasing the activity of both the NRLP3 and NLRP6 inflammasome or attenuate NLRP3 inflammasome activation in male mice despite displaying an increase in the gene expression of the NLRP3 sensor. The lack of statistical significance in our assessment of caspase-1 activation suggests that the above insight is only speculative, however. The causal factors behind these sex-specific differences as well as the effect of exercise on inflammasome activity remain elusive and require more rigorous analyses.

Conclusions

In all, the results of the present study provide new insight into the potential role of exercise in modulating inflammasome activity. Our findings also indicated that female mice may be more susceptible to regulation of inflammasome activity via exercise. Still however, the etiological factors that differentiate the NLRP3 inflammasome from its

pathogenic or protective activity are not well characterized. Further, the extent to which physical exercise modulates innate immune function via inflammasomes to promote (or disrupt) intestinal homeostasis is wholly unexplored.

Table 4.1. Analysis of caspase-1 cleavage by independent factors in mouse colon.

pairwise comparisons

parameter	activity status (AS)			diet (D)			sex (S)		
	sedentary	*exercise*	mean difference	*control 10% fat*	*very high 60% fat*	mean difference	*female*	*male*	mean difference
c-casp1/casp1[a]	0.8 ± 1.0	1.8 ± 0.6	-1.0 ± 1.1	1.5 ± 0.9	1.1 ± 0.7	0.4 ± 1.1	1.9 ± 0.9	0.7 ± 0.7	1.2 ± 1.1

3-way ANOVA *p*-values

parameter	AS	D	S	AS x D	AS x S	D x S	AS x D x S
c-casp1/casp1[a]	0.360	0.736	0.300	0.872	0.225	0.587	0.890

Values of each parameter are expressed the mean ± SEM. [a]Expressed as the ratio of normalized densities (to total protein) of c-casp1 to casp1. Casp1 (c-), caspase-1 (cleaved).

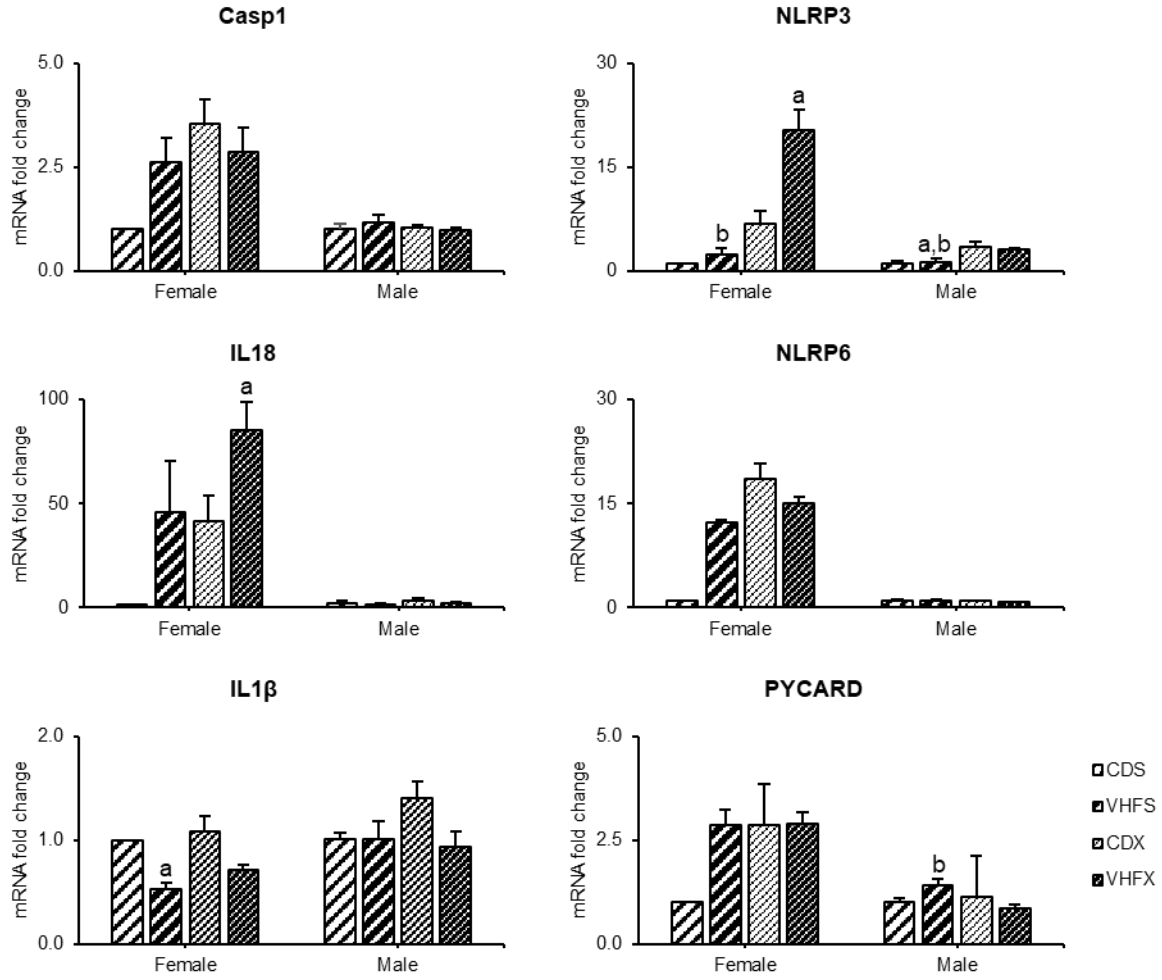

Figure 4.1. Effects of diet and voluntary wheel running on relative gene expression of the NLRP3 and NLRP6 inflammasomes in colon. Relative gene expression of inflammasome components and related cytokines following 12 weeks of treatment with control diet sedentary (CDS), very high-fat diet sedentary (VHFS), control diet exercise (CDX) and very high-fat diet running (VHFX) in female and male mice colon. Values are expressed as the fold change relative to CDS groups ± SEM, n = 1-7 mice/group. One-way ANOVA with Tukey's post-test for CDS vs VHFS; CDS vs CDX; CDS vs VHFX; VHFS vs CDX; VHFS vs VHFX and CDX vs VHFX for ΔCt values. ΔCt was calculated as $Ct_{target} - Ct_{reference}$. a, p = ≤ 0.05 compared to CDX; b, p = ≤ 0.05 compared to VHFX. Casp1; caspase-1; IL-18, interleukin-18; IL-1β, interleukin-beta; NLRP3 & 6, NOD-like receptor family pyrin domain containing 3 or 6; PYCARD, PYD and CARD domain containing.

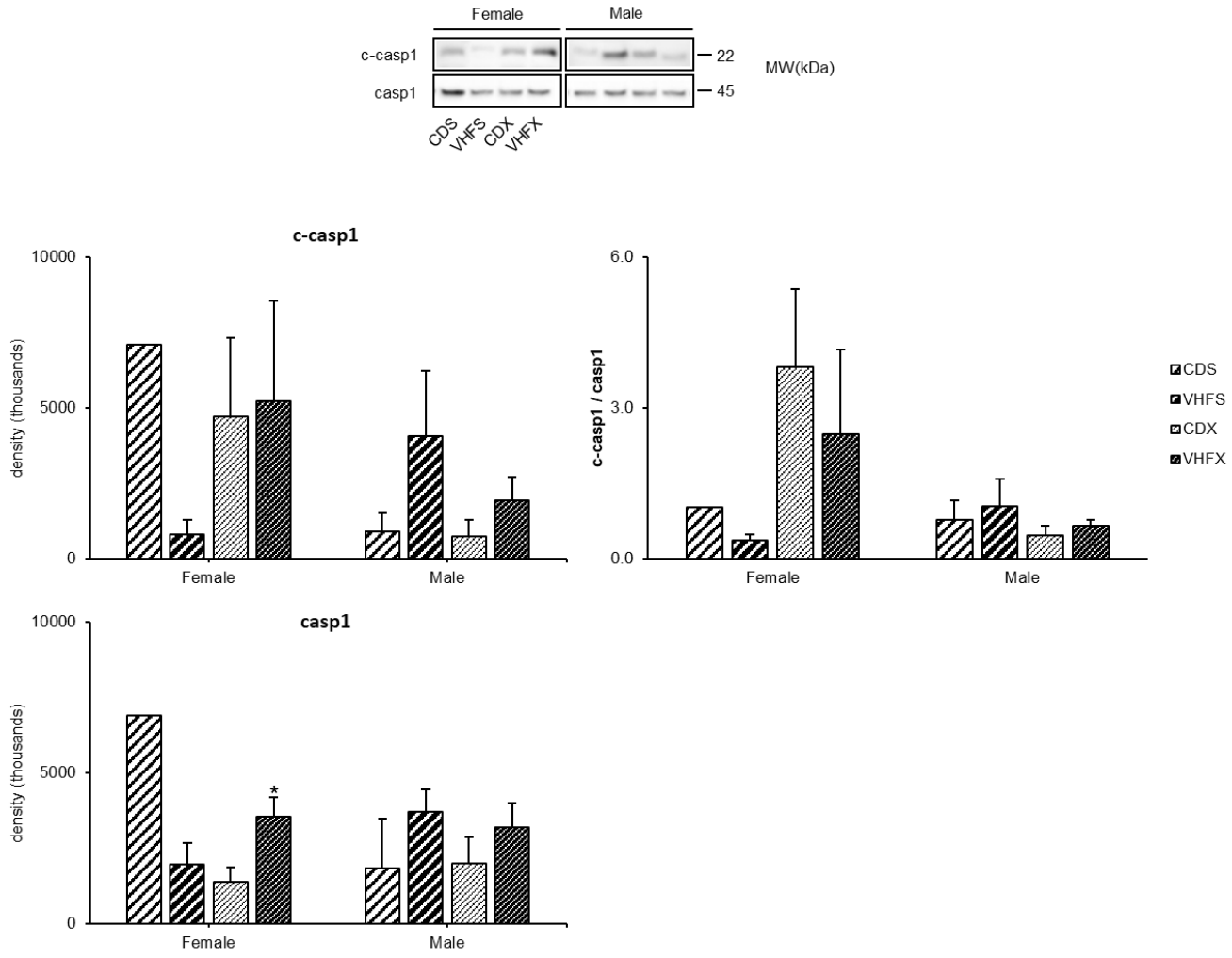

Figure 4.2. Effects of diet and voluntary wheel running on cleavage of casp1 in colon. Immunoblotting with antibodies for c-casp1 and casp1 following SDS-PAGE of colon lysates after 12 weeks of treatment with control diet sedentary (CDS), very high-fat diet sedentary (VHFS), control diet exercise (CDX) and very high-fat diet exercise (VHFX). Densities are expressed normalized to total protein as determined by ponceau S staining ± SEM, n = 1-7 mice/group. Ratio of normalized densities between c-casp1 and casp1 ± SEM. One-way ANOVA with Tukey's post-test for CDS vs HFS; CDS vs CDX; CDS vs VHFX; HFS vs CDX; VHFS vs VHFX and CDX vs VHFX for normalized densities and ratios. C-casp1, cleaved caspase-1; casp1, caspase-1.

General Discussion

Summary & Conclusions

The aim of Chapter 2 was to examine the extent to which 12 weeks of a 45% HFD and voluntary wheel running effect colon inflammation and microbiota localization, as measured by inner mucus layer thickness, in 6-week-old male and female C57BL/6NTac mice. Emerging evidence suggests that inflammatory status of the intestine appears to respond to and regulate the proximity and identity of gut microbes closest to the epithelium (95, 140-142). We therefore hypothesized that voluntary wheel running would attenuate HFD-induced colon inflammation and that consumption of an HFD results in the localization of the microbiota closer to the epithelial surface but is rescued by voluntary wheel running. We found voluntary wheel running to attenuate HFD-induced colon inflammation in female mice only and no significant differences in inner mucus layer thickness, challenging our initial hypothesis. Interestingly, sedentary males fed a control 10% fat diet demonstrated a similar degree of inflammation to that of their high-fat fed counterparts; this was not observed in females. These results indicate that there are distinct sex differences in colon inflammation in the absence of excess dietary fat intake suggesting an inherent protective benefit in female mice. Further, the lack of attenuation of inflammation in exercised high-fat fed male mice may be due to differences in exercise volume as females tend to adhere better to running wheels relative to their male counterparts (148).

The aims of Chapter 3 were to replicate aim 1 in a second cohort of 6-week-old male and female C57BL/6NTac mice but utilize a 60% HFD instead and employ additional measures of inflammatory status. Numerous high-fat feeding studies have employed a range of fat content in murine models of diet-induced inflammation, ranging from 45% to 72% weeks (78, 143, 144, 186). We chose 60% to compare our previous findings using a 45% HFD, to potentially accelerate the advent of overt colon pathologies

and to model a similar study that showed a reduction in mucus thickness using a 60% HFD (92). Additionally, we wanted to examine the impact of our dietary and exercise interventions on the induction of the UPR and colonic epithelial ER stress. In the colon the proportion of goblet cells, a secretory epithelial cell type, is increased (27). Given the high secretory rate of these cells as well as the myriad of secretory products produced to maintain intestinal homeostasis, it was surmised that HFD-induced colon inflammation would impose a heightened secretory burden to restore intestinal homeostasis and thus provoke ER stress. Taken together, we hypothesized that 60% HFD would result in the gut microbiota localizing closer to epithelial surface due to a thinner inner mucus layer and that this would be prevented by voluntary wheel running. We also hypothesized that voluntary wheel running would increase IL-10 production concomitantly with a reduction in mucosal inflammation and attenuate HFD-induced upregulation of the UPR gene expression. In contrast to our first hypothesis, we discovered a unique compensatory response in males characterized by a thickening of the inner mucus layer and an increase in muc2 production. In agreement with the findings of aim 1, we again found that sedentary male mice consuming a control 10% fat diet exhibited a similar degree of colon inflammation to that of their high-fat fed counterparts but in contrast, voluntary wheel running attenuated HFD-induced colon inflammation in both male and female mice suggesting that dietary sucrose content may have mediated these discrepant findings. Interestingly, we observed that female mice had an inherent increase in IL-10 compared to males further supporting the notion that females have a decreased propensity to colon pathologies. In contrast to our initial hypothesis, we observed a modest suppression in the gene expression of ER stress sensors ATF6 and IRE1β in female mice fed a HFD but no significant changes in the phosphorylation of eIF2α, which acts to arrest protein translation in the advent of ER stress (53), were observed. In contrast, a 60% HFD increased the phosphorylation of eIF2α in sedentary male mice but

this response was prevented with a control 10% fat diet or voluntary wheel running. These findings illustrate that male mice are more susceptible to HFD-induced ER stress but highlight, for the first time, that voluntary wheel running can attenuate HFD-induced ER stress in the colon.

The aims of Chapter 4 were to examine the impact of dietary fat and voluntary wheel running on the gene expression of inflammasome components and the activation of caspase-1 in the same cohort of animals from Chapter 3. Inflammasomes are comprised of three components: a sensor (e.g., NLRP), an adaptor (e.g., Pycard) and an inflammatory caspase (e.g., caspase-1) (72). Together, these components act as a staging platform for the activation of an inflammatory caspase and constitute an innate immune mechanism that contributes to a microbe-host mutualism or dysfunction. Our primary interest was the NLRP3 inflammasome which has been implicated in the pathogenesis of IBD (70) as well as the NLRP6 inflammasome which has shown to contribute extensively to the maintenance of colonic homeostasis (84). We hypothesized that voluntary wheel running would attenuate HFD-induced transcription of the NLRP3 sensor but promote the expression of the NLRP6 sensor and suppress HFD-induced caspase-1 activation. In partial fulfillment of our initial hypothesis, we observed marked increases in the gene expression of inflammasome components, including both the NLRP3 and NLRP6 sensor, in sedentary female mice fed an HFD and in exercised female mice fed either diet. Further, a non-significant increase in the activation of caspase-1, as determined by the ratio of cleaved caspase-1 to caspase-1, was observed in exercised female mice. In contrast, voluntary wheel running increased the gene expression of the NRLP3 sensor in exercised male mice fed either diet but resulted in a modest and non-significant decrease in the activation of caspase-1. Given the anti-inflammatory effects of voluntary wheel running demonstrated in Chapter 2 and 3, as

well as the inherent resistance to colon pathologies in females, these results suggest that exercise in females may confer an additional benefit to colon health via the activation of both the NLRP3 and NLRP6 inflammasomes. The non-significant findings in the activation of caspase-1 do demand caution, however. In summary, the findings from this dissertation highlight novel mechanisms by which exercise promotes colon health and attenuates HFD-induced colon pathologies. We have also demonstrated distinct sex differences in inflammation severity and disease risk stressing the contribution of sex as an outcome of disease. The complex interactions between sex, diet and activity status on intestinal homeostasis require further exploration as well as the extent to which these factors contribute to a host-microbe mutualism in the preservation of human health.

Literature Cited

1. Nicholson JK, Holmes E, Kinross J, Burcelin R, Gibson G, Jia W, Pettersson S. 2012. Host-gut microbiota metabolic interactions. *Science* 336: 1262-7

2. Helander HF, Fandriks L. 2014. Surface area of the digestive tract - revisited. *Scand J Gastroenterol* 49: 681-9

3. Mowat AM, Agace WW. 2014. Regional specialization within the intestinal immune system. *Nat Rev Immunol* 14: 667-85

4. Mathers CD, Boerma T, Ma Fat D. 2009. Global and regional causes of death. *Br Med Bull* 92: 7-32

5. Hooper LV, Macpherson AJ. 2010. Immune adaptations that maintain homeostasis with the intestinal microbiota. *Nat Rev Immunol* 10: 159-69

6. Marillier RG, Michels C, Smith EM, Fick LC, Leeto M, Dewals B, Horsnell WG, Brombacher F. 2008. IL-4/IL-13 independent goblet cell hyperplasia in experimental helminth infections. *BMC Immunol* 9: 11

7. Oeser K, Schwartz C, Voehringer D. 2015. Conditional IL-4/IL-13-deficient mice reveal a critical role of innate immune cells for protective immunity against gastrointestinal helminths. *Mucosal Immunol* 8: 672-82

8. Turner JE, Stockinger B, Helmby H. 2013. IL-22 mediates goblet cell hyperplasia and worm expulsion in intestinal helminth infection. *PLoS Pathog* 9: e1003698

9. Kondo M, Tamaoki J, Takeyama K, Nakata J, Nagai A. 2002. Interleukin-13 induces goblet cell differentiation in primary cell culture from Guinea pig tracheal epithelium. *Am J Respir Cell Mol Biol* 27: 536-41

10. Wlodarska M, Thaiss CA, Nowarski R, Henao-Mejia J, Zhang JP, Brown EM, Frankel G, Levy M, Katz MN, Philbrick WM, Elinav E, Finlay BB, Flavell RA. 2014. NLRP6 inflammasome orchestrates the colonic host-microbial interface by regulating goblet cell mucus secretion. *Cell* 156: 1045-59

11. Sheng YH, Triyana S, Wang R, Das I, Gerloff K, Florin TH, Sutton P, McGuckin MA. 2013. MUC1 and MUC13 differentially regulate epithelial inflammation in response to inflammatory and infectious stimuli. *Mucosal Immunol* 6: 557-68

12. Turner JR. 2009. Intestinal mucosal barrier function in health and disease. *Nat Rev Immunol* 9: 799-809

13. Gum JR, Jr., Hicks JW, Toribara NW, Siddiki B, Kim YS. 1994. Molecular cloning of human intestinal mucin (MUC2) cDNA. Identification of the amino terminus and overall sequence similarity to prepro-von Willebrand factor. *J Biol Chem* 269: 2440-6

14. Perez-Vilar J, Hill RL. 1999. The structure and assembly of secreted mucins. *J Biol Chem* 274: 31751-4

15. Lang T, Hansson GC, Samuelsson T. 2007. Gel-forming mucins appeared early in metazoan evolution. *Proc Natl Acad Sci U S A* 104: 16209-14

16. Johansson ME, Larsson JM, Hansson GC. 2011. The two mucus layers of colon are organized by the MUC2 mucin, whereas the outer layer is a legislator of host-microbial interactions. *Proc Natl Acad Sci U S A* 108 Suppl 1: 4659-65

17. Ambort D, Johansson ME, Gustafsson JK, Nilsson HE, Ermund A, Johansson BR, Koeck PJ, Hebert H, Hansson GC. 2012. Calcium and pH-dependent packing and release of the gel-forming MUC2 mucin. *Proc Natl Acad Sci U S A* 109: 5645-50

18. Shan M, Gentile M, Yeiser JR, Walland AC, Bornstein VU, Chen K, He B, Cassis L, Bigas A, Cols M, Comerma L, Huang B, Blander JM, Xiong H, Mayer L, Berin C, Augenlicht LH, Velcich A, Cerutti A. 2013. Mucus enhances gut homeostasis and oral tolerance by delivering immunoregulatory signals. *Science* 342: 447-53

19. Ermund A, Schutte A, Johansson ME, Gustafsson JK, Hansson GC. 2013. Studies of mucus in mouse stomach, small intestine, and colon. I. Gastrointestinal mucus layers have different properties depending on location as well as over the Peyer's patches. *Am J Physiol Gastrointest Liver Physiol* 305: G341-7

20. Johansson ME, Hansson GC. 2011. Microbiology. Keeping bacteria at a distance. *Science* 334: 182-3

21. Macpherson AJ, Uhr T. 2004. Induction of protective IgA by intestinal dendritic cells carrying commensal bacteria. *Science* 303: 1662-5

22. Rescigno M, Urbano M, Valzasina B, Francolini M, Rotta G, Bonasio R, Granucci F, Kraehenbuhl JP, Ricciardi-Castagnoli P. 2001. Dendritic cells express tight junction proteins and penetrate gut epithelial monolayers to sample bacteria. *Nat Immunol* 2: 361-7

23. Niess JH, Brand S, Gu X, Landsman L, Jung S, McCormick BA, Vyas JM, Boes M, Ploegh HL, Fox JG, Littman DR, Reinecker HC. 2005. CX3CR1-mediated dendritic cell access to the intestinal lumen and bacterial clearance. *Science* 307: 254-8

24. Suzuki K, Meek B, Doi Y, Muramatsu M, Chiba T, Honjo T, Fagarasan S. 2004. Aberrant expansion of segmented filamentous bacteria in IgA-deficient gut. *Proc Natl Acad Sci U S A* 101: 1981-6

25. Macpherson AJ, Gatto D, Sainsbury E, Harriman GR, Hengartner H, Zinkernagel RM. 2000. A primitive T cell-independent mechanism of intestinal mucosal IgA responses to commensal bacteria. *Science* 288: 2222-6

26. Cunliffe RN, Mahida YR. 2004. Expression and regulation of antimicrobial peptides in the gastrointestinal tract. *J Leukoc Biol* 75: 49-58

27. Karam SM. 1999. Lineage commitment and maturation of epithelial cells in the gut. *Front Biosci* 4: D286-98

28. Johansson ME, Phillipson M, Petersson J, Velcich A, Holm L, Hansson GC. 2008. The inner of the two Muc2 mucin-dependent mucus layers in colon is devoid of bacteria. *Proc Natl Acad Sci U S A* 105: 15064-9

29. Atuma C, Strugala V, Allen A, Holm L. 2001. The adherent gastrointestinal mucus gel layer: thickness and physical state in vivo. *Am J Physiol Gastrointest Liver Physiol* 280: G922-9

30. Nystrom EEL, Birchenough GMH, van der Post S, Arike L, Gruber AD, Hansson GC, Johansson MEV. 2018. Calcium-activated Chloride Channel Regulator 1 (CLCA1) Controls Mucus Expansion in Colon by Proteolytic Activity. *EBioMedicine* 33: 134-43

31. Birchenough GM, Johansson ME, Gustafsson JK, Bergstrom JH, Hansson GC. 2015. New developments in goblet cell mucus secretion and function. *Mucosal Immunol* 8: 712-9

32. Lee SH, Starkey PM, Gordon S. 1985. Quantitative analysis of total macrophage content in adult mouse tissues. Immunochemical studies with monoclonal antibody F4/80. *J Exp Med* 161: 475-89

33. Kelsall B. 2008. Recent progress in understanding the phenotype and function of intestinal dendritic cells and macrophages. *Mucosal Immunol* 1: 460-9

34. Pull SL, Doherty JM, Mills JC, Gordon JI, Stappenbeck TS. 2005. Activated macrophages are an adaptive element of the colonic epithelial

progenitor niche necessary for regenerative responses to injury. *Proc Natl Acad Sci U S A* 102: 99-104

35. Okumura R, Takeda K. 2017. Roles of intestinal epithelial cells in the maintenance of gut homeostasis. *Exp Mol Med* 49: e338

36. Borges da Silva H, Fonseca R, Pereira RM, Cassado Ados A, Alvarez JM, D'Imperio Lima MR. 2015. Splenic Macrophage Subsets and Their Function during Blood-Borne Infections. *Front Immunol* 6: 480

37. Gowans JL, Knight EJ. 1964. The Route of Re-Circulation of Lymphocytes in the Rat. *Proc R Soc Lond B Biol Sci* 159: 257-82

38. Husband AJ, Gowans JL. 1978. The origin and antigen-dependent distribution of IgA-containing cells in the intestine. *J Exp Med* 148: 1146-60

39. Pierce NF, Gowans JL. 1975. Cellular kinetics of the intestinal immune response to cholera toxoid in rats. *J Exp Med* 142: 1550-63

40. Abraham C, Cho JH. 2009. Inflammatory bowel disease. *N Engl J Med* 361: 2066-78

41. Tytgat KM, van der Wal JW, Einerhand AW, Buller HA, Dekker J. 1996. Quantitative analysis of MUC2 synthesis in ulcerative colitis. *Biochem Biophys Res Commun* 224: 397-405

42. Van Klinken BJ, Van der Wal JW, Einerhand AW, Buller HA, Dekker J. 1999. Sulphation and secretion of the predominant secretory human colonic mucin MUC2 in ulcerative colitis. *Gut* 44: 387-93

43. Velcich A, Yang W, Heyer J, Fragale A, Nicholas C, Viani S, Kucherlapati R, Lipkin M, Yang K, Augenlicht L. 2002. Colorectal cancer in mice genetically deficient in the mucin Muc2. *Science* 295: 1726-9

44. Van der Sluis M, De Koning BA, De Bruijn AC, Velcich A, Meijerink JP, Van Goudoever JB, Buller HA, Dekker J, Van Seuningen I, Renes IB, Einerhand AW. 2006. Muc2-deficient mice spontaneously develop colitis, indicating that MUC2 is critical for colonic protection. *Gastroenterology* 131: 117-29

45. Bu X, Li L, Li N, Tian X, Huang P. 2011. Suppression of mucin 2 enhances the proliferation and invasion of LS174T human colorectal cancer cells. *Cell Biol Int* 35: 1121-9

46. Shan YS, Hsu HP, Lai MD, Yen MC, Fang JH, Weng TY, Chen YL. 2014. Suppression of mucin 2 promotes interleukin-6 secretion and tumor

growth in an orthotopic immune-competent colon cancer animal model. *Oncol Rep* 32: 2335-42

47. Bergstrom KS, Kissoon-Singh V, Gibson DL, Ma C, Montero M, Sham HP, Ryz N, Huang T, Velcich A, Finlay BB, Chadee K, Vallance BA. 2010. Muc2 protects against lethal infectious colitis by disassociating pathogenic and commensal bacteria from the colonic mucosa. *PLoS Pathog* 6: e1000902

48. Sands BE, Podolsky DK. 1996. The trefoil peptide family. *Annu Rev Physiol* 58: 253-73

49. Luo K, Cao SS. 2015. Endoplasmic reticulum stress in intestinal epithelial cell function and inflammatory bowel disease. *Gastroenterol Res Pract* 2015: 328791

50. Leamy AK, Egnatchik RA, Young JD. 2013. Molecular mechanisms and the role of saturated fatty acids in the progression of non-alcoholic fatty liver disease. *Prog Lipid Res* 52: 165-74

51. McGuckin MA, Eri RD, Das I, Lourie R, Florin TH. 2010. ER stress and the unfolded protein response in intestinal inflammation. *Am J Physiol Gastrointest Liver Physiol* 298: G820-32

52. Bernales S, McDonald KL, Walter P. 2006. Autophagy counterbalances endoplasmic reticulum expansion during the unfolded protein response. *PLoS Biol* 4: e423

53. Fribley A, Zhang K, Kaufman RJ. 2009. Regulation of apoptosis by the unfolded protein response. *Methods Mol Biol* 559: 191-204

54. Hetz C. 2012. The unfolded protein response: controlling cell fate decisions under ER stress and beyond. *Nat Rev Mol Cell Biol* 13: 89-102

55. Kozutsumi Y, Segal M, Normington K, Gething MJ, Sambrook J. 1988. The presence of malfolded proteins in the endoplasmic reticulum signals the induction of glucose-regulated proteins. *Nature* 332: 462-4

56. Harding HP, Zhang Y, Bertolotti A, Zeng H, Ron D. 2000. Perk is essential for translational regulation and cell survival during the unfolded protein response. *Mol Cell* 5: 897-904

57. Kim I, Xu W, Reed JC. 2008. Cell death and endoplasmic reticulum stress: disease relevance and therapeutic opportunities. *Nat Rev Drug Discov* 7: 1013-30

58. Oyadomari S, Mori M. 2004. Roles of CHOP/GADD153 in endoplasmic reticulum stress. *Cell Death Differ* 11: 381-9

59. Tirasophon W, Welihinda AA, Kaufman RJ. 1998. A stress response pathway from the endoplasmic reticulum to the nucleus requires a novel bifunctional protein kinase/endoribonuclease (Ire1p) in mammalian cells. *Genes Dev* 12: 1812-24

60. Wang XZ, Harding HP, Zhang Y, Jolicoeur EM, Kuroda M, Ron D. 1998. Cloning of mammalian Ire1 reveals diversity in the ER stress responses. *EMBO J* 17: 5708-17

61. Lee K, Tirasophon W, Shen X, Michalak M, Prywes R, Okada T, Yoshida H, Mori K, Kaufman RJ. 2002. IRE1-mediated unconventional mRNA splicing and S2P-mediated ATF6 cleavage merge to regulate XBP1 in signaling the unfolded protein response. *Genes Dev* 16: 452-66

62. Olivari S, Molinari M. 2007. Glycoprotein folding and the role of EDEM1, EDEM2 and EDEM3 in degradation of folding-defective glycoproteins. *FEBS Lett* 581: 3658-64

63. Haze K, Yoshida H, Yanagi H, Yura T, Mori K. 1999. Mammalian transcription factor ATF6 is synthesized as a transmembrane protein and activated by proteolysis in response to endoplasmic reticulum stress. *Mol Biol Cell* 10: 3787-99

64. Thuerauf DJ, Morrison L, Glembotski CC. 2004. Opposing roles for ATF6alpha and ATF6beta in endoplasmic reticulum stress response gene induction. *J Biol Chem* 279: 21078-84

65. Johansson ME. 2012. Fast renewal of the distal colonic mucus layers by the surface goblet cells as measured by in vivo labeling of mucin glycoproteins. *PLoS One* 7: e41009

66. Taupin D, Podolsky DK. 2003. Trefoil factors: initiators of mucosal healing. *Nat Rev Mol Cell Biol* 4: 721-32

67. Hogan SP, Seidu L, Blanchard C, Groschwitz K, Mishra A, Karow ML, Ahrens R, Artis D, Murphy AJ, Valenzuela DM, Yancopoulos GD, Rothenberg ME. 2006. Resistin-like molecule beta regulates innate colonic function: barrier integrity and inflammation susceptibility. *J Allergy Clin Immunol* 118: 257-68

68. Johansson ME, Thomsson KA, Hansson GC. 2009. Proteomic analyses of the two mucus layers of the colon barrier reveal that their main component, the Muc2 mucin, is strongly bound to the Fcgbp protein. *J Proteome Res* 8: 3549-57

69. Ma X, Dai Z, Sun K, Zhang Y, Chen J, Yang Y, Tso P, Wu G, Wu Z. 2017. Intestinal Epithelial Cell Endoplasmic Reticulum Stress and Inflammatory Bowel Disease Pathogenesis: An Update Review. *Front Immunol* 8: 1271

70. Zmora N, Levy M, Pevsner-Fishcer M, Elinav E. 2017. Inflammasomes and intestinal inflammation. *Mucosal Immunol* 10: 865-83

71. Abreu MT. 2010. Toll-like receptor signalling in the intestinal epithelium: how bacterial recognition shapes intestinal function. *Nat Rev Immunol* 10: 131-44

72. Elinav E, Henao-Mejia J, Flavell RA. 2013. Integrative inflammasome activity in the regulation of intestinal mucosal immune responses. *Mucosal Immunol* 6: 4-13

73. Martinon F, Burns K, Tschopp J. 2002. The inflammasome: a molecular platform triggering activation of inflammatory caspases and processing of proIL-beta. *Mol Cell* 10: 417-26

74. Lamkanfi M, Dixit VM. 2014. Mechanisms and functions of inflammasomes. *Cell* 157: 1013-22

75. Zaki MH, Lamkanfi M, Kanneganti TD. 2011. The Nlrp3 inflammasome: contributions to intestinal homeostasis. *Trends Immunol* 32: 171-9

76. Shimada K, Crother TR, Karlin J, Dagvadorj J, Chiba N, Chen S, Ramanujan VK, Wolf AJ, Vergnes L, Ojcius DM, Rentsendorj A, Vargas M, Guerrero C, Wang Y, Fitzgerald KA, Underhill DM, Town T, Arditi M. 2012. Oxidized mitochondrial DNA activates the NLRP3 inflammasome during apoptosis. *Immunity* 36: 401-14

77. Murakami T, Ockinger J, Yu J, Byles V, McColl A, Hofer AM, Horng T. 2012. Critical role for calcium mobilization in activation of the NLRP3 inflammasome. *Proc Natl Acad Sci U S A* 109: 11282-7

78. Gulhane M, Murray L, Lourie R, Tong H, Sheng YH, Wang R, Kang A, Schreiber V, Wong KY, Magor G, Denman S, Begun J, Florin TH, Perkins A, Cuiv PO, McGuckin MA, Hasnain SZ. 2016. High Fat Diets Induce Colonic Epithelial Cell Stress and Inflammation that is Reversed by IL-22. *Sci Rep* 6: 28990

79. Campbell SC, Wisniewski PJ, Noji M, McGuinness LR, Haggblom MM, Lightfoot SA, Joseph LB, Kerkhof LJ. 2016. The Effect of Diet and Exercise on Intestinal Integrity and Microbial Diversity in Mice. *PLoS One* 11: e0150502

80. Normand S, Delanoye-Crespin A, Bressenot A, Huot L, Grandjean T, Peyrin-Biroulet L, Lemoine Y, Hot D, Chamaillard M. 2011. Nod-like receptor pyrin domain-containing protein 6 (NLRP6) controls epithelial self-renewal and colorectal carcinogenesis upon injury. *Proc Natl Acad Sci U S A* 108: 9601-6

81. Gremel G, Wanders A, Cedernaes J, Fagerberg L, Hallstrom B, Edlund K, Sjostedt E, Uhlen M, Ponten F. 2015. The human gastrointestinal tract-specific transcriptome and proteome as defined by RNA sequencing and antibody-based profiling. *J Gastroenterol* 50: 46-57

82. Birchenough GM, Nystrom EE, Johansson ME, Hansson GC. 2016. A sentinel goblet cell guards the colonic crypt by triggering Nlrp6-dependent Muc2 secretion. *Science* 352: 1535-42

83. Anand PK, Kanneganti TD. 2012. Targeting NLRP6 to enhance immunity against bacterial infections. *Future Microbiol* 7: 1239-42

84. Elinav E, Strowig T, Kau AL, Henao-Mejia J, Thaiss CA, Booth CJ, Peaper DR, Bertin J, Eisenbarth SC, Gordon JI, Flavell RA. 2011. NLRP6 inflammasome regulates colonic microbial ecology and risk for colitis. *Cell* 145: 745-57

85. Henao-Mejia J, Elinav E, Jin C, Hao L, Mehal WZ, Strowig T, Thaiss CA, Kau AL, Eisenbarth SC, Jurczak MJ, Camporez JP, Shulman GI, Gordon JI, Hoffman HM, Flavell RA. 2012. Inflammasome-mediated dysbiosis regulates progression of NAFLD and obesity. *Nature* 482: 179-85

86. Ikuta T, Kobayashi Y, Kitazawa M, Shiizaki K, Itano N, Noda T, Pettersson S, Poellinger L, Fujii-Kuriyama Y, Taniguchi S, Kawajiri K. 2013. ASC-associated inflammation promotes cecal tumorigenesis in aryl hydrocarbon receptor-deficient mice. *Carcinogenesis* 34: 1620-7

87. Levy M, Thaiss CA, Zeevi D, Dohnalova L, Zilberman-Schapira G, Mahdi JA, David E, Savidor A, Korem T, Herzig Y, Pevsner-Fischer M, Shapiro H, Christ A, Harmelin A, Halpern Z, Latz E, Flavell RA, Amit I, Segal E, Elinav E. 2015. Microbiota-Modulated Metabolites Shape the Intestinal Microenvironment by Regulating NLRP6 Inflammasome Signaling. *Cell* 163: 1428-43

88. Ng M, Fleming T, Robinson M, Thomson B, Graetz N, et al. 2014. Global, regional, and national prevalence of overweight and obesity in children and adults during 1980-2013: a systematic analysis for the Global Burden of Disease Study 2013. *Lancet* 384: 766-81

89. Singh S, Dulai PS, Zarrinpar A, Ramamoorthy S, Sandborn WJ. 2017. Obesity in IBD: epidemiology, pathogenesis, disease course and treatment outcomes. *Nat Rev Gastroenterol Hepatol* 14: 110-21

90. Aleksandrova K, Boeing H, Jenab M, Bas Bueno-de-Mesquita H, Jansen E, van Duijnhoven FJ, Fedirko V, Rinaldi S, Romieu I, Riboli E, Romaguera D, Overvad K, Ostergaard JN, Olsen A, Tjonneland A, Boutron-Ruault MC, Clavel-Chapelon F, Morois S, Masala G, Agnoli C, Panico S, Tumino R, Vineis P, Kaaks R, Lukanova A, Trichopoulou A,

Naska A, Bamia C, Peeters PH, Rodriguez L, Buckland G, Sanchez MJ, Dorronsoro M, Huerta JM, Barricarte A, Hallmans G, Palmqvist R, Khaw KT, Wareham N, Allen NE, Tsilidis KK, Pischon T. 2011. Metabolic syndrome and risks of colon and rectal cancer: the European prospective investigation into cancer and nutrition study. *Cancer Prev Res (Phila)* 4: 1873-83

91. Gruber L, Kisling S, Lichti P, Martin FP, May S, Klingenspor M, Lichtenegger M, Rychlik M, Haller D. 2013. High fat diet accelerates pathogenesis of murine Crohn's disease-like ileitis independently of obesity. *PLoS One* 8: e71661

92. Everard A, Belzer C, Geurts L, Ouwerkerk JP, Druart C, Bindels LB, Guiot Y, Derrien M, Muccioli GG, Delzenne NM, de Vos WM, Cani PD. 2013. Cross-talk between Akkermansia muciniphila and intestinal epithelium controls diet-induced obesity. *Proc Natl Acad Sci U S A* 110: 9066-71

93. Schroeder BO, Birchenough GMH, Stahlman M, Arike L, Johansson MEV, Hansson GC, Backhed F. 2018. Bifidobacteria or Fiber Protects against Diet-Induced Microbiota-Mediated Colonic Mucus Deterioration. *Cell Host Microbe* 23: 27-40 e7

94. Van Soest PJ, Robertson JB, Lewis BA. 1991. Methods for dietary fiber, neutral detergent fiber, and nonstarch polysaccharides in relation to animal nutrition. *J Dairy Sci* 74: 3583-97

95. Johansson ME, Gustafsson JK, Holmen-Larsson J, Jabbar KS, Xia L, Xu H, Ghishan FK, Carvalho FA, Gewirtz AT, Sjovall H, Hansson GC. 2014. Bacteria penetrate the normally impenetrable inner colon mucus layer in both murine colitis models and patients with ulcerative colitis. *Gut* 63: 281-91

96. Madsen J, Mollenhauer J, Holmskov U. 2010. Review: Gp-340/DMBT1 in mucosal innate immunity. *Innate Immun* 16: 160-7

97. Heazlewood CK, Cook MC, Eri R, Price GR, Tauro SB, Taupin D, Thornton DJ, Png CW, Crockford TL, Cornall RJ, Adams R, Kato M, Nelms KA, Hong NA, Florin TH, Goodnow CC, McGuckin MA. 2008. Aberrant mucin assembly in mice causes endoplasmic reticulum stress and spontaneous inflammation resembling ulcerative colitis. *PLoS Med* 5: e54

98. Hasnain SZ, Borg DJ, Harcourt BE, Tong H, Sheng YH, Ng CP, Das I, Wang R, Chen AC, Loudovaris T, Kay TW, Thomas HE, Whitehead JP, Forbes JM, Prins JB, McGuckin MA. 2014. Glycemic control in diabetes is restored by therapeutic manipulation of cytokines that regulate beta cell stress. *Nat Med* 20: 1417-26

99. Katz JP, Perreault N, Goldstein BG, Lee CS, Labosky PA, Yang VW, Kaestner KH. 2002. The zinc-finger transcription factor Klf4 is required for terminal differentiation of goblet cells in the colon. *Development* 129: 2619-28

100. Gregorieff A, Stange DE, Kujala P, Begthel H, van den Born M, Korving J, Peters PJ, Clevers H. 2009. The ets-domain transcription factor Spdef promotes maturation of goblet and paneth cells in the intestinal epithelium. *Gastroenterology* 137: 1333-45 e1-3

101. Benoit B, Bruno J, Kayal F, Estienne M, Debard C, Ducroc R, Plaisancie P. 2015. Saturated and Unsaturated Fatty Acids Differently Modulate Colonic Goblet Cells In Vitro and in Rat Pups. *J Nutr* 145: 1754-62

102. Robblee MM, Kim CC, Porter Abate J, Valdearcos M, Sandlund KL, Shenoy MK, Volmer R, Iwawaki T, Koliwad SK. 2016. Saturated Fatty Acids Engage an IRE1alpha-Dependent Pathway to Activate the NLRP3 Inflammasome in Myeloid Cells. *Cell Rep* 14: 2611-23

103. Volmer R, van der Ploeg K, Ron D. 2013. Membrane lipid saturation activates endoplasmic reticulum unfolded protein response transducers through their transmembrane domains. *Proc Natl Acad Sci U S A* 110: 4628-33

104. Cullberg KB, Larsen JO, Pedersen SB, Richelsen B. 2014. Effects of LPS and dietary free fatty acids on MCP-1 in 3T3-L1 adipocytes and macrophages in vitro. *Nutr Diabetes* 4: e113

105. Li Y, Lu Z, Ru JH, Lopes-Virella MF, Lyons TJ, Huang Y. 2018. Saturated Fatty Acid Combined with Lipopolysaccharide Stimulates a Strong Inflammatory Response in Hepatocytes in vivo and in vitro. *Am J Physiol Endocrinol Metab*

106. Vina J, Sanchis-Gomar F, Martinez-Bello V, Gomez-Cabrera MC. 2012. Exercise acts as a drug; the pharmacological benefits of exercise. *Br J Pharmacol* 167: 1-12

107. Martinez ME, Giovannucci E, Spiegelman D, Hunter DJ, Willett WC, Colditz GA. 1997. Leisure-time physical activity, body size, and colon cancer in women. Nurses' Health Study Research Group. *J Natl Cancer Inst* 89: 948-55

108. Slattery ML, Edwards SL, Ma KN, Friedman GD, Potter JD. 1997. Physical activity and colon cancer: a public health perspective. *Ann Epidemiol* 7: 137-45

109. Slattery ML, Potter J, Caan B, Edwards S, Coates A, Ma KN, Berry TD. 1997. Energy balance and colon cancer--beyond physical activity. *Cancer Res* 57: 75-80

110. Bilski J, Mazur-Bialy A, Brzozowski B, Magierowski M, Zahradnik-Bilska J, Wojcik D, Magierowska K, Kwiecien S, Mach T, Brzozowski T. 2016. Can exercise affect the course of inflammatory bowel disease? Experimental and clinical evidence. *Pharmacol Rep* 68: 827-36

111. Bruunsgaard H. 2005. Physical activity and modulation of systemic low-level inflammation. *J Leukoc Biol* 78: 819-35

112. Mathur N, Pedersen BK. 2008. Exercise as a mean to control low-grade systemic inflammation. *Mediators Inflamm* 2008: 109502

113. Pedersen BK. 2011. Muscles and their myokines. *J Exp Biol* 214: 337-46

114. Lira VA, Benton CR, Yan Z, Bonen A. 2010. PGC-1alpha regulation by exercise training and its influences on muscle function and insulin sensitivity. *Am J Physiol Endocrinol Metab* 299: E145-61

115. Eisele PS, Salatino S, Sobek J, Hottiger MO, Handschin C. 2013. The peroxisome proliferator-activated receptor gamma coactivator 1alpha/beta (PGC-1) coactivators repress the transcriptional activity of NF-kappaB in skeletal muscle cells. *J Biol Chem* 288: 2246-60

116. Liu WX, Wang T, Zhou F, Wang Y, Xing JW, Zhang S, Gu SZ, Sang LX, Dai C, Wang HL. 2015. Voluntary exercise prevents colonic inflammation in high-fat diet-induced obese mice by up-regulating PPAR-gamma activity. *Biochem Biophys Res Commun* 459: 475-80

117. Liu WX, Zhou F, Wang Y, Wang T, Xing JW, Zhang S, Sang LX, Gu SZ, Wang HL. 2015. Voluntary exercise protects against ulcerative colitis by up-regulating glucocorticoid-mediated PPAR-gamma activity in the colon in mice. *Acta Physiol (Oxf)* 215: 24-36

118. Demarzo MM, Martins LV, Fernandes CR, Herrero FA, Perez SE, Turatti A, Garcia SB. 2008. Exercise reduces inflammation and cell proliferation in rat colon carcinogenesis. *Med Sci Sports Exerc* 40: 618-21

119. Frajacomo FT, Kannen V, Deminice R, Geraldino TH, Pereira-Da-Silva G, Uyemura SA, Jordao-Jr AA, Garcia SB. 2015. Aerobic Training Activates Interleukin 10 for Colon Anticarcinogenic Effects. *Med Sci Sports Exerc* 47: 1806-13

120. Hasnain SZ, Tauro S, Das I, Tong H, Chen AC, Jeffery PL, McDonald V, Florin TH, McGuckin MA. 2013. IL-10 promotes production of intestinal

mucus by suppressing protein misfolding and endoplasmic reticulum stress in goblet cells. *Gastroenterology* 144: 357-68 e9

121. Wisniewski PJ, Joseph LB, Gardner C, Wahler G, Lightfoot SA, Campbell SC. 2018. Exercise Reduces Colon Inflammation in female but not Male Mice Fed a High-fat Diet. *Comparative Exercise Physiology (Accepted)*

122. Sun J, Shen X, Li Y, Guo Z, Zhu W, Zuo L, Zhao J, Gu L, Gong J, Li J. 2016. Therapeutic Potential to Modify the Mucus Barrier in Inflammatory Bowel Disease. *Nutrients* 8

123. Bergstrom KS, Xia L. 2013. Mucin-type O-glycans and their roles in intestinal homeostasis. *Glycobiology* 23: 1026-37

124. Lu P, Burger-van Paassen N, van der Sluis M, Witte-Bouma J, Kerckaert JP, van Goudoever JB, Van Seuningen I, Renes IB. 2011. Colonic gene expression patterns of mucin Muc2 knockout mice reveal various phases in colitis development. *Inflamm Bowel Dis* 17: 2047-57

125. Raouf AH, Tsai HH, Parker N, Hoffman J, Walker RJ, Rhodes JM. 1992. Sulphation of colonic and rectal mucin in inflammatory bowel disease: reduced sulphation of rectal mucus in ulcerative colitis. *Clin Sci (Lond)* 83: 623-6

126. Pullan RD, Thomas GA, Rhodes M, Newcombe RG, Williams GT, Allen A, Rhodes J. 1994. Thickness of adherent mucus gel on colonic mucosa in humans and its relevance to colitis. *Gut* 35: 353-9

127. Saitoh H, Takagaki K, Nakamura T, Munakata A, Yoshida Y, Endo M. 1996. Characterization of mucin in whole-gut lavage fluid obtained from patients with inflammatory bowel disease. *Dig Dis Sci* 41: 1768-74

128. Larsson JM, Karlsson H, Crespo JG, Johansson ME, Eklund L, Sjovall H, Hansson GC. 2011. Altered O-glycosylation profile of MUC2 mucin occurs in active ulcerative colitis and is associated with increased inflammation. *Inflamm Bowel Dis* 17: 2299-307

129. Monteiro R, Teixeira D, Calhau C. 2014. Estrogen signaling in metabolic inflammation. *Mediators Inflamm* 2014: 615917

130. Hajj Hussein I, Eid A, Maksoud R, Jambart S, Bou Assi T, Zgheib Z, Oueidat D, Chams N, Chams S, Diab R, Barada K, Jurjus R, Cappello F, Reimund J, Kreiker J, Leone A, Jurjus A. 2014. Estrogens control inflammation in experimental colitis. *J Biol Regul Homeost Agents* 28: 213-24

131. Caligioni CS. 2009. Assessing reproductive status/stages in mice. *Curr Protoc Neurosci* Appendix 4: Appendix 4I

132. Johansson ME, Hansson GC. 2012. Preservation of mucus in histological sections, immunostaining of mucins in fixed tissue, and localization of bacteria with FISH. In *Mucins: Methods and Protocols*, pp. 229-35

133. Amann RI, Binder BJ, Olson RJ, Chisholm SW, Devereux R, Stahl DA. 1990. Combination of 16S rRNA-targeted oligonucleotide probes with flow cytometry for analyzing mixed microbial populations. *Appl Environ Microbiol* 56: 1919-25

134. Thiagarajah JR, Yildiz H, Carlson T, Thomas AR, Steiger C, Pieretti A, Zukerberg LR, Carrier RL, Goldstein AM. 2014. Altered goblet cell differentiation and surface mucus properties in Hirschsprung disease. *PLoS One* 9: e99944

135. Bergstrom K, Liu X, Zhao Y, Gao N, Wu Q, Song K, Cui Y, Li Y, McDaniel JM, McGee S, Chen W, Huycke MM, Houchen CW, Zenewicz LA, West CM, Chen H, Braun J, Fu J, Xia L. 2016. Defective Intestinal Mucin-Type O-Glycosylation Causes Spontaneous Colitis-Associated Cancer in Mice. *Gastroenterology* 151: 152-64 e11

136. Vane JR, Mitchell JA, Appleton I, Tomlinson A, Bishop-Bailey D, Croxtall J, Willoughby DA. 1994. Inducible isoforms of cyclooxygenase and nitric-oxide synthase in inflammation. *Proc Natl Acad Sci U S A* 91: 2046-50

137. Luo C, Zhang H. 2017. The Role of Proinflammatory Pathways in the Pathogenesis of Colitis-Associated Colorectal Cancer. *Mediators Inflamm* 2017: 5126048

138. Johansson ME, Hansson GC. 2016. Immunological aspects of intestinal mucus and mucins. *Nat Rev Immunol* 16: 639-49

139. Specian RD, Neutra MR. 1980. Mechanism of rapid mucus secretion in goblet cells stimulated by acetylcholine. *J Cell Biol* 85: 626-40

140. Earle KA, Billings G, Sigal M, Lichtman JS, Hansson GC, Elias JE, Amieva MR, Huang KC, Sonnenburg JL. 2015. Quantitative Imaging of Gut Microbiota Spatial Organization. *Cell Host Microbe* 18: 478-88

141. Stecher B, Robbiani R, Walker AW, Westendorf AM, Barthel M, Kremer M, Chaffron S, Macpherson AJ, Buer J, Parkhill J, Dougan G, von Mering C, Hardt WD. 2007. Salmonella enterica serovar typhimurium exploits inflammation to compete with the intestinal microbiota. *PLoS Biol* 5: 2177-89

142. Swidsinski A, Weber J, Loening-Baucke V, Hale LP, Lochs H. 2005. Spatial organization and composition of the mucosal flora in patients with inflammatory bowel disease. *J Clin Microbiol* 43: 3380-9

143. Ohtomo T, Ino K, Miyashita R, Chigira M, Nakamura M, Someya K, Inaba N, Fujita M, Takagi M, Yamada J. 2017. Chronic high-fat feeding impairs adaptive induction of mitochondrial fatty acid combustion-associated proteins in brown adipose tissue of mice. *Biochem Biophys Rep* 10: 32-8

144. Zwamborn RA, Slieker RC, Mulder PC, Zoetemelk I, Verschuren L, Suchiman HE, Toet KH, Droog S, Slagboom PE, Kooistra T, Kleemann R, Heijmans BT. 2017. Prolonged high-fat diet induces gradual and fat depot-specific DNA methylation changes in adult mice. *Sci Rep* 7: 43261

145. Lambert MI, Van Zyl C, Jaunky R, Lambert EV, Noakes TD. 1996. Tests of running performance do not predict subsequent spontaneous running in rats. *Physiol Behav* 60: 171-6

146. Bernstein D. 2003. Exercise assessment of transgenic models of human cardiovascular disease. *Physiol Genomics* 13: 217-26

147. Cook MD, Martin SA, Williams C, Whitlock K, Wallig MA, Pence BD, Woods JA. 2013. Forced treadmill exercise training exacerbates inflammation and causes mortality while voluntary wheel training is protective in a mouse model of colitis. *Brain Behav Immun* 33: 46-56

148. Lightfoot JT, Turner MJ, Daves M, Vordermark A, Kleeberger SR. 2004. Genetic influence on daily wheel running activity level. *Physiol Genomics* 19: 270-6

149. Hou JK, Abraham B, El-Serag H. 2011. Dietary intake and risk of developing inflammatory bowel disease: a systematic review of the literature. *Am J Gastroenterol* 106: 563-73

150. Tschurtschenthaler M, Adolph TE, Ashcroft JW, Niederreiter L, Bharti R, Saveljeva S, Bhattacharyya J, Flak MB, Shih DQ, Fuhler GM, Parkes M, Kohno K, Iwawaki T, Janneke van der Woude C, Harding HP, Smith AM, Peppelenbosch MP, Targan SR, Ron D, Rosenstiel P, Blumberg RS, Kaser A. 2017. Defective ATG16L1-mediated removal of IRE1alpha drives Crohn's disease-like ileitis. *J Exp Med* 214: 401-22

151. Li XX, Zhang HS, Xu YM, Zhang RJ, Chen Y, Fan L, Qin YQ, Liu Y, Li M, Fang J. 2017. Knockdown of IRE1alpha inhibits colonic tumorigenesis through decreasing beta-catenin and IRE1alpha targeting suppresses colon cancer cells. *Oncogene* 36: 6738-46

152. Salah A, Bouaziz C, Prola A, Pires Da Silva J, Bacha H, Abid-Essefi S, Lemaire C. 2017. Citrinin induces apoptosis in human HCT116 colon cancer cells through endoplasmic reticulum stress. *J Toxicol Environ Health A* 80: 1230-41

153. Shimodaira Y, Takahashi S, Kinouchi Y, Endo K, Shiga H, Kakuta Y, Kuroha M, Shimosegawa T. 2014. Modulation of endoplasmic reticulum (ER) stress-induced autophagy by C/EBP homologous protein (CHOP) and inositol-requiring enzyme 1alpha (IRE1alpha) in human colon cancer cells. *Biochem Biophys Res Commun* 445: 524-33

154. Kubben FJ, Peeters-Haesevoets A, Engels LG, Baeten CG, Schutte B, Arends JW, Stockbrugger RW, Blijham GH. 1994. Proliferating cell nuclear antigen (PCNA): a new marker to study human colonic cell proliferation. *Gut* 35: 530-5

155. Welberg JW, de Vries EG, Hardonk MJ, Mulder NH, Harms G, Grond J, Zwart N, Koudstaal J, de Ley L, Kleibeuker JH. 1990. Proliferation rate of colonic mucosa in normal subjects and patients with colonic neoplasms: a refined immunohistochemical method. *J Clin Pathol* 43: 453-6

156. Birchenough G, Schroeder BO, Backhed F, Hansson GC. 2019. Dietary destabilisation of the balance between the microbiota and the colonic mucus barrier. *Gut Microbes* 10: 246-50

157. Desai MS, Seekatz AM, Koropatkin NM, Kamada N, Hickey CA, Wolter M, Pudlo NA, Kitamoto S, Terrapon N, Muller A, Young VB, Henrissat B, Wilmes P, Stappenbeck TS, Nunez G, Martens EC. 2016. A Dietary Fiber-Deprived Gut Microbiota Degrades the Colonic Mucus Barrier and Enhances Pathogen Susceptibility. *Cell* 167: 1339-53 e21

158. Yang X, Guo Y, He J, Zhang F, Sun X, Yang S, Dong H. 2017. Estrogen and estrogen receptors in the modulation of gastrointestinal epithelial secretion. *Oncotarget* 8: 97683-92

159. Diebel ME, Diebel LN, Manke CW, Liberati DM. 2015. Estrogen modulates intestinal mucus physiochemical properties and protects against oxidant injury. *J Trauma Acute Care Surg* 78: 94-9

160. Kim YS, Song BK, Oh JS, Woo SS. 2014. Aerobic exercise improves gastrointestinal motility in psychiatric inpatients. *World J Gastroenterol* 20: 10577-84

161. Reif S, Klein I, Lubin F, Farbstein M, Hallak A, Gilat T. 1997. Pre-illness dietary factors in inflammatory bowel disease. *Gut* 40: 754-60

162. Laffin M, Fedorak R, Zalasky A, Park H, Gill A, Agrawal A, Keshteli A, Hotte N, Madsen KL. 2019. A high-sugar diet rapidly enhances susceptibility to colitis via depletion of luminal short-chain fatty acids in mice. *Sci Rep* 9: 12294

163. De Schepper S, Verheijden S, Aguilera-Lizarraga J, Viola MF, Boesmans W, Stakenborg N, Voytyuk I, Schmidt I, Boeckx B, Dierckx de Casterle I,

Baekelandt V, Gonzalez Dominguez E, Mack M, Depoortere I, De Strooper B, Sprangers B, Himmelreich U, Soenen S, Guilliams M, Vanden Berghe P, Jones E, Lambrechts D, Boeckxstaens G. 2018. Self-Maintaining Gut Macrophages Are Essential for Intestinal Homeostasis. *Cell* 175: 400-15 e13

164. Lin HH, Faunce DE, Stacey M, Terajewicz A, Nakamura T, Zhang-Hoover J, Kerley M, Mucenski ML, Gordon S, Stein-Streilein J. 2005. The macrophage F4/80 receptor is required for the induction of antigen-specific efferent regulatory T cells in peripheral tolerance. *J Exp Med* 201: 1615-25

165. Liu T, Zhang L, Joo D, Sun SC. 2017. NF-kappaB signaling in inflammation. *Signal Transduct Target Ther* 2

166. Lawrence T, Fong C. 2010. The resolution of inflammation: anti-inflammatory roles for NF-kappaB. *Int J Biochem Cell Biol* 42: 519-23

167. Christian F, Smith EL, Carmody RJ. 2016. The Regulation of NF-kappaB Subunits by Phosphorylation. *Cells* 5

168. Hall PA, Levison DA, Woods AL, Yu CC, Kellock DB, Watkins JA, Barnes DM, Gillett CE, Camplejohn R, Dover R, et al. 1990. Proliferating cell nuclear antigen (PCNA) immunolocalization in paraffin sections: an index of cell proliferation with evidence of deregulated expression in some neoplasms. *J Pathol* 162: 285-94

169. Mayer A, Takimoto M, Fritz E, Schellander G, Kofler K, Ludwig H. 1993. The prognostic significance of proliferating cell nuclear antigen, epidermal growth factor receptor, and mdr gene expression in colorectal cancer. *Cancer* 71: 2454-60

170. Luo YQ, Ma LS, Zhao YL, Wu KC, Pan BR, Zhang XY. 1999. Expression of proliferating cell nuclear antigen in polyps from large intestine. *World J Gastroenterol* 5: 160-4

171. Richards TC. 1977. Early changes in the dynamics of crypt cell populations in mouse colon following administration of 1,2-dimethylhydrazine. *Cancer Res* 37: 1680-5

172. Deschner EE, Maskens AP. 1982. Significance of the labeling index and labeling distribution as kinetic parameters in colorectal mucosa of cancer patients and DMH treated animals. *Cancer* 50: 1136-41

173. McGarrity TJ, Peiffer LP, Colony PC. 1988. Cellular proliferation in proximal and distal rat colon during 1,2-dimethylhydrazine-induced carcinogenesis. *Gastroenterology* 95: 343-8

174. Bujisic B, Martinon F. 2017. IRE1 gives weight to obesity-associated inflammation. *Nat Immunol* 18: 479-80

175. Hillary RF, FitzGerald U. 2018. A lifetime of stress: ATF6 in development and homeostasis. *J Biomed Sci* 25: 48

176. Park HJ, Park SJ, Koo DB, Kong IK, Kim MK, Kim JM, Choi MS, Park YH, Kim SU, Chang KT, Park CK, Chae JI, Lee DS. 2013. Unfolding protein response signaling is involved in development, maintenance, and regression of the corpus luteum during the bovine estrous cycle. *Biochem Biophys Res Commun* 441: 344-50

177. Lin P, Yang Y, Li X, Chen F, Cui C, Hu L, Li Q, Liu W, Jin Y. 2012. Endoplasmic reticulum stress is involved in granulosa cell apoptosis during follicular atresia in goat ovaries. *Mol Reprod Dev* 79: 423-32

178. Xiong Y, Li W, Lin P, Wang L, Wang N, Chen F, Li X, Wang A, Jin Y. 2016. Expression and regulation of ATF6alpha in the mouse uterus during embryo implantation. *Reprod Biol Endocrinol* 14: 65

179. Lowe CE, Dennis RJ, Obi U, O'Rahilly S, Rochford JJ. 2012. Investigating the involvement of the ATF6alpha pathway of the unfolded protein response in adipogenesis. *Int J Obes (Lond)* 36: 1248-51

180. Chakraborty TR, Donthireddy L, Adhikary D, Chakraborty S. 2016. Long-Term High Fat Diet Has a Profound Effect on Body Weight, Hormone Levels, and Estrous Cycle in Mice. *Med Sci Monit* 22: 1601-8

181. Le Lay S, Krief S, Farnier C, Lefrere I, Le Liepvre X, Bazin R, Ferre P, Dugail I. 2001. Cholesterol, a cell size-dependent signal that regulates glucose metabolism and gene expression in adipocytes. *J Biol Chem* 276: 16904-10

182. Zaki MH, Boyd KL, Vogel P, Kastan MB, Lamkanfi M, Kanneganti TD. 2010. The NLRP3 inflammasome protects against loss of epithelial integrity and mortality during experimental colitis. *Immunity* 32: 379-91

183. Dupaul-Chicoine J, Yeretssian G, Doiron K, Bergstrom KS, McIntire CR, LeBlanc PM, Meunier C, Turbide C, Gros P, Beauchemin N, Vallance BA, Saleh M. 2010. Control of intestinal homeostasis, colitis, and colitis-associated colorectal cancer by the inflammatory caspases. *Immunity* 32: 367-78

184. Yao X, Zhang C, Xing Y, Xue G, Zhang Q, Pan F, Wu G, Hu Y, Guo Q, Lu A, Zhang X, Zhou R, Tian Z, Zeng B, Wei H, Strober W, Zhao L, Meng G. 2017. Remodelling of the gut microbiota by hyperactive NLRP3 induces regulatory T cells to maintain homeostasis. *Nat Commun* 8: 1896

185. Nowarski R, Jackson R, Gagliani N, de Zoete MR, Palm NW, Bailis W, Low JS, Harman CC, Graham M, Elinav E, Flavell RA. 2015. Epithelial IL-18 Equilibrium Controls Barrier Function in Colitis. *Cell* 163: 1444-56

186. Cani PD, Amar J, Iglesias MA, Poggi M, Knauf C, Bastelica D, Neyrinck AM, Fava F, Tuohy KM, Chabo C, Waget A, Delmee E, Cousin B, Sulpice T, Chamontin B, Ferrieres J, Tanti JF, Gibson GR, Casteilla L, Delzenne NM, Alessi MC, Burcelin R. 2007. Metabolic endotoxemia initiates obesity and insulin resistance. *Diabetes* 56: 1761-7